Semi-analytical Modelling of Fluid Flow in Unconventional Fractured Reservoirs Including Branch-fracture Permeability Field

by

©Ayon Kumar Das

A thesis submitted to the School of Graduate Studies in partial fulfillment of the requirements for the degree of

Master of Engineering

Department of Process Engineering

Memorial University of Newfoundland

October 2018

St. John's Newfoundland

Abstract

Growing demand for energy and unavailability of new viable energy resources have played a crucial role in the persistent exploitation of unconventional resources through multistage hydraulic fracturing. Currently, standard modelling approaches idealize a fractured media as an interplay of several homogeneous continuum of normal diffusive characteristics. However, evolved branch-fractures generate a space with extreme heterogeneity around primary fracture plane. The precise characterization of these branch-fractures is imperative for well performance analysis along with subdiffusive behaviour of unconventional matrices. This study presents two semi-analytical models that account for the branch-fracture permeability field and subdiffusion.

The first model, Induced Branch-fracture Subdiffusive Flow model (SIBFF), accounts for exponential permeability field concept and subdiffusive transport behaviour of matrices. Compared to the earlier analytical models, the SIBFF model accounts for more comprehensive transport mechanisms and medium properties. The other model, Fractal Branch-fracture model, couples fractal porosity/permeability distribution of branch-fracture and subdiffusion to account for more detailed description of stimulated reservoir volume (SRV) and unfractured inner region.

The wellbore pressure solution is derived by discretizing the reservoir into several flow regions and imposing both flux and pressure continuity at the interface between contiguous segments. The inclusion of permeability field and fractional flux law introduces important complexities to the mathematical model that are carefully resolved by implementing Bessel functions and Laplace transformation (LT). Finally, the solution is inverted to time domain using Gaver-Wynn-Rho (GWR) algorithm. This study also assessed the applicability of four numerical inversion methods and found GWR method more suitable and predictive.

The sensitivity of important model parameters is presented. Results were verified analytically and validated against Niobrara and Eagleford field data. It is shown that the models could be implemented to quantify the efficiency of a stimulation job, to decide on the necessity of re-fracturing a formation and to analyze horizontal well performance with better predictive capability. The proposed models could further be employed to characterize different flow regimes for unconventional reservoirs.

Acknowledgements

I would like to express my deepest appreciation to my supervisor, Dr. Syed Imtiaz, who showed me endless support, guidance, patience and dedication despite his heavy work load. I would also like to express my sincere gratitude to my former supervisor Dr. M. Enamul Hossain.

I truly acknowledge the support and guidance from Dr. Greg F. Naterer and Dr. Faisal Khan throughout the course of my study and research. I would also like to extend my gratitude to the administrative staff of Graduate Studies and School of Graduate Studies. Thanks to the entire stuff of the Process Engineering department for sharing their knowledge and experience.

I would like to thank Statoil for their financial and academic support and for granting me this opportunity to complete my advance degree. I would also like to thank all of my colleagues at MUN who supported me during this journey.

Finally, I would like to thank my family, friends and everyone who added value to the work described in this thesis and gave continuous support at every stem of this challenging yet exciting journey.

Table of Contents

List of Tables

List of Figures

To my father Okhil Chandra Das, my mother Sabita Rani Das
& my grandmother Bela Rani Das

Chapter 1

Introduction

1.1 Unconventional Fractured Reservoir

Unconventional resources have made a significant paradigm shift in the business of energy exploration and exploitation, with shale and ultralow permeability reservoirs contributing as the leading hydrocarbon producer through complementing hydraulic stimulation and horizontal well technology. Unconventional resources typically include shale gas and shale oil in low permeability shales, tight oil and gas, coal bed methane (CBM), oil/gas sands and hydrates. The resource triangle concept introduced by Gray (1977) is the best way to categorize the unconventional resources in nature. The concept explains that all natural resources are distributed log-normally in nature. As the figure 1.1 depicts, the high quality reservoirs with high permeability are small in volume, hard to find but are easy to extract when they are discovered. Going deeper into the resource triangle requires advanced technology to produce economically as the quality of the reservoirs severely deteriorates in terms of conductivity. For instance, in the 1980s, tight gas sands and coal seams were unlocked by the advent of vertical wells with hydraulic fracturing. However, the economic production from unconventional shale and tight formations requires multistage hydraulic stimulation and horizontal well technology. In the literature of reservoir engineering, unconventional fractured reservoirs are therefore synonymous to the shale and tight formations upgraded by hydraulic fracturing and horizontal well completion.

The enormous volume of hydrocarbon reserve in shale and ultralow formations

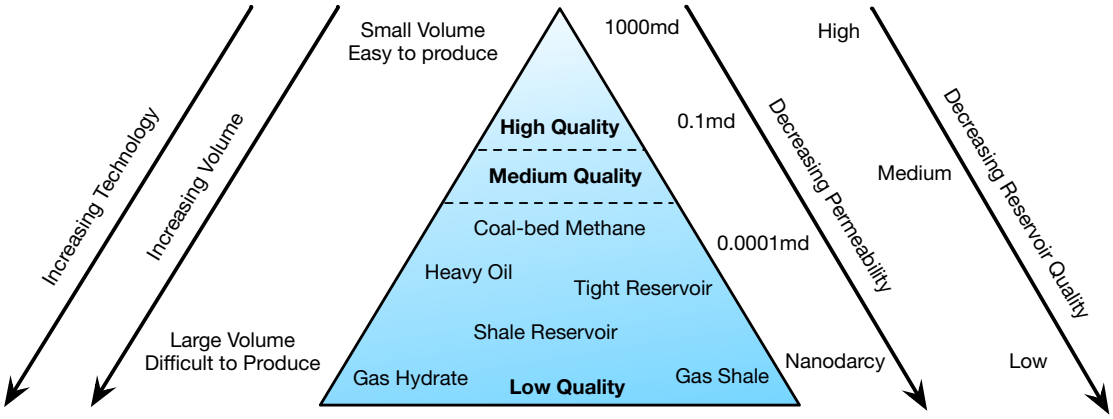

Figure 1.1: The concept of resource triangle (adapted from Gray, 1977)

has been a major stimulant for carrying out more investigation in fluid flow through hydraulically fractured media. The intense heterogeneity in shale and tight plays is inherited from the diagenesis of those reservoirs. The application of hydraulic fracturing further complicates the geometry and environment of the flow paths in the reservoir. The multistage fracturing enhances the productivity by generating an invasive fracture network in the vicinity of the horizontal well. The affected space is usually referred to as stimulated reservoir volume.

1.2 Branch-fracture Permeability Field

The practice of inducing hydraulic fracturing to exploit energy from unconventional resources has been a common practice in the oil and gas industry. The advances in horizontal drilling and stimulation technology has made many countries to produce from their unconventional reservoirs. However, in order to ensure economic recovery from unconventional reservoirs, an efficient stimulation technique and realistic modelling of fluid flow in induced fractures are necessary. During the fracturing treatment, a number of perforations are performed to inject fracturing fluid into the formation. The high velocity fluid induce a primary fracture plane of greater permeability around the perforation point. In this study, it is assumed that the primary fracture plane is highly permeable and rectangular in shape to facilitate the analytical solution for fluid flow. However, the fracturing treatment also induces numerous branch fractures stemming from the primary fracture plane due to the shear and tensile failure of the

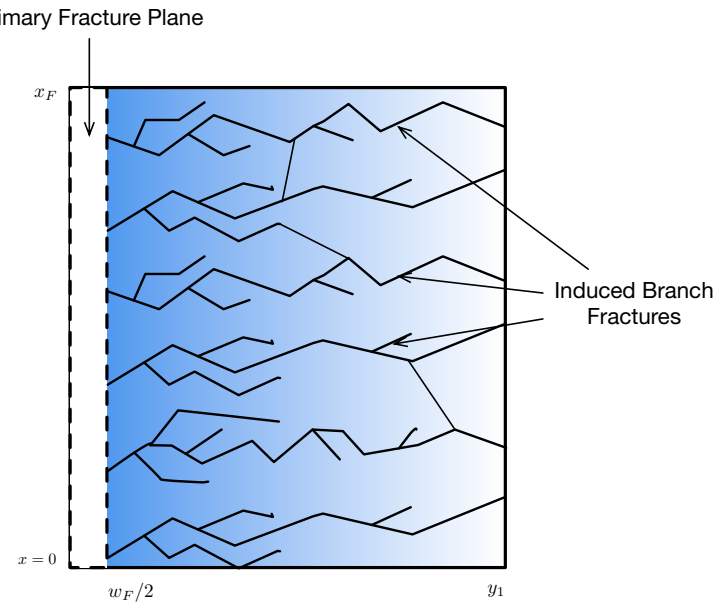

Figure 1.2: Schematic of induced branch fractures around a main fracture plane

natural fractures away from the main fracture plane (Palmer et al., 2007; Ge et al., 2011; Fuentes-Cruz, Gildin, Valkó, et al., 2014). According to Taleghani et al. (2011), in an event of fluid driven stimulation, different types of critical situation may arise inside the reservoir:

- Pre-existing transverse natural fractures may arrest the propagation of the induced fracture
- The propagation of induced fractures may reactivate the stationary fractures
- The aperture of the pre-existing fracture may decrease or begin to close permanently

Therefore, the growth of the interactive induced fractures creates a network of branch fractures. The aperture and the density of those fractures decreases away from the primary fracture plane creating a field of altered permeability in the stimulated reservoir volume. These secondary branch fractures enhances the reservoir contact area and maximizes hydrocarbon recovery from low permeability reservoirs.

1.3 Problem Description

An inherent difficulty in developing a mathematical model for fluid flow in fractured media comes from translating the flow through complex fractures in analytical form. The particle displacement in a well-connected fracture network follows Fickian or normal diffusion and the fluid flux can be described by the Darcy's law. Most of the developed analytical models idealize the fracture continuum as a homogeneous but highly permeable media in the SRV of stimulated reservoir. However, the spatial variation of branch-fracture permeability introduces heterogeneity in the fracture continuum. The diffusivity can no longer be assumed constant in the fracture continuum.

Conventional formulations of transient diffusion in heterogeneous media assume that fluid flux changes proportionally with the change in imposed pressure gradient. This formulation performs well only when fracture network or matrix medium is well connected. However, the unconventional matrix possess heterogeneity in different scales that results in a flow field that cannot be described by Gaussian distribution. This shift from Gaussian diffusion to non-Gaussian diffusion are well described by the sub-diffusion phenomena assuming that mean square displacement of fluid particles is no longer linearly dependent on time. Raghavan (2011) accounted for this deviation and proposed a fractional flux law for sub-diffusive flow behaviour. The fractional flux law defines production rate at a point as a reflection of the pressures and gradients that extend to the previous times.

In order to produce a fractured reservoir efficiently, engineers must be able to simulate the fluid flow as realistic as the formulation and problem geometry permits. We believe that the coupling of the spatial variation of induced fracture permeability and subdiffusion with appropriate transfer function between different continua is necessary for a better understanding of the unconventional fractured reservoirs. This will enhance the performance of the prevailing analytical models and predict well performance with a high degree of accuracy.

1.4 Research Objectives

The main objective of this work is to perform a rigorous analytical study to account for branch-fracture permeability field in SRV and subdiffusion phenomena in unconventional matrix and present semi-analytical solutions simulating single-phase fluid flow in hydraulically stimulated unconventional reservoirs. The semi-analytical models include a significant segment which is numerical and prone to errors if proper care is not taken in the implementation of inversion algorithm. Therefore, this research will:

- assess the applicability and accuracy of the widely used Laplace inversion methods and compare results from these methods with the analytical and numerical results for fracture flow problems.
- develop semi-analytical solution for fluid flow in multifractured horizontal reservoir incorporating exponential branch-fracture permeability field and subdiffusion in unconventional matrix. Also, analyze field data to introduce practical guidelines and establish confidence in applying the derived solution
- develop fractal branch-fracture flow model assuming the generated branch-fracture network around the horizontal well as a fractal object. Also, validate the model with field data to extract useful information about the SRV and USRV of ultralow unconventional reservoirs.

1.5 Thesis Outline

This thesis is divided into six chapters:

Chapter 1 introduces the thesis and discusses about the necessity of including the branch-fracture permeability field in hydraulically stimulated reservoirs.

Chapter 2 outlines standard modelling approaches, especially dual-porosity and anomalous diffusion approaches, applied to simulate fluid flow in fractured media.

Chapter 3 presents a comparative study of four numerical Laplace inversion methods that are widely used in the semi-analytical modelling of fluid flow through porous

media. In addition, it also discusses about the background, limitations and applicability of those four methods.

Chapter 4 describes the formulation of the Induced Branch-fracture Sub-diffusive Flow model. We discretize the whole reservoir into five flow regions and present a detailed description of the mathematical models for each flow regions, defining the governing relations and assumptions. It also presents a section where the SIBFF model is validated against an analytical model and the field data from Niobrara Shale field.

Chapter 5 presents the fractal branch-fracture flow model. The governing equations and the mathematical formulations of SRV and USRV flow region is documented in this chapter. It also presents a sensitivity study of the influential parameters to illustrate the constraints and the capabilities of the presented fractal model. Finally, we provide a field example (with Eagle Ford data) to establish the model as the finest tool for the characterization of ultra-low unconventional reservoirs.

Chapter 6 summarizes the main conclusions of this research along with recommendations for possible future work.

Chapter 2

Standard Approaches to Model Fluid Flow in Fractured Reservoirs

This chapter reviews a number of standard fluid flow models that have bolstered the understanding of fluid flow in fractured reservoirs. The underlying assumptions, geometry of the fractured media and the transfer functions between fracture and matrix continuum are the vital features of any of those analytical models. Based on the idealization scheme and diffusion, we divide the these model into two approach: Continuum and Anomalous approach. These approaches are discussed in the following sections.

2.1 Continuum Approach

Fluid flow modelling in fractured unconventional reservoirs is of paramount importance as the hydraulic fracking treatment to those reservoirs has been a promising option. As we know the fluid flow through fractured media is controlled by the continuous interaction and interplay of fracture and matrix. Researchers have studied fractured reservoirs for decades and proposed several idealistic and oversimplified models of dual porosity type to capture the physics of fluid flow in fractured media. The basic idea behind dual porosity models is the assumption that the total reservoir system is composed of two uniform continua. One continuum is the uniform rock matrix and another continuum is the uniform fracture network. This continuum assumption simplifies that any infinitesimal chunk of reservoir volume contains both fractures and

matrix components. Consequently, at every point in space, there exist two different pressures: the matrix pressure and fracture pressure. The exchange of fluid between these two continuum takes place by a coupling equation, termed as transfer function, under specific flow condition. But there is no exchange of fluid among matrix blocks and no direct communication between the matrix and the wellbore. As the fluid production begins, a significant pressure drop occurs in the fracture medium due to the depletion of fluid. As fluid production continues, differential pressure between the matrix and fractures causes the matrix fluid flow towards the fractures. This flow, termed as interporosity flow, continues until the pressures in both continua reach equilibrium.

For a slightly compressible fluid, the fluid pressure in the fracture continuum is governed by the diffusion equation (Matthews and Russell, 1967).

$$\nabla \cdot \left(\frac{k_f}{\mu} \nabla p_f \right) + \dot{Q} = \phi_f c_f \frac{\partial p_f}{\partial t} \tag{2.1}$$

Diffusion equation in matrix continuum,

$$\nabla \cdot \left(\frac{k_m}{\mu} \nabla p_m \right) = \phi_m c_m \frac{\partial p_m}{\partial t} \tag{2.2}$$

These two equations are usually coupled by a source/sink term that can be evaluated from a surface integral of Darcy's law at the matrix block boundary.

$$\dot{Q} = -\frac{1}{V_m} \oiint_{\partial V_m} \frac{k_m}{\mu} \left(\nabla p_m \cdot n \right) \, dS \tag{2.3}$$

Barenblatt (1962) proposed the very first concept of dual porosity model to define heterogeneity of fractured reservoirs. They assumed the total complex reservoir as a system of two overlapping media: fissures or fractures and Matrix blocks. They reported that each media is defined by its own average liquid pressure where fissures have the highest conductivity but very low porosity. On the other hand, the matrix blocks have the highest storativity but low permeability. They wrote two different set of equations for the two continua and coupled them together by a transfer function under pseudo steady state condition.

Warren and Root (1963) developed the very first comprehensive dual porosity model, called Sugar-Cube model and introduced dual porosity concept into petroleum

engineering literature. According to this model, the reservoir comprises of uniformly structured fractures immersed in a uniform setting of matrix grains. The fracture network possesses a significantly higher conductivity but low storativity. All the matrix blocks acts as a source of fluid and feeds to the fractures. All the fractures are the only flow medium that feeds to the wellbore. Figure 2.1 illustrates the idealization of Warren and Root model as proposed. They assumed an average pressure distribution in each block. The average pressure in the matrix block is given by,

$$\overline{p}_m = \int_{V_m} \frac{1}{V_m} p_m \partial V \tag{2.4}$$

Integrating over the entire matrix block and applying divergence theorem to convert the volume integral into surface integral:

$$\phi_m c_m \frac{\partial p_m}{\partial t} = \frac{1}{V_m} \oiint_{\partial V_m} \frac{k_m}{\mu} \left(\nabla p_m \cdot n\right) dS = -Q \tag{2.5}$$

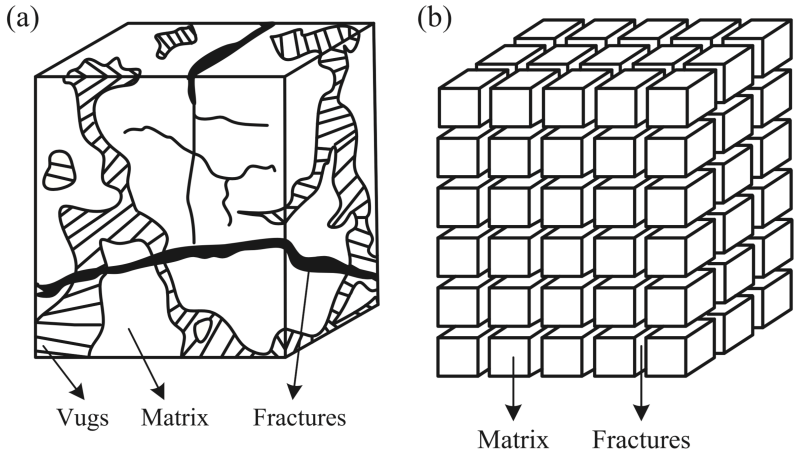

Figure 2.1: Idealization of a comprehensive model of dual porosity models. (a) Actual reservoir (b) Reservoir model (adapted from Wu, 2016)

The most distinctive assumption of this model is that it assumes pseudo steady state interporosity flow between matrix and fractures. This means that the average pres-

sure in the matrix blocks decline linearly as a function of time. To couple fracture equation and matrix equation together, they assumed the source term $\dot{Q}$ to be directly proportional to $(p_f - p_m)$.

$$Q = -\frac{\alpha k_m}{\mu}\left(p_f - \overline{p}_m\right) = -\phi_m c_m \frac{\partial \overline{p}_m}{\partial t} \tag{2.6}$$

Where, α is referred to as shape factor, which is used to eliminate the matrix geometry effect. The difference between the average matrix pressure and the average pressure of the contiguous fracture is used as a main driving force in the interporosity flow. As pseudo steady state condition is assumed, the pressure at the middle of the matrix elements gets affected from time zero. Besides that, as the fluid pressure in the matrix continuum is governed by ordinary differential equation, the computational time needed to evaluate the source term becomes remarkably negligible when implemented in a reservoir simulator (Zimmerman et al., 1993).The diffusion equation for fracture continuum in Warren and Root model takes the following form.

$$\nabla \cdot \left(\frac{k_f}{\mu}\nabla p_f\right) - \phi_m C_m \frac{\partial p_m}{\partial t} = \phi_f C_f \frac{\partial p_f}{\partial t} \tag{2.7}$$

Figure 2.2 illustrates the pressure profile in the matrix blocks and contiguous fractures. This model proposed that only two parameters are sufficient to effectively describe the deviation from single porosity reservoirs to dual porosity reservoirs. One is a measure of the fluid capacitance of the secondary porosity and the other one is a measure related to the scale of heterogeneity. The first parameter, ω, is the ratio between the storativity of fracture and the storativity of the total system:

$$\omega = \frac{(\phi V c)_f}{(\phi V c)_f + (\phi V c)_m} \tag{2.8}$$

$$\lambda = \alpha r_w^2 \frac{k_m}{k_f} \tag{2.9}$$

The other parameter,λ, is the interporosity flow coefficient. It represents the ability of the fluid to flow the storage continuum to the conductive continuum. It determines how rapidly storage continuum feeds to the fracture media. Warren and Root analyzed the pressure transient responses by utilizing these two parameters. However, Odeh (1965) analyzed pressures transient behaviour of fractured media and proved

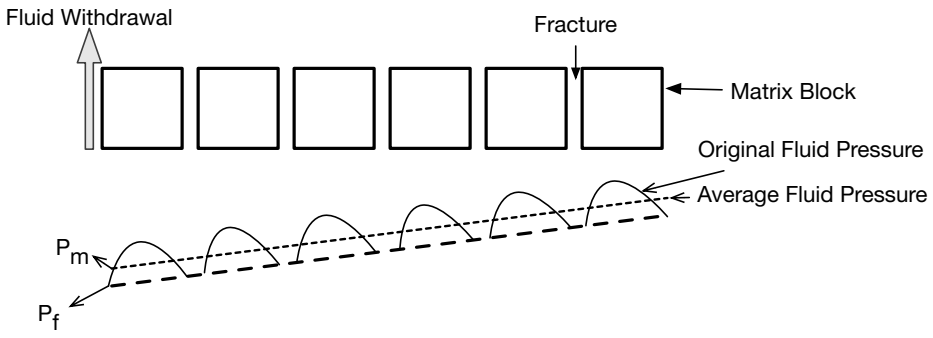

Figure 2.2: Pressure profile along the cube shaped matrix in the idealization of Sugar-cube model

mathematically that the build-up and drawdown data of fractured reservoirs look identical to those of a homogeneous reservoir.

Kazemi et al. (1976) extended the Warren and Root model to two phase flow which incorporates the effects of relative fluid permeabilities, imbibition, gravitation and variation in formation properties. They idealized the fractured reservoir as an equivalent system of horizontal fractures immersed in between two matrix layers. Unlike the Warren and Root model, they assumed that the fluid exchange between matrix domain and fracture domain occurs under transient flow condition. The application of transient flow condition into dual porosity model eliminates the limitations of early time flow in Warren and Root model. As with sugar cube model, two differential equations are written to describe the dual porosity system-one for flow in fractures and another for flow in matrix. They discretized the governing differential equations in three-dimensional system and solved the model numerically. The finite difference form of governing differential equations for fracture and matrix continuum are given as below:

$$\left[\sum T_l \lambda_p \rho_p \Delta \left(p_p - \gamma_p D\right) + \rho_p q_p^w\right] - \tau_{mf} = \left[\frac{V}{\Delta t}\Delta_t \left(\phi S_p \rho_p\right)\right]_f \tag{2.10}$$

$$\tau_{mf} = \left[\frac{V}{\Delta t}\Delta_t \left(\varnothing S_p \rho_p\right)\right]_m \tag{2.11}$$

The transfer function for fluid exchange is given as:

$$\tau_{mf} = K_m V \lambda_p \rho_p \left[(p_p - \gamma_p D)_f - (p_p - \gamma_p D)_m \right] \tag{2.12}$$

de Swaan O et al. (1976) developed an analytical model for transient flow condition in fractured reservoirs. This model doesn't require any adjusting parameters like shape factors. Only fluid and reservoir properties are enough to explain a fractured reservoir. The matrix elements were assumed as horizontal layered slabs between high permeable fractures. Flow in the matrix slab is unidirectional and perpendicular to the flow direction within the fractures. This type of flow is usually referred to as bilinear flow. Having a layered continuum of matrix elements, the solution of diffusion equation for the matrix was more convenient and easier. Unlike the Warren and Root model the matrix layers are not assumed as an overlapped source when fracture diffusion equation was written. Rather, the fluid transfer from the matrix layers is included according to the Darcy's law at the interface of matrix and fracture. In the model, he showed that the two straight-line well pressure responses during well test, a key feature of Warren and Root model, is preserved. However, the approach presented in the model does not describe the transition between these two straight lines.

Ozkan et al. (2009) implemented the dual porosity concept to simulate fluid fluid flow in a multiply fractured horizontal well and proposed a trilinear dual-porosity (TDP) model. They subdivided a multifractured reservoir into three linear flow regions: rectangular hydraulic fracture, dual porosity inner region and a homogeneous outer region. However, the TDP model did not account for any unfractured region in the inner reservoir that would produce erroneous result when the inner reservoir is not fully affected by the fracturing job. The inner region was modelled as a dual porosity idealization and the results for assuming the matrix-fracture fluid transfer as the pseudosteady(Warren & Root, 1963) or transient transfer function(de Swaan O et al., 1976; Kazemi et al., 1976) was shown in the study. The laplace solution of each flow domain was coupled at the interface by applying pressure and flow continuity. It was shown that TDP model was a predictive tool for evaluating productivity of

multifractured horizontal reservoir when the available reservoir data is very low. It was determined that the increase in the number of natural fractures in inner region is the most efficient way to improve the productivity of unconventional reservoirs.

Stalgorova and Mattar (2013) accounted for an unfractured region in between two hydraulic fractures assuming that the stimulated region did not traverse the total space between any two transverse hydraulic fracture and developed a Five Region model with five linear flow domain. The analytical derivation of the model follows the same lines as Trilinear Dual-porosity model by Ozkan et al. (2009). The inner region divided into two flow regions: homogeneous SRV with higher permeability and USRV with reservoir's inherent permeability. This assumption enables it to be used in a wide range of geometries for multifractured reservoir and produces realistic estimation for productivity. They verified their solution with existing semianalytical solution and found useful for practical analysis of horizontal well performance. However, the assumption of homogeneous SRV region is not realistic as the fracturing fluid generates a space with spatially altered permeability. The spatial variation of permeability and dual-continuum in SRV should be considered in order to delineate a comprehensive picture of SRV.

2.2 Anomalous Diffusion Approach

The flow field generated by the particles in unconventional reservoirs is significantly different from the field of a conventional reservoirs. In order to incorporate the heterogeneity in the flow domain, generalized diffusion concept has gained popularity in the las few decades(Fomin, Chugunov, & Hashida, 2011; Caputo, 1998; Chang & Yortsos, 1990; Raghavan, 2011). The generalized diffusion concept includes normal diffusion: when mean square displacement (MSD) of particles follows linear relationships with time; and anomalous diffusion: when the MSD is nonlinearly dependent on time. According to Holy (2016), the anomalous diffusion concept applied to an unconventional reservoirs are based on the following three hypotheses:

- The deviation of straight line slopes observed on log-log plots of rate vs time in unconventional reservoirs from the slopes of conventional reservoirs are the result of anomalous diffusion

- The fractional relation between the flux and pressure gradient captures the physics of the anomalous diffusion and the conservation law of mass still holds.

- The hydraulically stimulated space in unconventional reservoirs can be regarded as an disordered media in which particle displacement is nonlinearly dependent on time.

In the continuum approach, the fracture medium is idealized as a homogeneous, continuous and uniformly distributed medium. However, the geometry of the fracture network generates a flow field which resembles with the anomalously diffusive flow field. The anomalous diffusion due to the geometric irregularity is analytically modelled with fractal concepts (Chang & Yortsos, 1990; J. Acuna & Yortsos, 1991; Beier et al., 1994; Camacho Velazquez, Fuentes-Cruz, Vasquez-Cruz, et al., 2006).

Metzler et al. (1994); Park et al. (2000) presented a generailized fractal diffusivity equation that accounts for temporal dependencies on fluid flux in the form of a time fractional derivative. Raghavan (2011) upgraded the time fractional model and revealed that the application of fractional constitutive flux law is inherent in the nature of the unconventional fractured reservoirs that exhibits a number of scales in the form of obstacles and channels as well as induced changes affected by the stimulation job. Assuming a Continuous-Tine-Random-Walk process in the particle displacement of the diffusion in porous media, a fractional velocity equation incorporating subdiffusion is given by (Fomin et al., 2011; C. Chen & Raghavan, 2015; Raghavan, 2011),

$$\vec{v}_x = -\frac{k_\beta}{\mu}\frac{\partial^{1-\beta}}{\partial t^{1-\beta}}\frac{\partial \Delta p}{\partial x} \tag{2.13}$$

Where, β is the anomalous diffusion parameter. When, $\beta < 1$, hindrance to fluid flow is more pronounced than the normal diffusion case ($\beta = 1$). Superdiffusion occurs when $\beta > 1$. The fractional derivative term in (2.13) is defined using Caputo's definition,

$$\frac{\partial^{1-\beta}}{\partial t^{1-\beta}}\left\{p\left(x,t\right)\right\} = \frac{1}{\Gamma\left(\beta\right)}\int_0^t \frac{\partial p\left(x,t\right)}{\partial t}\left(t-\tau\right)^{-(1-\beta)} d\tau \tag{2.14}$$

Ozcan (2014a) proposed an Trilinear Anomalous Diffusion (TAD) model that idealizes the nano-porous inner reservoir as a space where the conditions for anomalous

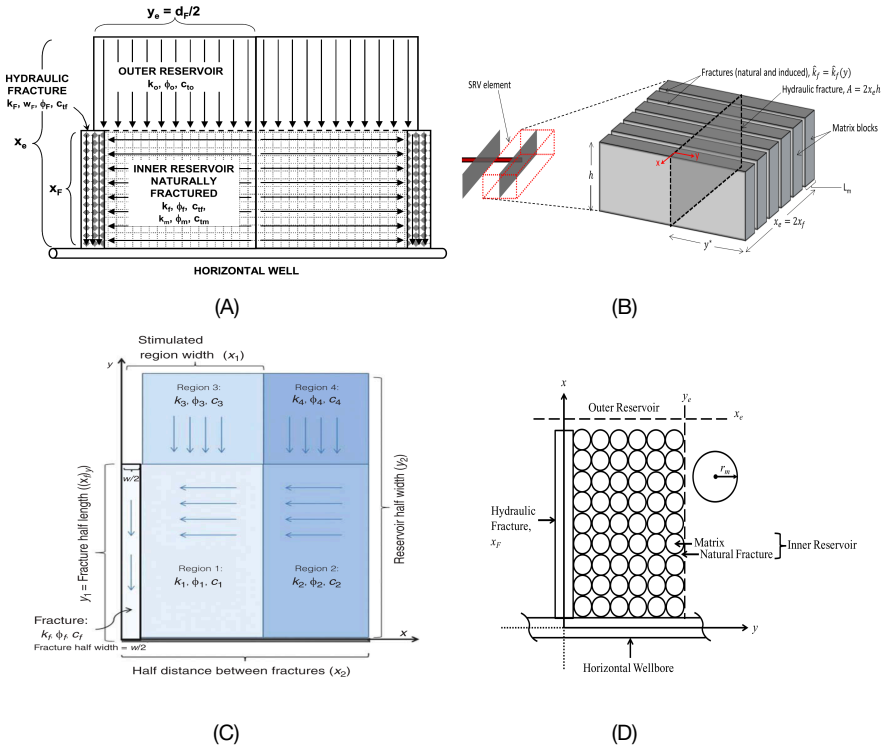

Figure 2.3: (A). Trilinear Model (Ozkan et al., 2009) , (B). Induced Permeability-double Porosity Model (Fuentes-Cruz, Gildin, & Valkó, 2014), (C). Five Region Model (Stalgorova & Mattar, 2013) and (D) TADDP Model (Albinali, 2016)(Figures are taken from the respective papers)

diffusion holds. This model assumes that the fracturing job generates a disordered and fractured space between any two hydraulic fractures. The temporal fractional equation was applied to capture the hereditary effects of anomalous diffusion in the inner reservoir. The normal diffusion was idealized in hydraulic fracture and outer regions and the Darcy's law was applied to represent the relationships between pressure gradient and fluid velocity in the porous media. The derivation of the TAD model follows the similar procedure to that in trilinear model(Ozkan et al., 2009).

Albinali et al. (2016) proposed a Trilinear Anomalous Diffusion and Dual Porosity model (TADDP) which idealizes the SRV as a dual porosity continuum: Spherical matrix with anomalous diffusion and induced fractures with uniform properties ($k_{\alpha f}$ is uniform for the fracture continuum). TADDP model is one of the established anomalous diffusion models that was validated against the standard analytical models

and field data. Like TAD model, they applied the generalized diffusion equation to account for anomalous behaviour of disordered medium. However, this model coupled dual porosity representation with anomalous diffusion that enables the model to study the effect of flow hindrance of matrix and fracture continuum independently. They concluded that the unconventional matrix shows subdiffusive flow behaviour that could be taken into account by time fractional Darcy's law by Raghavan (2011). It was also shown that the induced fracture network can be simulated by normal diffusion formula when the connectivity of fracture network is good. However, the TADDP model did not incorporate the effect of unfractured region between two fracture planes.

Chapter 3

Numerical Laplace Inversion of Fracture Flow Solution

3.1 Introduction

The economic production from unconventional plays compliments the stimulation by hydraulic fracturing and horizontal drilling. Reservoir engineers make their investment decisions based on two classes of fluid flow models of fractured reservoir with embedded hydraulic fractures (Xu, Li, Du, et al., 2011). The first class of those models includes the decline curve models which are developed by following the decline trend of the rates. These models, developed by Arps et al. (1945), requires knowledge of a distinctive line between the transient and boundary dominated flow periods and do not involve reservoir parameters in the analysis of forecasting rates. These limitations of decline models made the other class, analytical models, attractive for predicting rates and estimating reserves. The development of a fully analytical model for a complex geometry posed by multifractured reservoir is always cumbersome and if the solution is found, it often involves infinite series solution which is not well suited for forecasting and history matching with field data. However, the semi-analytical models, that requires a part of the model to be dealt with numerical methods, have been the best tool that allow reservoir engineers to obtain solutions to the complex problems of different geometries (Furman & Neuman, 2003). Unlike the common practice, the history matching with the developed model is much easier when it is performed entirely in Laplace domain (La, 2015). In all of these applications of LT,

numerical inversion from Laplace domain to the real time domain is a crucial part and the possible errors form this segment is often neglected in the process. The numerical inversion of LT could be a potential source of errors if the accurate method with a desirable range of method parameter is not chosen for the inversion job. There is a large volume of published studies describing the methods of inverting Laplace transform from the complex domain to the real-time domain. So, it is natural and timely to assess the applicability of these methods in the problems of fluid flow through fractured media. We investigate the applicability of these methods in solving flow problems of fractured reservoir.This study has focused on the two directions of the inverse problems associated with the fractured reservoir modelling: First is to investigate the applicability to a wide range of inversion problems and the other one is the numerical accuracy of the approximant which can be obtained on a digital computer. We start off the discussion of the four methods by defining the Laplace transform and inverse Laplace transform equation:

$$F(s) = \int_0^\infty e^{-st} f(t)\, dt \tag{3.1}$$

$$f(t) = \lim_{T\to\infty} \frac{1}{2\pi i} \int_{a-iT}^{a+iT} e^{st} F(s)\, ds \tag{3.2}$$

Here, s is a complex variable in the Laplace domain. $F(s)$ represents the function defined in Laplace domain that needs to be inverted to the time domain to obtain $f(t)$.

3.2 Numerical Laplace Inversion Methods

3.2.1 Fourier Series Method

A considerable amount of literature has been published on the Fourier series method of Laplace transform inversion. The main idea of these methods lies in converting the basic Laplace inversion equation into a Fourier transform and then approximating the time function using a certain Fourier series. The development of this method starts with replacing s with $(a + iv)$ in the original inverse equation (Abate & Valkó, 2004).

$$f(t) = \frac{2e^{at}}{\pi} \int_0^{\infty} \left[\mathrm{Re}\left\{ f(a+iv) \right\} cos(vt) - \mathrm{Im}\left\{ f(a+iv)\, sin(vt) \right\} \right] dv \tag{3.3}$$

Crump(1976) showed that the function $\hat{f}(s)$ and $f(t)$ can be written in terms of Fourier Cosine transform.

$$\mathrm{Re}\left\{ f(s) \right\} = \int_0^{\infty} e^{at} f(t)\, cosvtdt \tag{3.4}$$

$$f(t) = \frac{2e^{at}}{\pi} \int_0^{\infty} \mathrm{Re}\left\{ f(s) \right\} cosvtdv \tag{3.5}$$

Therefore, it is evident that the continuous function $f(t)$ should be completely determined from the frequency spectrum of $\mathrm{Re}\{\hat{f}(t)\}$.Dubner and Abate (1968) have derived an approximation formula for evaluating $f(t)$ with the application of trapezoidal rule. The approximate inversion formula is given by:

$$f(t) = \frac{2e^{at}}{T} \left[\frac{1}{2} Re\left\{ f(a) \right\} + \sum_{k=1}^{\infty} \mathrm{Re}\left\{ f\left(a + \frac{k\pi i}{T} \right) \right\} cos\left(\frac{k\pi}{T} t \right) \right] \tag{3.6}$$

They eliminated the cosine factor by letting $T = 2t$ in the above equation to accelerate the computation as there are no cosines and presented the following equation:

$$f(t) = \frac{e^{at}}{t} \left\{ \frac{1}{2} F(a) + Re \sum_{k=1}^{n} F\left(a + i\frac{k\pi}{t} \right) (-1)^k \right\} \tag{3.7}$$

3.2.2 Fixed Talbot Method

Talbot (1979) proposed an approach to invert a function defined in Laplace domain by deforming the standard contour in the Bromwich integral. Later, Abate and Valkó (2004) upgraded the method by fixing the contour path which led to Fixed Talbot algorithm. This method approximates the inverse of any Laplace transform by the following equation,

$$f(t) = \frac{r}{M} \left\{ \frac{1}{2} f(r)\, exp(rt) + \sum_{k=1}^{M-1} \mathrm{Re}\left[exp\left(ts\left(\theta_k \right) \right) f\left(s\left(\theta_k \right) \right) \left(1 + i\sigma\left(\theta_k \right) \right) \right] \right\} \tag{3.8}$$

Where, $s(\theta)$ and $\sigma(\theta)$ are defined as below:

$$\begin{aligned} s(\theta) &= r\theta\left(cot\theta i\right), \quad -\pi < \theta < +\pi \\ \sigma(\theta) &= \theta + \left(\theta cot\theta - 1\right) cot\theta \end{aligned} \tag{3.9}$$

And, θ_k is defined as,

$$\theta_k = \frac{k\pi}{M},\ r = \frac{2M}{5t} \tag{3.10}$$

3.2.3 Gaver-Stehfest Method

Stehfest algorithm (Stehfest, 1970) is the one which has been widely used to invert Laplace transform irrespective of fields and problem types due to its simplicity for implementation and the reported accuracy level. It should be remarkably noted here that almost every research work concerning the pressure behaviour of wells over the last few decades has based on the Gaver-Stehfest method (C.-C. Chen et al., 1996). This method has been derived from, an alternative way of evaluating inverse problem, the Post-Widder method proposed by Abate and Whitt (1995). Post Widder method evaluates $f(t)$ as a pointwise limit of $\phi_k(t)$ as $\phi \to \infty$.

$$\phi_k(t) = \frac{(-1)^k}{k!}\left(\frac{k}{t}\right)^{k+1} f^{(k)}\left(\frac{k}{t}\right) \tag{3.11}$$

Where $\hat{f}^{(k)}(s)$ represent the n^{th} derivative of $\hat{f}(s)$. One main advantage of this formula is that it avoids the computation for complex arguments and also it computes $f(t)$ from the value of and its derivatives. However, the evaluation of $\hat{f}(s)$ and it's derivatives. However, the evaluation of $\hat{f}(s)$ to the n^{th} derivative and the associated round-off errors in computing binomial coefficient makes the formula less accurate and less efficient. During the investigation for the assessment of time dependent behaviour of stochastic processes, it was found that the Post Widder's formula can be transformed into a discrete equation which does not require to evaluate the high order derivatives. Those discrete version of equation 13 are known as Gaver functionals and can be written as (Gaver Jr, 1966),

$$f_k(t) = (-1)^k \left(\frac{2k}{k}\right) \Delta^k f(k\tau) = k\tau \left(\frac{2k}{k}\right) \sum_{j=0}^{k} (-1)^j \left(\frac{k}{j}\right) f((k+j)\tau) \tag{3.12}$$

Where $\tau = \frac{ln2}{t}$ and Δ denotes the forward difference operator,

$$\Delta f(n\tau) = f((n+1)\tau) - f(n\tau) \tag{3.13}$$

Gaver Jr (1966) also showed that $f_k(t)$ can be represented by an asymptotic expansion which leads to $f(t)$ as k approaches to ∞.

$$f_k(t) \sim (t) + \frac{\alpha_1}{k} + \frac{\alpha_2}{k^2} + \dots \tag{3.14}$$

Where $\alpha_1, \alpha_2....$ are the functions of t. This asymptotic expansion suggests that the value of k should be chosen as a very large number to obtain (t) with desirable accuracy. However, this expansion provides an insight to apply different sequence acceleration methods to obtain the convergence of the sequence faster than the usual. The Gaver functionals can also be computed by the following recursive relations.

$$G_0^n = n\tau \hat{f}(n\tau), \ n \geq 1 \tag{3.15}$$

$$G_k^{(n)} = \left(1 + \frac{n}{k}\right) G_{k-1}^{(n)} - \left(\frac{n}{k}\right) G_{k-1}^{(n+1)}, \ k \geq 1, n \geq k \tag{3.16}$$

$$f_k(t) = G_k^{(k)} \tag{3.17}$$

Stehfest (1970) exploited the useful features of Salzer sequence acceleration scheme and applied it on the Gaver functionals to find the inversion of Laplace transform (Salzer, 1954). The approximation of (t) using Stehfest algorithm can be written as,

$$f(t) = \frac{ln2}{t} \sum_{j=1}^{N} A_j f\left(\frac{jln2}{t}\right) \tag{3.18}$$

$$A_j = (-1)^{\left(\frac{N}{2}+1\right)} \sum_{k=\left(\frac{j+1}{2}\right)}^{min\left(j,\frac{N}{2}\right)} \frac{k^{\left(\frac{N}{2}+1\right)}(2k)!}{\left(\frac{N}{2}-k\right)!k!(j-k)!(2k-1)!} \tag{3.19}$$

Where N, Stehfest number, should necessarily be even and it represents the number of the total coefficients. The value of the coefficients does not depend on the elements of the time domain. In a fixed machine precision, as the value of M increases, the accuracy of the approximant $f(t, M)$ also increases to a certain limit, thereafter the instability and the error of the approximation become pronounced.

3.2.4 Gaver-Wynn-Rho Method

Abate and Valkó (2004) exploited the ability of nonlinear sequence acceleration methods and presented an effective Laplace inversion method which produces accurate results in a multiprecision computing environment. The sequence of Gaver functionals shows a logarithmic convergence behaviour, which can be mathematically written by the following equation,

$$\lim_{k\to\infty} \frac{f(t) - f_{k+1}(t)}{f(t) - f_k(t)} = 1 \tag{3.20}$$

The authors assessed the acceleration of convergence for the sequence of Gaver functionals by applying five sequence acceleration methods and conclusively showed that Wynn's Rho algorithm is the most effective acceleration scheme and it provides reliable performance on a wide variety of time functions. Other sequence transformations used in that study were Levin's u-transformation, Lubkin's iterated w-transformation and Brzezinski's theta algorithm. The recursive Wynn rho algorithm is given by (Wimp, 1981),

$$\rho_{-1}^{(n)} = 0,\ \rho_0^{(n)} = f_n(t),\ n \geq 0 \tag{3.21}$$

$$\rho_k^{(n)} = \rho_{k-2}^{(n+1)} + \frac{k}{\rho_{k-1}^{(n+1)} - \rho_{k-1}^{(n)}},\ k \geq 1 \tag{3.22}$$

Here $f_n(t)$ are the Gaver Functionals with n representing the number of elements of Gaver sequence that have been used in the corresponding transformation. The value of the approximant to $f(t)$ is evaluated from the following term of the algorithm,

$$f(t, M) = \rho_M^{(0)} \tag{3.23}$$

Where M must be an even integer. The recursive algorithms produce a matrix which takes the form of the following:,

$$\begin{array}{cccccccc}
\rho_{-1}^{(0)} & f_0(t) & \rho_1^{(0)} & \rho_2^{(0)} & \rho_3^{(0)} & \cdots & \cdots & \rho_{n-2}^{(0)} \\
\rho_{-1}^{(1)} & f_1(t) & \rho_1^{(1)} & \rho_2^{(1)} & \rho_3^{(1)} & \cdots & \cdots & \rho_{n-2}^{(1)} \\
\rho_{-1}^{(2)} & f_2(t) & \rho_1^{(2)} & \rho_2^{(2)} & \vdots & \cdots & & \\
\rho_{-1}^{(3)} & f_3(t) & \vdots & \vdots & \vdots & & & \\
\vdots & \vdots & \vdots & \vdots & \rho_3^{(n-4)} & & & \\
\vdots & \vdots & \vdots & \rho_2^{(n-3)} & & & & \\
\vdots & \vdots & \rho_1^{(n-2)} & & & & & \\
\rho_{-1}^{(n)} & f_{n-1}(t) & & & & & &
\end{array} \tag{3.24}$$

From the above matrix, the value of $f(t)$ is approximated from the last element of the first row which is $\rho_{n-2}^{(0)}$. It should be noted that the alternating signs and the binomial coefficients are the good source of round-off errors in the computation of Gaver functionals in a fixed precision environment. As the value of M increases the accuracy of the approximant is supposed to increase too, but the round off errors eclipses the effect of choosing large M. Hence, Abate and Valkó (2004) suggested that the computation should be performed in a multiprecision computational environment which allows for the following requirement,

$$Number\ of\ precision\ decimal\ digits = (2.1)\, M$$

The relative error estimate for the Gaver Wynn Rho algorithm was found to be the following,

$$\left| \frac{f(t) - f(t, M)}{f(t)} \right| \sim 10^{-0.8M} \tag{3.25}$$

That is the obtained accuracy in the evaluation of $f(t)$ is about $0.8M$ significant digits.

3.3 Comparative Analysis with Analytical and Numerical Results

A significant number of inversion methods are available in the literature. As we are focusing on the capability of inverting a fracture flow solution, two general test functions and one fracture flow solution will be tested here.

3.3.1 Comparison with Example Functions

Two test functions were selected to analyze the applicability of the discussed four methods. The tested functions were carefully chosen where the first one represents an oscillating function and the other one shows an exponential decline. From the discussion of the four methods, it is evident that all of these methods are subjected to the round off and truncation errors. The elimination of truncation errors could be minimized by considering a large number as the algorithm's characteristic number. However, the effect of round off errors is tested using computing environments with different precisions.

- ☐ Test function 1

$$f(s) = \frac{1}{(1+s^2)^{0.6}} \tag{3.26}$$

- ☐ Test function 2

$$f(s) = \frac{1}{(1+s)^2} \tag{3.27}$$

Figure 3.1 shows the performance of the inversion methods applied to the test functions. In this figure, it can be seen that GWR, Fixed Talbot and Fourier methods are in good agreement with the analytical solution. The computation was done in MATLAB where the default precision is Double (to the 16 significant digits). However, the Stehfest method show a diversion from the analytical solution. The Stehfest number, N, was chosen 14 to invert the test function 1. The Stehfest number is important in achieving precision in the inversion. The inversion of second test function provides excellent match with the analytical result. Only the Fourier method diverges in the late time periods in a small extant.

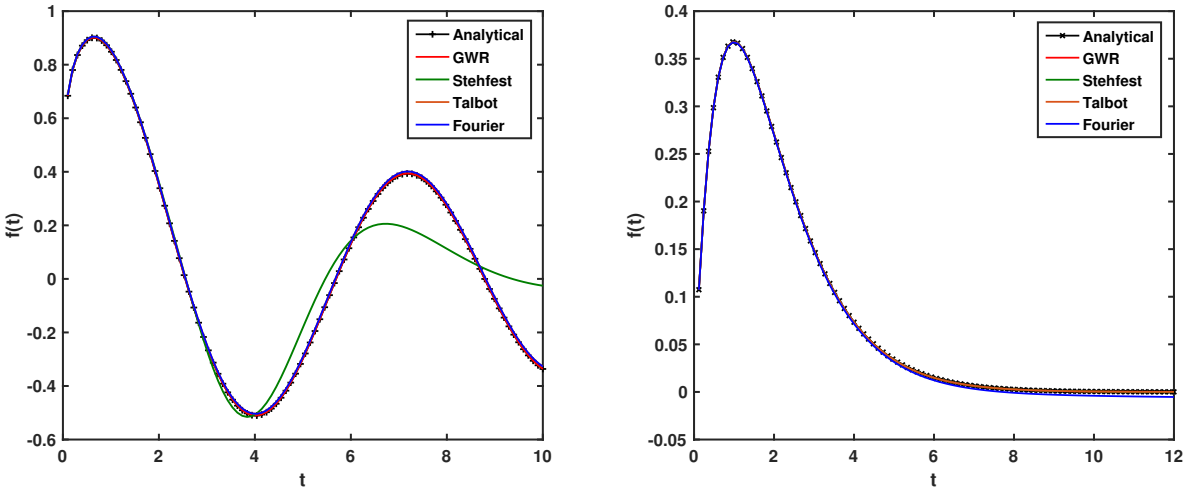

Figure 3.1: Inversion of test function 1 and 2 compared against the analytical solution

As the accuracy of the Gaver-stehfest method, at 32 significant digits, is poor in comparison with the exact analytical solution, the inversion of function 1 with big Stehfest number ($N = 26$) is computed and shown graphically in Figure 3.2. In this case, the default precision was changed and set to the 100 significant digits. The plot shows a comparison that how a computing environment can affect the inversion results. The left plot was computed in double precision with $N = 26$ and the right plot was computed in symbolic environment of MATAB with precision level 100. As can be seen from the plot, the inversion overlapped with the exact solution perfectly ultimately improving the accuracy. Therefore, the accuracy of finding an accurate inversion result from Gaver-stehfest depends on both computing environment and the number of Sthefest coefficient to be considered. From the analysis it can be summarized that GWR, Talbot and Fourier methods perform well in a double precision environment. The Stehfest algorithm should be used in a symbolic environment to achieve high accuracy.

3.3.2 Comparison with Single Compartment Fracture Solution

In order to analyze the applicability and accuracy of the presented four methods to the solution of fracture flow, a simplistic yet standard model is chosen. The solutions derived in a multi-fractured horizontal reservoir requires the Laplace variable to be

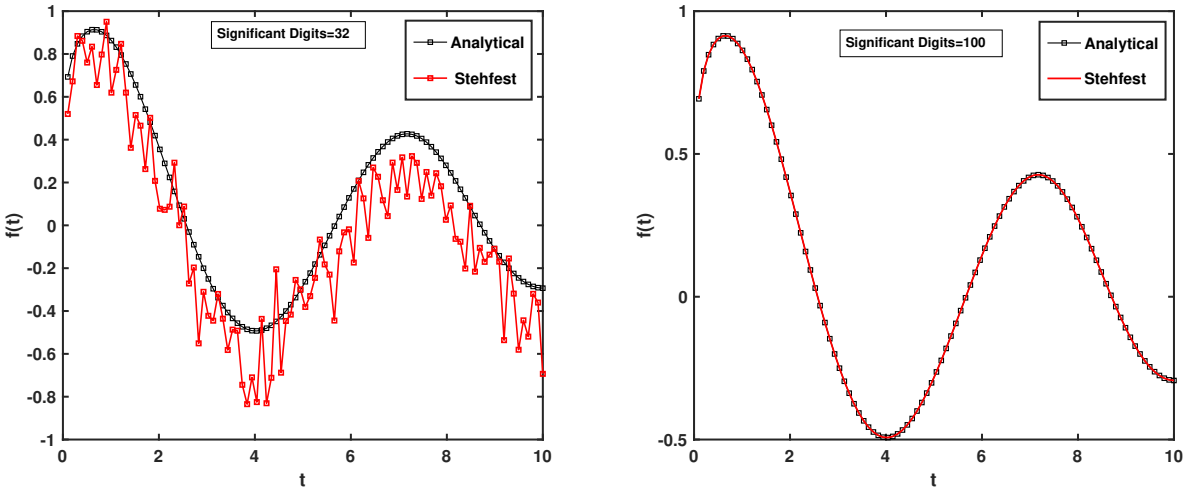

Figure 3.2: Inversion of Test function by Gaver-stehfest method; Left: when computed with the default precision level (to the 32 significant digits); Right: when computed in higher precision level (to the 100 significant digits)

nested a number of lumped parameters. The nesting of the Laplace variable makes it difficult to arrive at an analytically inverted result. The numerical inversion of those problems become the last resort to achieve the result and interpret well data. The model simulates single phase oil flow from a multi-fractured reservoir into an infinitely conductive fracture. The single compartment system consists of evenly-spaced, transverse hydro-fractures in a rock matrix. The geometry of the problem is shown in Figure 3.3.

The diffusivity equations that governs fluid flow in matrix are,

$$\begin{aligned} \frac{\partial^2 p_{Dm}}{\partial y_D^2} &= \frac{\partial p_{Dm}}{\partial t_D} \\ p_{Dm}\left(y_D, 0\right) &= 0 \\ p_{Dm}\left(-1, t_D\right) &= 0 \\ p_{Dm}\left(=1, t_D\right) &= 0 \end{aligned} \tag{3.28}$$

We can solve the equation (3.28) at least three ways: fully analytically , semi-analytically and numerically. The results from the semi-analytical solution using the four inversion methods are compared against the results from analytical solution and

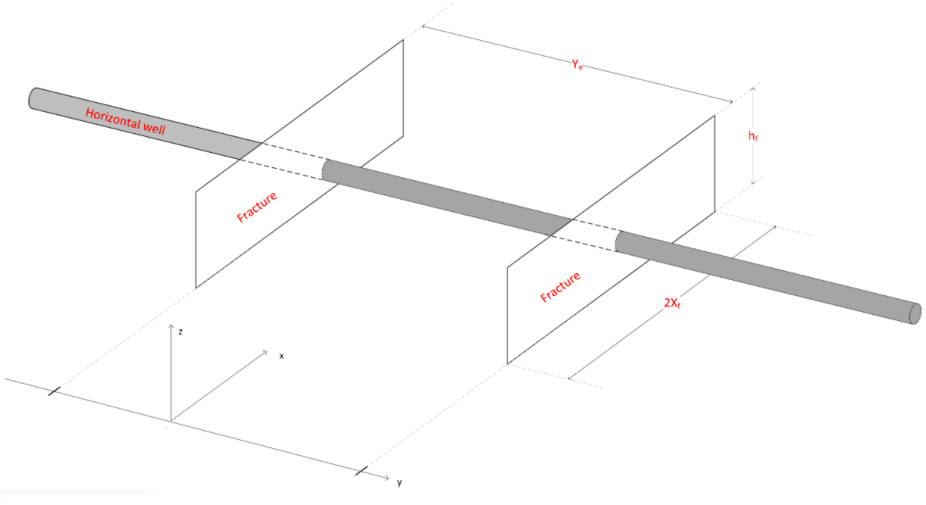

Figure 3.3: Flow geometry of single compartment multi-fractured horizontal reservoir (adapted from La, 2015)

a numerical simulator. The results of numerical solution was adopted from La (2015). The problem was simulated in CMG simulator. Reservoir specification used in the simulation and the analytical solution process are listed in Table 3.1.

- The analytical solution

$$q_t(t) = \frac{2E}{F} \sum_{n=1}^{\infty} e^{\frac{-\phi^2(2n-1)^2 t}{4F^2}} \tag{3.29}$$

- The semi-analytical solution using Laplace Transform

$$\begin{aligned} \overline{q}(s) &= \frac{E}{\sqrt{s}} \tanh\left(F\sqrt{s}\right) \\ E &= \frac{4(N-1)A_f k_m (p_i - p_{wf})}{\mu\sqrt{\alpha_m}} \\ F &= \frac{y_e}{2\sqrt{\alpha_m}} \end{aligned} \tag{3.30}$$

The analytical solution of the equation (3.28) involves infinite series which is incompatible and somewhat cumbersome in the history matching and well test data in-

Table 3.1: Reservoir specifications used in the reservoir simulation model by La (2015)

Parameters	Values
Reservoir grid configuration	$101 \times 1 \times 1$
Reservoir size	50.5ft $\times$ 1000ft $\times$ 10ft
Initial reservoir pressure, p_i, psia	5000
Bottom hole flowing pressure, p_{wf}, psia	2000
Matrix permeability, k_m, md	0.01
Matrix porosity, ϕ_m	6.5×10^{-2}
Fracture width, w_F, ft	0.5
Oil viscosity, μ, cp	2.0
Oil saturation, S_w	1.0
Total compressibility, c_t, psi^{-1}	3.7×10^{-5}

terpretation. On the other hand, the Laplace solution provides advantages in history matching as reported by (La, 2015). The figure 3.4 presents analytical and numerical solution of the problem and comparison of the four methods. Because the analytical solution itself is an infinite series approximation, the coherence of the results from numerical simulator and analytical approximate solution was checked and found in good agreement. The comparison with the inversion methods shows that GWR and Talbot method performs excellent in achieving accuracy. In order to quantitatively evaluate the performance of these methods, we calculate four error measures of these algorithms. The error measures are defined below,

☐ Root Mean Squared Error (RMSE)

$$\text{RMSE} = \sqrt{\frac{\sum_{i=1}^{n} (X_{act} - X_{semi})}{n}}$$

☐ Mean Absolute Percentage Error (MAPE)

$$\text{MAPE} = \frac{1}{n} \sum_{i=1}^{n} \left| \frac{X_{act} - X_{semi}}{X_{act}} \right| \times 100\%$$

☐ Normalized Root Mean Squared Error (NRMSE)

$$\text{NRMSE} = \frac{\text{RMSE}}{X_{max} - X_{min}}$$

☐ L_e (Davies & Martin, 1979)

$$\text{L}_e = \frac{\sum_{i=1}^{n} \left(X_{act} - X_{semi}\right)^2 e^{-i}}{\sqrt{\sum_{i=1}^{n} e^{-i}}}$$

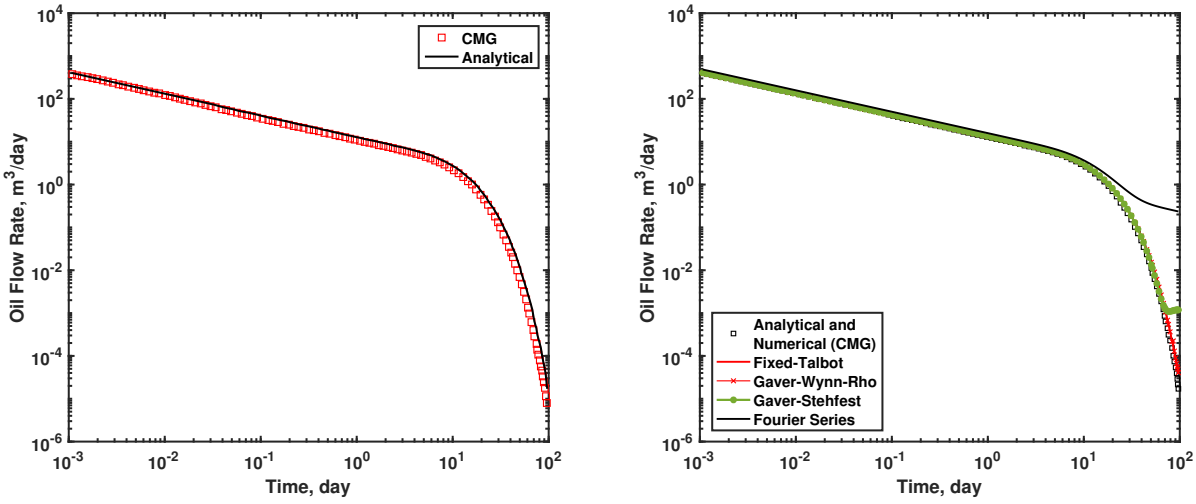

Figure 3.4: Results from analytical and numerical simulator (Left) and; Comparison of four methods against analytical and numerical results (Right);

Table 3.2 lists the error measures of the four algorithms for the initial values and Table 3.3 lists the errors when the entire data set is taken into account. From a close inspection of the errors, it can be seen that Fourier method completely fails to converge with the analytical result at the late time periods as the MAPE error measures are increasing in a significant way. The Stehfest show a little diversion in the late time periods and the MAPE measure is also greatly increased when full dataset was accounted for. The accuracy from Stehfest could be increased if it is applied in a symbolic environment (sym and vpa function in MATLAB, MAPLE, Mathematica) with high number of Stehfest coefficients. However, the Gaver-Wynn-Rho and Fixed Talbot algorithms performs well in accurately inverting the fracture

flow solution.

Table 3.2: Error measures for the initial time values (first 50 points) of the fracture flow problem

Inversion Methods	RMSE	NRMSE	MAPE	L_e
Fourier Series Method	34.7749	0.0911	20.8873	35.6501
Fixed Talbot Method	0.5195	0.0014	0.7878	0.4928
Gaver-stehfest Method	0.5195	0.0014	0.7878	0.4928
Gaver-Wynn-Rho Method	0.5195	0.0014	0.7879	0.4928

Table 3.3: Error measure for the full data set values (118 points) of the fracture flow problem

Inversion Methods	RMSE	NRMSE	MAPE	L_e
Fourier Series Method	22.6830	0.0561	4.6853×10^4	33.2056
Fixed Talbot Method	0.4012	9.914×10^{-4}	0.7879	0.5018
Gaver-stehfest Method	0.4012	9.914×10^{-4}	219.9678	0.5017
Gaver-Wynn-Rho Method	0.4012	9.914×10^{-4}	0.7879	0.5018

From the above analysis, it can be concluded that the possible truncation errors and round off errors could be minimized if a perfect combination of precise computing environment and large number of inversion coefficient is considered. The analysis is important because it establishes confidence in employing a particular inversion method to a obtain a solution in time domain. GWR methods performs very well irrespective of the function types and show excellent agreement with the compartmentalized solution of multi-fractured well. It should be noted that Fixed Talbot is also a good candidate for choosing as a tool for inversion, however special attention should be taken as it involves imaginary values in the computations. The most popular Gaver-stehfest algorithms shows poor convergence when applied in double precision computing environment with big/small number of Stehfest coefficient. Also,

It is recommended that the large Stehfest number should be considered and the computation should be employed in symbolic environment to obtain high accuracy at late time periods of fracture flow solution.

3.4 Conclusion

The following conclusions can be drawn from the assessment of four widely used Laplace inversion methods:

- ☐ Gaver-Wynn-Rho algorithm and Fixed Talbot performs well in the inversion of a variety of functions. The algorithms also produce accurate result in the inversion of nested fracture flow solution.
- ☐ Stehfest algorithm accumulates round off errors when it is used in the inversion of oscillating function. In order to obtain good result with Stehfest algorithm, big Stehfest number should be chosen for the inversion and the computation should be done in symbolic environment.
- ☐ If MATLAB is used as a computational tool for the inversion, the Sym and VPA function should be used for better result.

Chapter 4

Induced Branch-fracture Subdiffusive Flow Model

4.1 Introduction

The Induced Branch-fracture Subdiffusive Flow (SIBFF) [1] model couples hydraulically induced fracture network and subdiffusive flow in tight or shale matrix into a new semi-analytical flow model. Most of the analytical flow models including the proposed SIBFF model are the upgrades of the classical trilinear flow model developed by Ozkan et al. (2009). In most cases, earlier models have based their idealization on the assumption of constant, isotropic and homogeneous reservoir properties. Although, few models have incorporated spatial variation of the reservoir properties in their formulation, they carry with them a number of limitations. Table 4.1 presents a comprehensive comparison of the features of the proposed model with the other standard analytical models. The newly developed model connects a realistic physical model with the subdiffusive flow in unconventional reservoir. In order to capture the field scale heterogeneity after stimulation, this study incorporates the spatial variation of branch-fracture permeability in the stimulated reservoir volume (SRV). The flow domain, derivation steps and pseudo-function assumptions are analogous to those of Five Region model by Stalgorova and Mattar (2013). However, the proposed model brings unique complexity due to the incorporation of exponential branch-fracture per-

[1] For the ease of pronounciation, we rearranged the exact acronym "IBFSF" to "SIBFF". The word "SIBFF" can easily be pronounced as "siff"

meability field into the diffusion equation and it was taken care of by applying Bessel functions and an integral transform.

The major features of the SIBFF model can be summarized as:

- Multi-Region flow with sub or normal diffusion: Two regions in the outer reservoir, Induced fracture and spherical matrix idealization in SRV, inner unfractured region and hydraulic fracture.
- Anisotropic stimulated reservoir volume
- Subdiffusive flow in the spherical matrix blocks of SRV matrix
- Subdiffusion in the two regions of the outer reservoir
- Normal diffusion in induced fracture network due to the well connectivity of induced branch fractures and reopened natural fractures
- Transient fluid transfer from sub diffusive spherical matrix to the induced fracture with classical diffusion
- Application of innovative analytical methods to ease the complexities of the SIBFF model, such as Laplace Transform, Bessel Transform and asymptotic expansion; use of multiprecision Laplace inversion method (Gaver-Wynn-Rho Method).

4.2 Physical Model Description

The skeleton of the proposed model is analogous to that of the Five-Region model which was developed by Stalgorova and Mattar (2013). However, the SRV segment of the new model assumes dual porosity idealization, whereas Five-Region model assumed a homogeneous SRV with higher permeability. Figure 4.1 depicts a top view of a multiple fractured horizontal well (MFHW) in an unconventional reservoir. The reservoir segment in each symmetry element (red dotted in Figure 4.1) is divided into five flow regions: hydraulic fracture, SRV and region 2 in inner reservoir and region 3 and 4 in the outer reservoir. This model assumes that the hydraulic fracture in each stage is of a biwing transverse shape and maintains an equal distance

Table 4.1: Model features comparison of the proposed model with standard analytical models

Model Features	Models					
	Ozkan et al. (2009)	Stalgorova and Mattar (2013)	Ozcan (2014b)	Fuentes-Cruz, Gildin, Valkó, et al. (2014)	Albinali et al. (2016)	The proposed Model
1. Transport Medium in SRV	Isotropic	Isotropic	Isotropic	Isotropic	Isotropic	*Anisotropic*
2. Scale Variability of Permeability	Uniform	Uniform	Uniform	Exponential	Uniform	*Exponential*
3. Regions in Outer Reservoir	One region	Two regions	One region	None	One region	*Two regions*
4. USRV in inner reservoir	Not Considered	Considered	Not considered	Not considered	Not considered	*Considered*
5. Matrix blocks in SRV	Horizontal slab	N/A	N/A	Vertical slab	Spherical	*Spherical*
6. Diffusion in SRV Matrix	Classical	Classical	Subdiffusion	Classical	Subdiffusion	*Subdiffusion*
7. Diffusion in SRV Fracture	Classical	N/A	N/A	Classical	Subdiffusion	*Classical*
8. Diffusion in Outer Region	Classical	Classical	Classical	Classical	Subdiffusion	*Subdiffusion*

from the nearby hydraulic fracture stages. The uniform spacing assumption between hydraulic fractures is realistic because it is a completion norm for MFHW to design equally spaced hydraulic fractures with similar properties. Necessarily, a complex branch fracture network composed of induced fractures and reopened natural fracture is created around each of the hydraulic fractures during the stimulation operation. Since, the complexity and orientation of the induced fracture network is so convoluted, the exact idealization of the induced network is difficult to simulate in a realistic way. Hence for simplicity, the SRV segment is considered as an alternating stack of spherical matrix and induced fracture continuum. The half-length of the hydraulic fractures indicates the spread of the inner reservoir and the range of the stimulation job. Region 2 indicates that there lies an unfractured region between two consecutive hydraulic fractures.

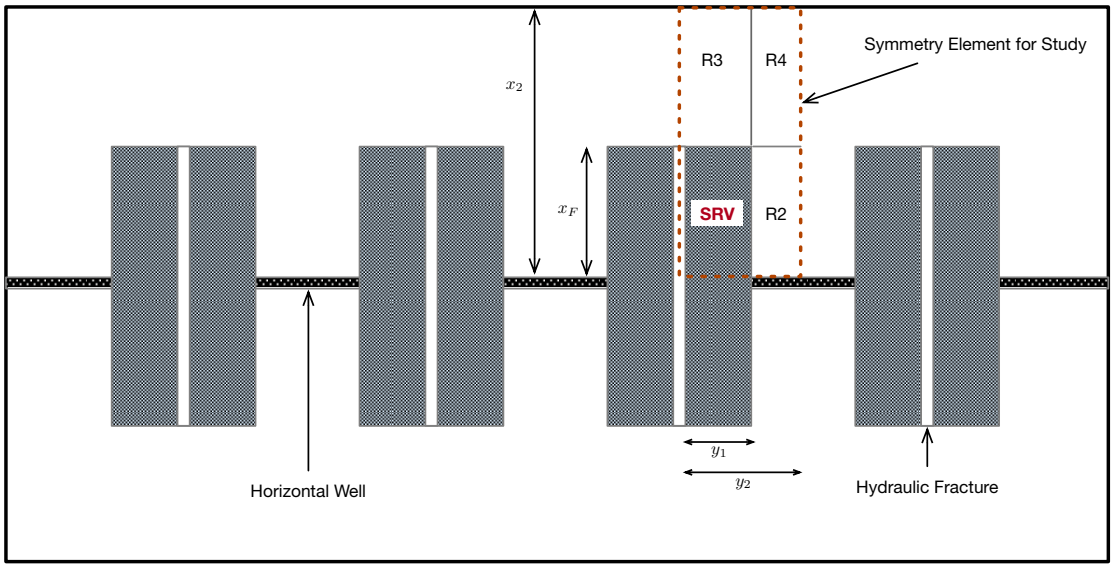

Figure 4.1: Top view of a horizontal well and symmetry element (red dotted) of the proposed model; R2= region 2, R3= region 3, R4=region 4, SRV= Stimulated Reservoir Volume

4.3 Development of the Semi-analytical Solution

This section presents a description of the governing flow equations with necessary boundary conditions for five different regions of multi-fractured reservoirs and derivation to find the bottomhole pressure solution. The formulation of analytical solution for fluid flow in fractured reservoir always poses a difficulty to couple different regions. In this study, the pressure continuity and flux continuity at the interface of every two regions has been considered to couple the pressure diffusion. In the proposed model, fluid flows from the outer reservoir (Region 3 and Region 4) to the inner reservoir following subdiffusion phenomenon, then to the induced branch-fractures to the SRV, then to the primary hydraulic fracture plane and ultimately to the wellbore. For each segment of the reservoir, there exist a different governing diffusivity equation with different boundary conditions. With the help of Laplace transform, the pressure solution for each segment of figure 4.1 is achieved. The pressure solution is then coupled through flux continuity and pressure continuity. A representative term from each segment carries diffusion information to the other segment and finally yields a pressure solution for the bottomhole of the horizontal well. The obtained bottomhole pressure

in Laplace domain is then inverted back to real time domain using Gaver-Wynn-Rho algorithm.

The mathematical derivation of the proposed model starts with honouring the laws of physics. The mass balance or continuity equation with a source from the neighbouring matrix stack or fracture stack could be written as,

$$\nabla \cdot (\rho \vec{v}) + \dot{Q_m} = -\frac{\partial (\phi \rho)}{\partial t} \tag{4.1}$$

where ρ = fluid density, $\vec{v}$ = fluid velocity, ϕ = porosity of the medium and $\dot{Q_m}$ denotes the source term from the neighbouring matrix/fracture stack representing the influx of mass into the control volume for a time interval of dt. Equation (4.1) is the most fundamental diffusivity equation for fluid flow in a media with a source and it is a starting point for the models to derived and analyzed here. The ∇ notation is used here for the compatibility of Equation to the various flow geometry, appropriate operators will be used in the later developments of the derivation corresponding to rectangular flow geometry. To incorporate pressure in the derivation we need a description of the velocity term in terms of pressure. During the classical diffusion in the porous media, the Darcy's law predict the velocity of the fluid. Darcy's law,

$$\vec{v} = -\frac{k}{\mu} (\nabla p + \rho \vec{g}) \tag{4.2}$$

where $\rho \vec{g}$ denotes the gravitational effect. However, since we are assuming horizontal linear flow in each of the flow medium, this term can be neglected. Then using the definition of the fluid compressibility, Equation (4.2) reduces to,

$$c(\nabla p)^2 + \nabla \cdot \left(\frac{k}{\mu} \nabla p \right) + \dot{Q} = \phi c \frac{\partial p}{\partial t} \tag{4.3}$$

The $c\,(\nabla p)^2$ in Equation (4.3) is nonlinear, as this term squares the gradient of pressure and multiplies this group by another weak function of pressure, fluid compressibility. Solution of nonlinear equation with a source term poses multiple difficulty to achieve an analytical pressure equation. An analytical solution developed by Finjord, Aadnoy, et al. (1989) using perturbation method is not well suited for the interpretation of well test data. However, $c\,(\nabla p)^2$ term approaches to zero for the assumption of small and constant fluid compressibility value. Therefore, for a slightly compressible fluid ,

the governing diffusivity equation reduces to,

$$\nabla \cdot \left(\frac{k}{\mu} \nabla p \right) + \dot{Q} = \phi c_t \frac{\partial p}{\partial t} \tag{4.4}$$

Before moving on to the core derivation segment, the pressure variable is changed to the pressure difference $\Delta p = p_i - p$, where p_i is the initial reservoir pressure. This transformation facilitates the derivation in making initial condition zero and boundary conditions favourable. In terms of pressure difference Δp while velocity is positive in the opposite direction of positive gradient, we write,

$$\vec{v} = -\frac{k}{\mu} \nabla (\Delta p) \tag{4.5}$$

As the dominant fluid flow in unconventional matrix conituum is sub-diffusion, a fractional velocity term should be used in the 4.1. Assuming a Continuous-Tine-Random-Walk process in the particle displacement of the diffusion in porous media, a fractional velocity equation incorporating subdiffusion is given by (Fomin et al., 2011; C. Chen & Raghavan, 2015; Raghavan, 2011),

$$\vec{v_x} = -\frac{k_\beta}{\mu} \frac{\partial^{1-\beta}}{\partial t^{1-\beta}} \frac{\partial \Delta p}{\partial x} \tag{4.6}$$

In this study, we only focus on the subiffusive behaviour of unconventional matrices, the anomalous diffusion term, β, is therefore referred to subdiffusion exponent in the rest of the thesis. The fractional derivative term in (4.6) is defined using Caputo's definition,

$$\frac{\partial^{1-\beta}}{\partial t^{1-\beta}} \left\{ p\left(x,t\right) \right\} = \frac{1}{\Gamma\left(\beta\right)} \int_0^t \frac{\partial p\left(x,t\right)}{\partial t} \left(t-\tau\right)^{-(1-\beta)} d\tau \tag{4.7}$$

4.3.1 Subdiffusive Fluid Transport in Region 4

Governing diffusivity equation to be applied in the region 4 of the figure 4.1 can be derived from Equation (4.1) and (4.6). That is:

$$\frac{\partial}{\partial x} \left(\frac{k_\beta}{\mu} \frac{\partial^{1-\beta}}{\partial t^{1-\beta}} \frac{\partial \Delta p_4}{\partial x} \right) = \left(\phi c_t\right) \frac{\partial \Delta p_4}{\partial t} \tag{4.8}$$

Equation (4.8) is subjected to the following initial and boundary conditions which

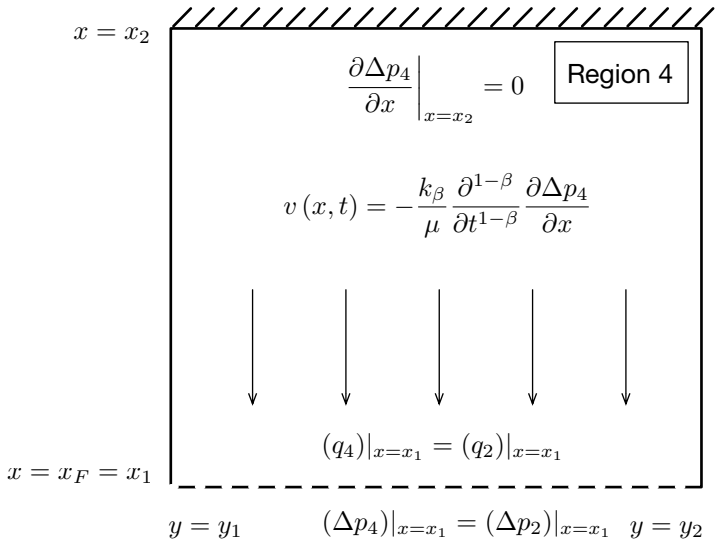

Figure 4.2: Schematic of region 4 of the outer reservoir and its governing equations

facilitate to find the pressure solution for Region 4. Figure 4.2 depicts the boundary of the region 4 and also presents the governing diffusivity equation and boundary conditions.

- ☐ Initial condition (Initial reservoir pressure prevails everywhere at $t = 0$):

$$\Delta p|_{t=0} = 0 \tag{4.9}$$

- ☐ Boundary condition 1 (No flow boundary at $x = x_2$):

$$\left.\frac{\partial \Delta p_4}{\partial x}\right|_{x=x_2} = 0 \tag{4.10}$$

- ☐ Boundary condition 2 (Pressure continuity at the interface of Region 4 and Region 2):

$$(\Delta p_4)\,|_{x=x_1} = (\Delta p_2)\,|_{x=x_1} \tag{4.11}$$

By exploiting the features of Laplace transform and the dimensionless variables defined in Table 4.2, the pressure solution is derived in Appendix A.1. Therefore, the derived pressure solution for the domain of region 4 is,

$$\overline{p}_{4D} = (\overline{p}_{2D})\,\frac{\cosh\left[\sqrt{\epsilon_4}\,(\,x_{2D} - \,x_D)\right]}{\cosh\left[\sqrt{\epsilon_4}\,(\,x_{2D} - \,x_{1D})\right]} \tag{4.12}$$

It should be stated that the bar over the function represents the Laplace transform of that function. In Equation (4.12), ϵ_4 carries all the necessary subdiffusion information to the neighbouring reservoir segment while coupling is performed.

$$\epsilon_4 = \left(\frac{x_F^2}{\eta_\beta}\right)\left(\frac{\eta_i}{x_F^2}\right)^{\beta} s^{\beta} \tag{4.13}$$

Table 4.2: Dimensionless and scaled variables used in the formulation of the proposed SIBFF model

Dimensionless and scaled variables	
Pressure differential, Δp	$(p_i - p)$
Dimensionless length in the x-direction	$x_D = \frac{x}{x_F}$
Dimensionless length in the y-direction	$y_D = \frac{y}{x_F}$
Dimensionless radius	$r_D = \frac{r}{x_F}$
Dimensionless pressure	$p_D = \frac{2\pi k_i h_{ft}(p-p_i)}{qB\mu} = \frac{2\pi k_i h_{ft}}{qB\mu}(\Delta p)$
Dimensionless time	$t_D = \frac{k_i t}{(\phi\mu c_t)_i} x_F^2 = \left(\frac{\eta_i}{x_F^2}\right) t$
Dimensionless flowrate	$q_D = \frac{qB\mu}{2\pi k_i h_{ft}(p-p_i)} = \frac{qB\mu}{2\pi k_i h_{ft}(\Delta p)}$
Dimensionless diffusivity	$\eta_D = \frac{\eta}{\eta_i}$
Hydraulic fracture conductivity	$C_{FD} = \frac{k_F w_F h}{k_i x_F h_{ft}}$
Average intrinsic branch-fracture permeability in x-direction	$k_x = k_i \left(\frac{k_{\beta D}-1}{\beta D}\right)$
Bulk permeability in x-direction	$\tilde{k}_x = \frac{\overline{k_x} h_{ft}}{h}$
Bulk permeability in y-direction	$\tilde{k}_y = \frac{k_{\beta i} h_{ft}}{h}$

Also, derivative of Equation (4.12) at $x_D = x_{1D}$ is calculated for flux from the region 4 to the region 2:

$$\left.\frac{\partial \Delta \overline{p}_{4D}}{\partial x_D}\right|_{x_D=x_{iD}} = -\left(\overline{p}_{2D}\right)|_{x_D=x_{iD}} \sqrt{\epsilon_4} \tanh\left[\sqrt{\epsilon_4}\left(x_{2D}-x_{1D}\right)\right] \tag{4.14}$$

4.3.2 Subdiffusive Fluid Transport in Region 3

Region 3 and Region 4 are two part of the outer reservoir. In most cases the characteristic parameters in both regions are same. The governing diffusivity equation is same as region 3. However, the boundary conditions differs from one another as this region is contiguous with the SRV. The governing diffusivity equation can be written as,

$$\frac{\partial}{\partial x}\left(\frac{k_\beta}{\mu}\frac{\partial^{1-\beta}}{\partial t^{1-\beta}}\frac{\partial \Delta p_3}{\partial x}\right) = \left(\phi c_t\right)_3 \frac{\partial \Delta p_3}{\partial t} \tag{4.15}$$

Equation (4.15) is subjected to the following initial and boundary conditions which facilitate with finding an exact solution for the Region 3. Figure 4.3 depicts the boundary of the region 3 and also presents the governing diffusivity equation and boundary conditions.

☐ Boundary Condition 1 (No flow boundary at $x = x_2$):

$$\left.\frac{\partial \Delta p_3}{\partial x}\right|_{x=x_2} = 0 \tag{4.16}$$

☐ Boundary condition 2 (Pressure continuity at the interface of region 3 and SRV branch-fractures):

$$\left(\Delta p_3\right)|_{x=x_1} = \left(\Delta p_i\right)|_{x=x_1} \tag{4.17}$$

By applying Laplace transform and the dimensionless variables defined in Table 4.2, the pressure solution is derived in Appendix A.2. Therefore, the derived pressure solution for the domain of region 3 is,

$$\overline{p}_{3D} = \left(\overline{p}_{iD}\right)|_{x_D=x_{1D}} \frac{\cosh\left[\sqrt{\epsilon_3}\left(x_{2D}-x_D\right)\right]}{\cosh\left[\sqrt{\epsilon_3}\left(x_{2D}-x_{1D}\right)\right]} \tag{4.18}$$

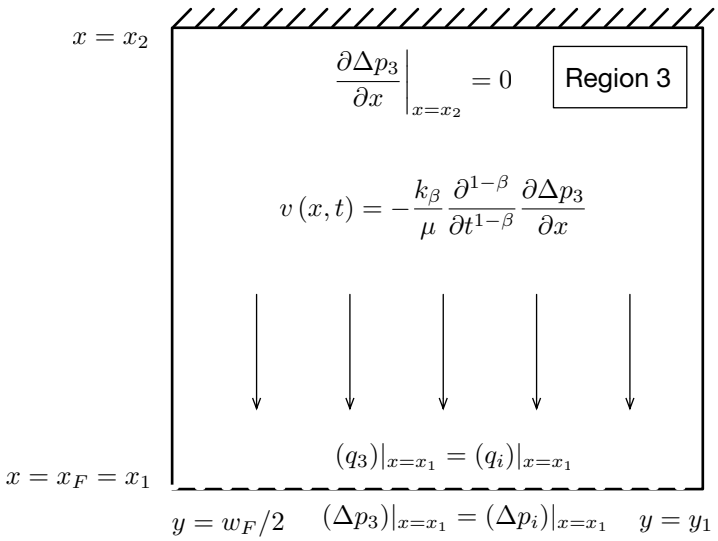

Figure 4.3: Schematic of region 3 of the outer reservoir and its governing equations

Like ϵ_4 of the region 4, ϵ_3 carries all the necessary subdiffusive information to the neighbouring SRV segment while coupling is performed by transfer functions.

$$\epsilon_3 = \left(\frac{x_F^2}{\eta_\beta}\right)\left(\frac{\eta_i}{x_F^2}\right)^\beta s^\beta \tag{4.19}$$

The derivative of Equation (4.18) at $x_D = x_{1D}$ is evaluated as this function will be used in SRV branch-fracture solution.

$$\left.\frac{\partial \overline{p}_{3D}}{\partial x_D}\right|_{x_D=x_{1D}} = -\left(\overline{p}_{iD}\right)|_{x_D=x_{1D}}\sqrt{\epsilon_3}\tanh\left[\sqrt{\epsilon_3}\left(x_{2D}-x_{1D}\right)\right] \tag{4.20}$$

4.3.3 Subdiffusive Fluid Transport in Region 2

The diffusion equation in region 2 involves x and y component of the fluid flux due to the need for coupling of region 4 influx. The governing diffusivity equation can be written as,

$$\frac{\partial}{\partial x}\left(\frac{k_\beta}{\mu}\frac{\partial^{1-\beta}}{\partial t^{1-\beta}}\frac{\partial \Delta p_2}{\partial x}\right) + \frac{\partial}{\partial y}\left(\frac{k_\beta}{\mu}\frac{\partial^{1-\beta}}{\partial t^{1-\beta}}\frac{\partial \Delta p_2}{\partial y}\right) = \left(\phi c_t\right)_2\frac{\partial \Delta p_2}{\partial t} \tag{4.21}$$

The diffusivity equation (4.21) is subjected to the following initial and boundary conditions that will be used to search for a exact solution for the domain of region

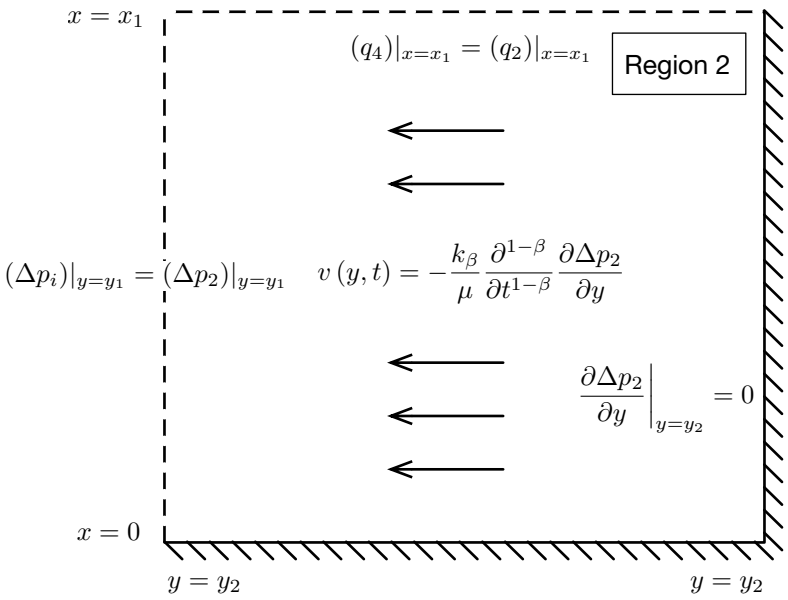

Figure 4.4: Schematic of region 2 of the outer reservoir and its governing equations

2. The necessary boundary conditions and governing equations are also depicted in figure 4.4.

- ☐ Boundary condition 1 (Flux continuity at the interface of region 4 and region 2)

$$(q_4)|_{x=x_1} = (q_2)|_{x=x_1} \tag{4.22}$$

- ☐ Boundary condition 2 (No flow boundary at $y = y_2$)

$$\left.\frac{\partial \Delta p_2}{\partial y}\right|_{y=y_2} = 0 \tag{4.23}$$

- ☐ Boundary condition 3 (Pressure continuity at the interface of SRV branch-fracture and region 2)

$$(\Delta p_2)|_{y=y_1} = (\Delta p_i)|_{y=y_1} \tag{4.24}$$

By applying Laplace transform and the dimensionless variables defined in Table 4.2, the pressure solution is derived in Appendix A.3. Therefore, the derived pressure solution for the domain of region 2 is,

$$\overline{p}_{2D} = (\overline{p}_{iD})|_{y=y_{1D}} \frac{\cosh\left[\sqrt{\epsilon_2}\,(y_{2D} - y_D)\right]}{\cosh\left[\sqrt{\epsilon_2}\,(y_{2D} - y_{1D})\right]} \tag{4.25}$$

In Equation (4.25), ϵ_2 carries all the important information about region 2 to the SRV branch-fracture. It should be noted that, the branch-fractures are the only medium for fluid transport in SRV whereas spherical matrix acts as a storage of fluid.

$$\epsilon_2 = \left[\sqrt{\epsilon_4}\tanh\left[\sqrt{\epsilon_4}\,(x_{2D} - x_{1D})\right] + \frac{x_F^2}{\eta_\beta}\left(\frac{\eta_i}{x_F^2}\right)^\beta s^\beta\right] \tag{4.26}$$

Also, derivative of (4.25) is calculated at $y_D = y_{1D}$ for flux from region 2 to the SRV branch-fractures.

$$\left.\frac{\partial \overline{p}_{2D}}{\partial y_D}\right|_{y_D = y_{1D}} = -(\overline{p}_{iD})|_{y_D = y_{1D}} \sqrt{\epsilon_2}\tanh\left[\sqrt{\epsilon_2}\,(y_{2D} - y_{1D})\right] \tag{4.27}$$

4.3.4 Exponential Branch-fracture Permeability Field in SRV

The fracturing job alters the permeability of the SRV region by generating branch-fractures. The density and the size of the aperture of those fractures decreases away from the primary fracture plane. It is assumed in this study that the generated fractures are well-connected but having varying spatial permeability. Therefore, the classic diffusion in the branch-fracture medium is a natural choice. The porosity of the fracture medium is kept constant and the aperture of the fracture is also constant along the width of the SRV. However, the assumption of constant aperture is compensated by the consideration of the variation of permeability in the fracture continuum. The fracturing treatment generates numerous branch fractures stemming from the primary fracture plane due to the shear and tensile failure of the natural fractures away from the main fracture plane (Palmer et al., 2007; Ge et al., 2011; Fuentes-Cruz, Gildin, Valkó, et al., 2014). Fuentes-Cruz, Gildin, Valkó, et al. (2014) concluded that the monotonic increase of permeability enhancement due to the induced branch-fractures follows exponential trends after a stimulation job is carried out in unconventional reservoirs. They defines the variability of permeability in single-porosity reservoir by the following equation,

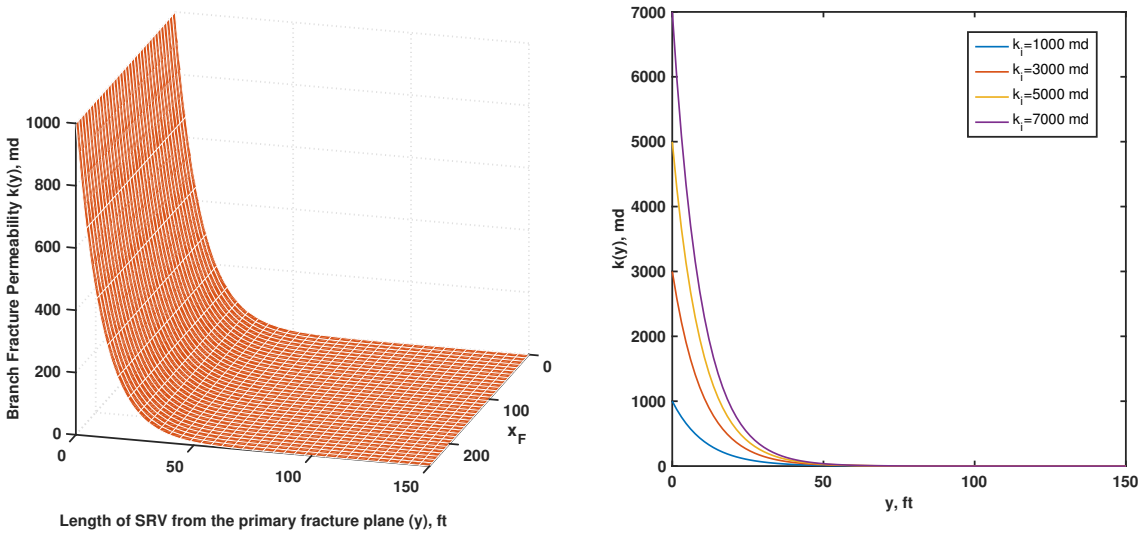

Figure 4.5: Exponential branch-fracture permeability field (left); The variation of fields in terms of different k_i (right)

$$k\left(y\right) = k^0 \left(\frac{k^*}{k^0}\right)^{\frac{y}{y_e}} \tag{4.28}$$

This exponential variation of single porosity SRV is adopted and modified to the geometry of the problem considering in this study. Therefore, the branch-fracture permeability field for the proposed model is presented as,

$$k\left(y\right) = k_i \left(\frac{k_{\beta i}}{k_i}\right)^{\frac{y-w_F/2}{y_1-w_F/2}} \tag{4.29}$$

Where, k_i is the highest permeability in the branch-fracture that happens in vicinity of the primary fracture plane; $k_{\beta i}$ is the lowest permeability in the stimulation affected space generated by hydraulic fracturing. $k_{\beta i}$ can be same as the matrix permeability k_β. However, the quantity of $k_{\beta i}$ depends on the formation characteristics and stimulation job. When $k_{\beta i}$ is same as the matrix inherent permeability, the ratio of k_i to $k_{\beta i}$ represents the stimulation ratio (SR) of SRV region. The stimulation ratio is an indicator of stimulation job efficiency that could be determined if the branch-fracture permeability is accounted for in the flow modelling multi-fractured reservoir.

In order to facilitate the incorporation of the field into the fracture diffusivity equation, we convert Equation (4.29) into dimensionless form:

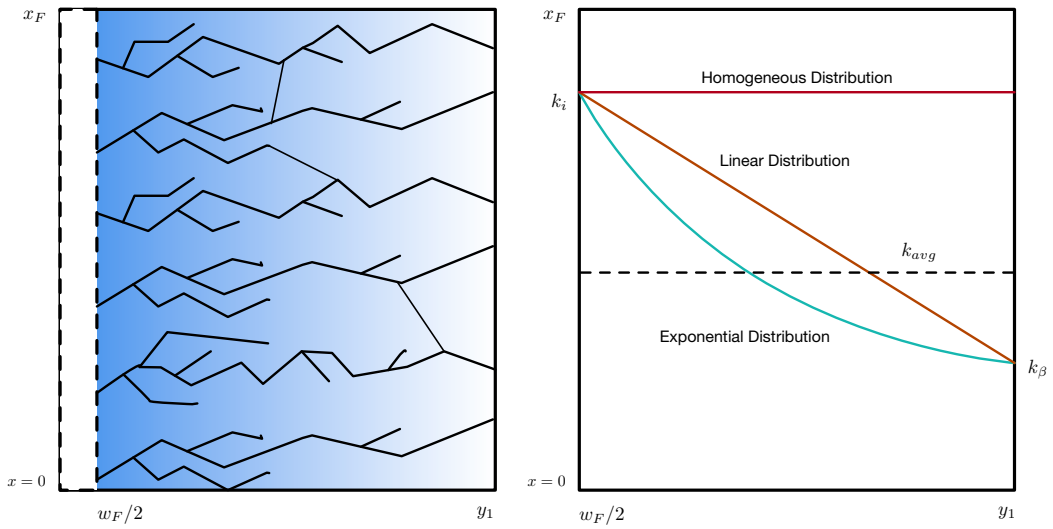

Figure 4.6: Schematic of branch fracture network; Various forms of permeability distributions

$$k_D\left(y_D\right) = \left(k_{\beta D}\right)^{\frac{y_D - w_D/2}{y_{1D} - w_D/2}} \tag{4.30}$$

Where, $k_{\beta D} = \frac{k_{\beta i}}{k_i}$ and $k_{\beta D}$ represents the reciprocal of the stimulation ratio of the stimulated reservoir volume.

$$\mathrm{SR} = \frac{k_i}{k_{\beta i}} = \frac{1}{k_{\beta D}} \tag{4.31}$$

In the SRV region, the permeability of branch fractures in y-direction is represented by Equation (4.29). However, all the previous analytical models calculate the fluid transfer at the interface of SRV and outer reservoir assuming isotropic condition in SRV. However, The SIBFF model accounts for the anisotropy in permeability of SRV. The permeability in the x-direction is assumed to be equal to the permeability averaged over the interface of SRV branch-fracture and region 3. Therefore, the permeability in the x-direction,

$$k_x = \overline{k_x} \tag{4.32}$$

4.3.5 Subdiffusive Fluid Transport in SRV Matrix

Stimulated reservoir Volume (SRV) region is assumed to be consisted of two continua: one is spherical matrix continuum which is governed by fractional diffusion equation and another is induced (exponential distribution) branch-fracture region which is governed by normal diffusion. It should be noted that, in a well-connected fractured region, the assumption of normal diffusion is a natural choice. The normal diffusion in induced fractured permeability field not only captures the heterogeneity in a realistic way, but also involves less number of unknown variables than the fractional diffusion assumption. In this section, we resent the pressure solution derived in Appendix A.4 for the SRV spherical matrix which will subsequently be incorporated into the branch-fracture diffusivity equation. The governing diffusivity equation in spherical matrix:

$$\frac{1}{r^2}\frac{\partial}{\partial r}\left(r^2\frac{k_\beta}{\mu}\frac{\partial^{1-\beta}}{\partial t^{1-\beta}}\frac{\partial \Delta p_m}{\partial r}\right) = (\phi c_t)_\beta \frac{\partial \Delta p_m}{\partial t} \tag{4.33}$$

The initial and boundary conditions that are imposed in the spherical matrix domain are:

- ☐ Boundary condition 1

$$\Delta p_m\left(r=0,t\right)=0 \tag{4.34}$$

- ☐ Boundary condition 2 (Pressure continuity at the interface of spherical matrix and branch-fracture medium)

$$\Delta p_m|_{r=r_m} = (\Delta p_i)|_{r=r_m} \tag{4.35}$$

By applying the above boundary conditions , Laplace transform and dimensionless variables (Table 4.2), the pressure solution for the spherical matrix domain is derived in Appendix A.4. Therefore, the pressure solution:

$$\overline{p}_{mD} = \frac{r_{mD}}{r_D}\frac{\sinh\left(\sqrt{\epsilon_m}\, r_D\right)}{\sinh\left(\sqrt{\epsilon_m}\, r_{mD}\right)}\ (\overline{p}_{iD})|_{r_D=r_{mD}} \tag{4.36}$$

Where,

$$\epsilon_m = \left(\frac{x_F^2}{\eta_\beta}\right)\left(\frac{\eta_i}{x_F^2}\right)^\beta s^\beta \tag{4.37}$$

Also, the derivative of Equation (4.36) is calculated at $r_D = r_{mD}$ for fluid influx from spherical matrix to the SRV branch-fractures (see Appendix A.5).

$$\left(\frac{\partial \overline{p}_{mD}}{\partial r_D}\right)\Bigg|_{r_D=r_{mD}} = \frac{(\overline{p}_{iD})|_{r_D=r_{mD}}}{r_{mD}} \left[r_{mD}\sqrt{\epsilon_{\mathrm{m}}}\coth\left(\sqrt{\epsilon_m}\ r_{mD}\right)\ -1\right] \tag{4.38}$$

4.3.6 Classic Diffusion in Branch-fracture Network

The branch fracture network is assumed well-connected and the gaussian distribution of particle displacements prevail over a given time. Therefore, Fickian or classical diffusion defines the fluid movement in branch-fracture medium. The spatial variation of permeability described in section 1.2 and 4.3.4 is incorporated in the governing diffusivity equation of branch-fractures. The governing equation can be written as,

$$\frac{\partial}{\partial x}\left(\frac{\overline{k_x}}{\mu}\frac{\partial \Delta p_i}{\partial x}\right) + \frac{\partial}{\partial y}\left(\frac{k\,(y)}{\mu}\frac{\partial \Delta p_i}{\partial y}\right) + \dot{Q} = (\phi c_t)_i \frac{\partial \Delta p_i}{\partial t} \tag{4.39}$$

Figure 4.7 depicts the necessary boundary conditions and the underlying governing equations. The branch-fracture diffusivity equation is subjected to the following boundary conditions,

- ☐ Boundary condition 1 (Flux continuity at the interface of SRV branch-fracture and region 3)

$$(q_i)|_{x=x_1} = (q_3)|_{x=x_1} \tag{4.40}$$

- ☐ Boundary condition 2 (Flux continuity at the interface of SRV branch-fracture and region 2)

$$(q_i)|_{y=y_1} = (q_2)|_{y=y_1} \tag{4.41}$$

- ☐ Boundary condition 3 (Pressure continuity at $y = w_F/2$)

$$(\Delta p_i)|_{y=w_F/2} = (\Delta p_F)|_{y=w_F/2} \tag{4.42}$$

- ☐ Boundary condition 4 (Pressure continuity at $y = y_1$)

$$(\Delta p_i)|_{y=y_1} = (\Delta p_2)|_{y=y_1} \tag{4.43}$$

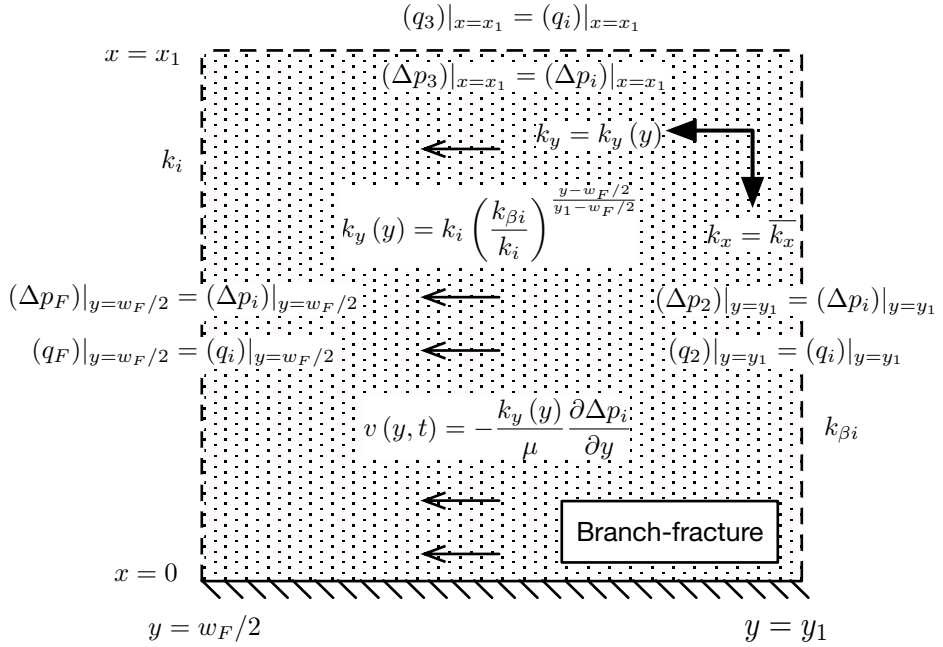

Figure 4.7: Schematic of the top view SRV branch-fracture domain and its governing equations

In Equation (4.39), $\dot{Q}$ denotes the transient fluid transfer from the SRV matrix spheres into the branch-fracture. According to de Swaan O et al. (1976), the matrix source term should be the ratio of the total flux across the surface of a spherical matrix to the half of the fracture volume envelope around each sphere. As shown in 4.8, the SRV region is composed of repetitive n_f units of array of spherical matrix and branch-fracture slabs. The figure also shows a fracture volume envelope that is assumed to be filled by the fluid influx from a single spherical matrix.
In the light of above discussion, the matrix source term can be written as,

$$\dot{Q} = -\frac{k_\beta\,(4\pi r_m^2)}{\mu}\frac{\partial^{1-\beta}}{\partial t^{1-\beta}}\left(\frac{\partial \Delta p_m}{\partial r}\right)_{r=r_m}\frac{1}{4\pi r_m^2(h_f/2\ )} \tag{4.44}$$

After the source term of Equation (4.44) is incorporated in Equation (4.40), the exploitation of dimensionless variables and Laplace transform lead to,

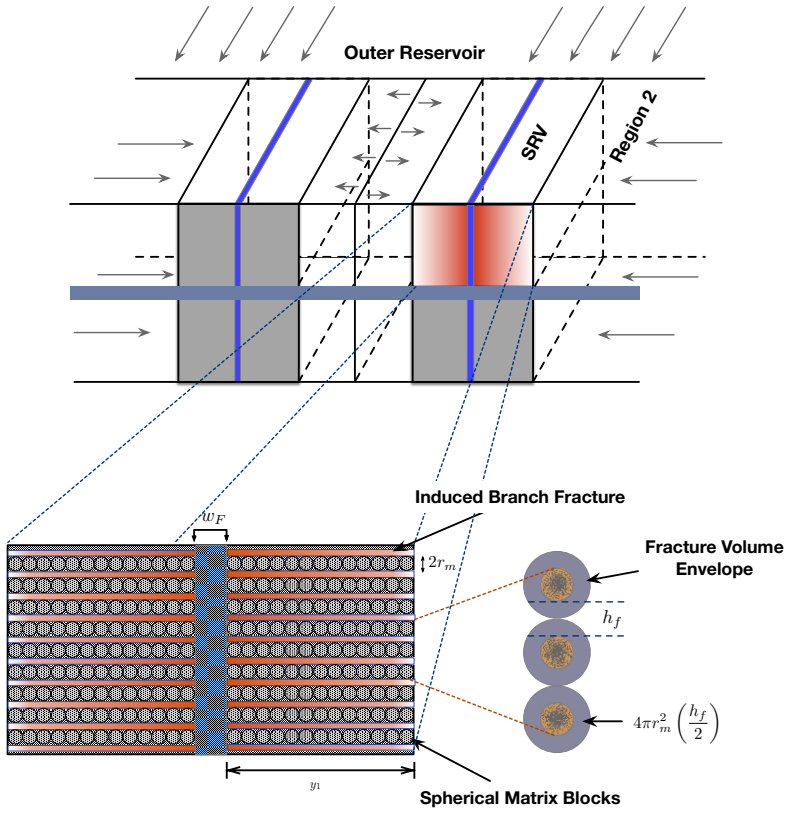

Figure 4.8: Distribution of matrix flux in the fracture volume envelope

$$k_{xD}\left(\frac{\partial \overline{p}_{iD}}{\partial x_D}\right)\Big|_{x_D=x_{1D}} + \frac{\partial}{\partial y_D}\left(k_D\left(y_D\right)\frac{\partial \overline{p}_{iD}}{\partial y_D}\right) - \frac{2k_\beta}{k_i h_{fD}}\left(\frac{\eta_i}{x_F^2}\right)^{1-\beta} s^{1-\beta}\left(\frac{\partial \overline{p}_{mD}}{\partial r_D}\right)_{r_D=r_{mD}} = s\left(\overline{p}_{iD}\right) \tag{4.45}$$

Recalling the derivative of pressure solution for spherical matrix presented in Equation (4.38),

$$\left(\frac{\partial \overline{p}_{mD}}{\partial r_D}\right)\Big|_{r_D=r_{mD}} = \frac{\left(\overline{p}_{iD}\right)|_{r_D=r_{mD}}}{r_{mD}}\left[r_{mD}\sqrt{\epsilon_{\mathrm{m}}}\coth\left(\sqrt{\epsilon_m}\ r_{mD}\right) - 1\right] \tag{4.46}$$

Recalling Equation (4.20) and applying the flux continuity condition stated in Equa-

tion (4.40), we can obtain the following,

$$\left(\frac{\partial \overline{p}_{iD}}{\partial x_D}\right)\Big|_{x_D=x_{1D}} = -\frac{k_\beta}{\widetilde{k_x}} \left(\frac{\eta_i}{x_F^2}s\right)^{1-\beta} \sqrt{\epsilon_3}\tanh\left[\sqrt{\epsilon_3}\left(x_{2D}-x_{1D}\right)\right] \left(\overline{p}_{iD}\right)|_{x_D=x_{1D}} \quad (4.47)$$

Plugging Equation (4.46) and (4.47) in Equation (4.45) results in,

$$\begin{aligned} &-\frac{k_{xD}k_\beta}{\widetilde{k_x}} \left(\frac{\eta_i}{x_F^2}s\right)^{1-\beta} \sqrt{\epsilon_3}\tanh\left[\sqrt{\epsilon_3}\left(x_{2D}-x_{1D}\right)\right] \left(\overline{p}_{iD}\right)|_{x_D=x_{1D}} + \frac{\partial}{\partial y_D}\left(k_D\left(y_D\right)\frac{\partial \overline{p}_{iD}}{\partial y_D}\right) \\ &-\frac{2k_\beta}{k_i h_{fD}}\left(\frac{\eta_i}{x_F^2}s\right)^{1-\beta} \frac{\left(p_{iD}\right)|_{r_D=r_{mD}}}{r_{mD}} \left[r_{mD}\sqrt{\epsilon_{\mathrm{m}}}\coth\left(\sqrt{\epsilon_m}\ r_{mD}\right)\ -1\right] = s\ \left(\overline{p}_{iD}\right) \end{aligned} \quad (4.48)$$

Now, identifying the terms that are independent of y_D and lumping them together into a function of Laplace variable s reduces Equation (4.48) to,

$$\frac{\partial}{\partial y_D}\left(k_D\left(y_D\right)\frac{\partial \overline{p}_{iD}}{\partial y_D}\right) - \epsilon_i\ \left(\overline{p}_{iD}\right) = 0 \quad (4.49)$$

Where,

$$\epsilon_i = \epsilon_a + \epsilon_b + s \quad (4.50)$$

And, the lumped model functions ϵ_a and ϵ_b are defined as:

$$\begin{aligned} \epsilon_a &= \frac{k_{xD}k_\beta}{\widetilde{k_x}} \left(\frac{\eta_i}{x_F^2}s\right)^{1-\beta} \sqrt{\epsilon_3}\tanh\left[\sqrt{\epsilon_3}\left(x_{2D}-x_{1D}\right)\right] \\ \epsilon_b &= \frac{2k_{\beta D}}{h_{fD}r_{mD}}\left(\frac{\eta_i}{x_F^2}s\right)^{1-\beta} \left[r_{mD}\sqrt{\epsilon_{\mathrm{m}}}\coth\left(\sqrt{\epsilon_m}\ r_{mD}\right)\ -1\right] \end{aligned} \quad (4.51)$$

Next, we incorporate the exponential branch-fracture permeability field to the diffusivity equation of fracture medium. Recalling the branch-fracture permeability field in dimensionless form from Equation (4.30),

$$k_D(y_D) = (k_{\beta D})^{\left(\frac{y_D - w_D/2}{y_{1D} - w_D/2}\right)} \quad (4.52)$$

To simplify branch-fracture diffusivity equation, we let the following:

$$M = \left(\frac{\ln k_{\beta D}}{y_{1D} - w_D/2}\right), \quad z_D \ = e^{M(y_D - w_D/2)} \tag{4.53}$$

Therefore, the diffusivity equation for branch-fracture can be simplified to the following equation. (Details of this transformation is derived in Appendix A.5)

$$z_D^2 \frac{\partial^2 \overline{p}_{iD}}{\partial z_D} + 2 z_D \frac{\partial \overline{p}_{iD}}{\partial z_D} - \left(\frac{\epsilon_i}{M^2}\right)\left(\frac{1}{z_D}\right)\overline{p}_{iD} = 0 \tag{4.54}$$

Equation (4.54) resembles to the modified Bessel differential equation. In order to find the solution to this equation, we complement the techniques of determining solutions from a standard Bessel differential equation. Therefore, the general solution to the modified Bessel differential equation can be written as below:

$$\overline{p}_{iD} = z_D^{-1/2} \ \left[A I_1 \left(\frac{2\sqrt{\epsilon_i}}{M} \ z_D^{-\frac{1}{2}} \right) + B K_1 \left(\frac{2\sqrt{\epsilon_i}}{M} \ z_D^{-\frac{1}{2}} \right) \right] \tag{4.55}$$

Here, I_1 and K_1 are the modified Bessel function of first and second kind.A and B are two constants which needs to be evaluated with the available boundary conditions. For the ease of algebraic manipulation, we let the argument of Bessel functions as:

$$X = \frac{2\sqrt{\epsilon_i}}{M} \ z_D^{-\frac{1}{2}} \tag{4.56}$$

This simplifies Equation 4.55 to,

$$\overline{p}_{iD} = z_D^{-1/2} \ \left[A I_1 (X) + B K_1 (X) \right] \tag{4.57}$$

In order to obtain the exact pressure solution for branch-fracture domain, we need to transform the constants A and B in terms of $(\overline{p}_{iD})|_{y_D = y_{1D}}$. Then, applying pressure continuity at the interface of branch-fracture and primary fracture plane, we can obtain the desired pressure solution for branch-fracture domain.

Now, the differentiation rules for I_ν and K_ν are given by,

$$\begin{aligned} I_\nu^{'}(x) &= I_{\nu-1}(x) - \frac{\nu}{x} \ I_\nu (x) \\ K_\nu^{'}(x) &= -K_{\nu-1}(x) - \frac{\nu}{x} \ K_\nu (x) \end{aligned} \tag{4.58}$$

Taking the derivative of Equation (4.57) and evaluating at $y_D = y_{1D}$,

$$\left(\frac{\partial \overline{p}_{iD}}{\partial y_D}\right)\Big|_{y_D=y_{1D}} = \frac{\sqrt{\epsilon_i}}{k_{\beta D}}\left[BK_0\left(X_1\right) - AI_0\left(X_1\right)\right] \tag{4.59}$$

Recalling Equation (4.27) from Region 2 and implementing the boundary condition stated in Equation (4.41), we can transform the constants A and B to:

$$\begin{aligned} A &= D\left(\overline{p}_{iD}\right)\big|_{y_D=y_{1D}} \\ B &= C\ \left(\overline{p}_{iD}\right)\big|_{y_D=y_{1D}} \end{aligned} \tag{4.60}$$

Where, the lumped functions C, D and ϵ_α are defined as below,

$$\begin{aligned} C &= \left[\frac{\sqrt{k_{\beta D}}I_0\left(X_1\right) - \epsilon_\alpha I_1\left(X_1\right)}{K_1\left(X_1\right)I_0\left(X_1\right) + K_0\left(X_1\right)I_1\left(X_1\right)}\right] \\ D &= \left[\frac{\sqrt{k_{\beta D}}}{I_1\left(X_1\right)} - \left(\frac{K_1\left(X_1\right)}{I_1\left(X_1\right)}\right)C\right] \\ \epsilon_\alpha &= \left(\frac{\sqrt{\epsilon_2}}{\sqrt{\epsilon_i}}\right)\left(\frac{k_\beta k_{\beta D}}{\widetilde{k_y}}\right)\ \left(\frac{\eta_i}{x_F^2}s\right)^{1-\beta}\tanh\left[\sqrt{\epsilon_2}\left(y_{2D} - y_{1D}\right)\right] \end{aligned} \tag{4.61}$$

This simplifies Equation (4.57) to:

$$\left(\overline{p}_{iD}\right)| = z_D^{-1/2}[DI_1\left(X\right) + CK_1\left(X\right)\ ]\ \left(\overline{p}_{iD}\right)\big|_{y_D=y_{1D}} \tag{4.62}$$

Now, applying the pressure continuity condition stated in Equation (4.42) into Equation (4.62), we obtain,

$$\overline{p}_{iD} = z_D^{-\frac{1}{2}}\left[\frac{DI_1\left(X\right) + CK_1\left(X\right)}{DI_1\left(X_0\right) + CK_1\left(X_0\right)}\right]\left(\overline{p}_{FD}\right)\big|_{y_D=\frac{w_D}{2}} \tag{4.63}$$

Equation (4.63) represents the exact pressure solution for branch-fracture domain in terms of hydraulic fracture pressure. Where, X,$X_1$and X_0 are the arguments of I and K and they are defined as below:

$$
\begin{aligned}
X &= \frac{2\sqrt{\epsilon_i}\ln\left(\frac{1}{k_{\beta D}}\right)}{y_{1D}-w_D}\ e^{(\ln k_{\beta D})\ \left(\frac{y_D-w_D/2}{y_{1D}-w_D/2}\right)} \\
X_1 &= \frac{2\sqrt{\epsilon_i}\ln\left(\frac{1}{k_{\beta D}}\right)}{y_{1D}-w_D/2}\ \frac{1}{\sqrt{k_{\beta D}}} \\
X_0 &= \frac{2\sqrt{\epsilon_i}\ln\left(\frac{1}{k_{\beta D}}\right)}{y_{1D}-w_D/2}
\end{aligned}
\tag{4.64}
$$

The derivative of Equation (4.63) at $y_D = w_D/2$ is evaluated, as this function is required to couple the branch-fracture solution with the primary fracture solution. Therefore,

$$
\left(\frac{\partial \overline{p}_{iD}}{\partial y_D}\right)\Bigg|_{y_D=w_D/2} = \epsilon_\gamma\ \left(\overline{p}_{FD}\right)|_{y_D=\frac{w_D}{2}} \tag{4.65}
$$

Where,

$$
\epsilon_\gamma = \delta\sqrt{\epsilon_i}\left[\frac{C\ K_0\left(X_0\right) - D\ I_0\left(X_0\right)}{DI_1\left(X_0\right) + CK_1\left(X_0\right)}\right] \tag{4.66}
$$

In the above equation, when $k_{\beta D} = \frac{k_\beta}{k_i} < 1, \delta = -1$. Equation (4.65) is now ready to be coupled with the hydraulic fracture region to incorporate the effect of all the four regions. The term ϵ_γ accounts for the effect of outer regions, inner unfractured region, the branch-fracture permeability distribution in the SRV and the effect of fractional diffusion in spherical matrix.

4.3.7 Classic Diffusion in Primary Fracture Plane

In the analytical modelling of fluid flow through multi-fractured reservoirs, the primary fracture plane is usually assumed as a porous medium with high permeability. In this study, primary hydraulic fracture is modelled as a vertical rectangular slab intersecting the horizontal wellbore. This medium is well connected and provides less hindrance to flow. Therefore, the diffusion phenomena can be defined by using classical diffusion formula. Fluid flows linearly from branch-fracture network to hydraulic fracture in the y-direction, then flows along the x-direction to the wellbore. Flow inside the hydraulic fracture is also assumed linear. The diffusivity equation for

hydraulic fracture region is,

$$\frac{\partial}{\partial x}\left(\frac{k_F}{\mu}\frac{\partial \Delta p_F}{\partial x}\right)+\frac{\partial}{\partial y}\left(\frac{k_F}{\mu}\frac{\partial \Delta p_F}{\partial y}\right)=(\phi c_t)_F\frac{\partial \Delta p_F}{\partial t} \tag{4.67}$$

Figure 4.9 shows a schematic of the cross-section of primary fracture plane and its governing equations. Equation (4.67) is subjected to the following boundary conditions,

- ☐ Boundary condition 1 (Flux continuity at the interface of SRV branch-fracture and primary fracture region)

$$(q_F)|_{y=w_F/2}=(q_i)|_{y=w_F/2} \tag{4.68}$$

- ☐ Boundary condition 2 (Flux continuity at the interface of primary fracture plane and the wellbore)

$$\left(\frac{Bq_f}{4}\right)\Big|_{x=0}=(q_F)|_{x=0} \tag{4.69}$$

- ☐ Boundary condition 3 (No flow boundary at $x=x_1$)

$$\left(\frac{\partial \Delta p_F}{\partial x}\right)\Big|_{x=x_1}=0 \tag{4.70}$$

By applying Laplace transform and the dimensionless variables defined in Table 4.2, the wellbore pressure solution is derived in Appendix A.6. Therefore, the derived wellbore pressure solution in Laplace domain is,

$$\overline{p}_{FD}|_{x_D=0}=\overline{p}_{WD}=\frac{\pi}{s\ C_{FD}\ \sqrt{\epsilon_F}\tanh\left[\sqrt{\epsilon_F}\ \right]} \tag{4.71}$$

Where, ϵ_F is a nested function of Laplace variable s and it carries the diffusion characteristics and effect of all the other flow regions. C_{FD} is hydraulic fracture conductivity. The definition of C_{FD} and ϵ_F are given below.

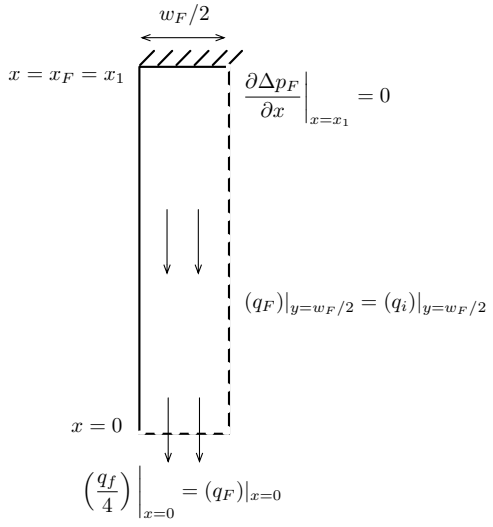

Figure 4.9: Schematic of the cross-section of primary fracture plane and its governing equations

$$C_{FD} = \frac{k_F w_D}{\widetilde{k_i}} = \frac{k_F w_F h}{k_i x_F h_{ft}}$$
$$\epsilon_F = \frac{s}{\eta_{FD}} - \frac{2}{C_{FD}}\epsilon_\gamma \tag{4.72}$$

Therefore, Equation (4.71) presents the constant rate solution for the buttomhole pressure of the proposed SIBFF model in Laplace domain. It should be noted that the calculation of ϵ_F requires the evaluation of ϵ_4,ϵ_3,ϵ_m,ϵ_2,ϵ_i,ϵ_α and ϵ_γ and these parameters are functions of Laplace variable, s. Finally, we accumulate the final set of model functions that should be evaluated to obtain the wellbore pressure in Laplace domain.

$$\epsilon_4 = \epsilon_3 = \epsilon_m = \left(\frac{x_F^2}{\eta_\beta}\right)\left(\frac{\eta_i}{x_F^2}\right)^{\beta} s^{\beta}, \qquad \epsilon_i = \epsilon_a + \epsilon_b + s$$

$$\epsilon_2 = \left[\sqrt{\epsilon_4}\tanh\left[\sqrt{\epsilon_4}\left(x_{2D} - x_{1D}\right)\right] + \frac{x_F^2}{\eta_\beta}\left(\frac{\eta_i}{x_F^2}\right)^{\beta} s^{\beta}\right]$$

$$\epsilon_a = \frac{k_{xD} k_\beta}{\widetilde{k_x}} \left(\frac{\eta_i}{x_F^2} s\right)^{1-\beta} \sqrt{\epsilon_3}\tanh\left[\sqrt{\epsilon_3}\left(x_{2D} - x_{1D}\right)\right]$$

$$\epsilon_b = \frac{2k_{\beta D}}{h_{fD} r_{mD}}\left(\frac{\eta_i}{x_F^2} s\right)^{1-\beta} \left[r_{mD}\sqrt{\epsilon_{\mathrm{m}}}\coth\left(\sqrt{\epsilon_m}\ r_{mD}\right)\ - 1\right]$$

$$\epsilon_\alpha = \left(\frac{\sqrt{\epsilon_2}}{\sqrt{\epsilon_i}}\right)\left(\frac{k_\beta k_{\beta D}}{\widetilde{k_y}}\right)\ \left(\frac{\eta_i}{x_F^2} s\right)^{1-\beta} \tanh\left[\sqrt{\epsilon_2}\left(y_{2D} - y_{1D}\right)\right]$$

$$C = \left[\frac{\sqrt{k_{\beta D}} I_0\left(X_1\right) - \epsilon_\alpha I_1\left(X_1\right)}{K_1\left(X_1\right) I_0\left(X_1\right) + K_0\left(X_1\right) I_1\left(X_1\right)}\right]$$

$$D = \left[\frac{\sqrt{k_{\beta D}}}{I_1\left(X_1\right)} - \left(\frac{K_1\left(X_1\right)}{I_1\left(X_1\right)}\right) C\right]$$

$$\epsilon_\gamma = \delta\sqrt{\epsilon_i}\left[\frac{C\ K_0\left(X_0\right) - D\ I_0\left(X_0\right)}{D I_1\left(X_0\right) + C K_1\left(X_0\right)}\right]$$

$$\epsilon_F = \frac{s}{\eta_{FD}} - \frac{2}{C_{FD}}\epsilon_\gamma$$

$$\overline{p}_{FD}|_{x_D=0} = \overline{p}_{WD} = \frac{\pi}{s\ C_{FD}\ \sqrt{\epsilon_F}\tanh\left[\sqrt{\epsilon_F}\ \right]}$$

A computational code for the developed model equations was written in MATLAB and the model solution in real domain is obtained applying the multiprecision Gaver-Wynn-Rho algorithm in a symbolic environment to avoid the round-off error. In the subsequent segments, the analysis of the derived solution is presented.

4.4 Results, Verification and Validation

In this chapter, we determine the applicability of the proposed SIBFF model by comparing the results with the standard analytical model and the field data obtained from the literature. By imposing asymptotic conditions, the solution have been verified with an established analytical model. A sensitivity analysis on the effect of various model parameter is carried out in this section. The flow rate solution for constant bottom hole pressure case is developed by using superposition theory on Laplace space. Then the flowrate solution is used to analyze rate transient behaviour of the presented model. Finally, with the knowledge of sensitivity analysis, the proposed model is matched with Niobrara shale oil field data and evaluated the values of constrained parameters.

4.4.1 Analytical Verification with TADDP Model

Asymptotic cases of this model can be used to verify the model with the existing simplified models. Albinali et al. (2016) proposed a Trilinear Anomalous Diffusion and Dual Porosity model (TADDP) which idealizes the SRV as a dual porosity continuum: Spherical matrix with anomalous diffusion and induced fractures with uniform $k_{\alpha f}$. TADDP model is one of the established anomalous diffusion models that was validated against the standard analytical models and field data. However, the TADDP model did not incorporate the effect of unfractured region between two fracture planes, which was accounted for in this model. The wellbore pressure solution of SIBFF model should yield the solution of TADDP model when applied necessary asymptotic conditions. Table 4.3 summarizes the necessary modifications that should be made to the TADDP model to yield the SIBFF model.

The wellbore pressure solution for TADDP model can be summarized as below,

$$\beta_o = \left(\frac{x_F^2}{\eta_\beta}\right)\left(\frac{\eta_f}{x_F^2}\right)^\beta s^\beta \tag{4.74}$$

$$\beta_m = \left(\frac{x_F^2}{\eta_\beta}\right)\left(\frac{\eta_i}{x_F^2}\right)^\beta s^\beta \tag{4.75}$$

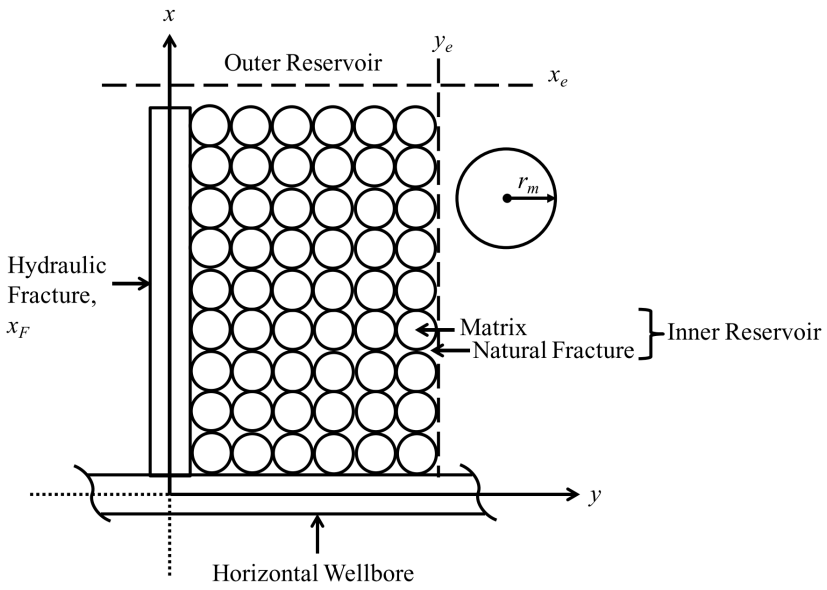

Figure 4.10: Schematic of the TADDP model idealization (adapted from Albinali et al., 2016)

$$\begin{aligned}\beta_{ff} = \frac{k_\beta}{\tilde{k}_i}\left(s\ \frac{\eta_i}{x_F^2}\right)^{\beta}\sqrt{\beta_o}\tanh\left[\sqrt{\beta_o}\,(x_{1D}-1)\right] \\ +\ \left[\frac{2k_\beta}{h_{fD}k_i r_{mD}}\left(\frac{\eta_i}{x_F^2}\ s\right)^{1-\beta}\left\{r_{mD}\sqrt{\beta_m}\coth\left(\sqrt{\beta_m}\ r_{mD}\right)\ -1\right\}\right]+s\end{aligned} \tag{4.76}$$

$$\beta_{HF} = \sqrt{\beta_{ff}}\tanh\left[\sqrt{\beta_{ff}}\,(y_{1D}-w_D/2)\right] \tag{4.77}$$

$$\alpha_{HF} = \frac{s}{\eta_{FD}} + \ \frac{2}{C_{FD}}\ \beta_{HF} \tag{4.78}$$

Therefore, setting $y_{1D} = y_{2D}$, $\tilde{k}_X = \tilde{k}_i$, $\lim_{k_{\beta D}\to 1}\epsilon_i$ and $\lim_{k_{\beta D}\to 1}\epsilon_\gamma$ in the proposed model should yield the above solution of TADDP.

Setting $y_{1D} = y_{2D}$ results in:

$$\epsilon_\alpha = 0,\ \epsilon_2 = 0$$

Table 4.3: Feature comparisons and necessary modifications needed to verify the proposed SIBFF model with TADDP model

Regions	The TADDP model	The proposed model	Necessary modifications
Outer Reservoir	Only one region with isotropic transfer function coupling with SRV fracture	Two regions with anisotropic coupling of region 3 and SRV branch-fracture	$y_{1D} = y_{2D}$
	Fluid flows directly to SRV fractures only	Fluid flows to both SRV branch-fracture and unfractured region 2	
Inner Reservoir	SRV spans from one fracture plane to the other fracture plane	SRV spans from the fracture plane to the onset of the unfractured region	$\lim_{k_{\beta D}\to 1} \epsilon_i$
	Isotropic fracture continuum with anomalous diffusion	Anisotropic fracture continuum with normal diffusion	$\tilde{k}_x = \tilde{k}_y = \tilde{k}_i$

$$\epsilon_3 = \beta_o \qquad \epsilon_m = \beta_m$$

Since SRV is isotropic in TADDP model. Setting $k_{xD} = 1, \quad \tilde{k}_Y = \tilde{k}_i$ confirms that SIBFF has isotropic SRV. This results in,

$$\begin{aligned}\epsilon_i = \beta_{ff} = \frac{k_\beta}{\tilde{k}_i}\left(s\ \frac{\eta_i}{x_F^2}\right)^\beta \sqrt{\epsilon_3}\tanh\left[\sqrt{\epsilon_3}\,(x_{1D}-1)\right] \\ + \left[\frac{2k_\beta}{h_{fD}k_i r_{mD}}\left(\frac{\eta_i}{x_F^2}\ s\right)^{1-\beta}\left\{r_{mD}\sqrt{\beta_m}\coth\left(\sqrt{\beta_m}\ r_{mD}\right)\ -1\right\}\right] + s\end{aligned} \tag{4.79}$$

As $k_{\beta D}$ approaches to 1, the permeability distribution in the SRV branch-fractures approaches to as like as in the TADDP model (Uniform Permeability Distribution). Now, applying $\epsilon_\alpha = 0$ and $\lim_{k_{\beta D}\to 1}$ into the solution of SIBFF model yields,

$$C = \left[\frac{I_0(X_1)}{K_1(X_1)\ I_0(X_1) + K_0(X_1)\ I_1(X_1)}\right]$$

$$D = \left[\frac{K_0(X_1)}{K_1(X_1)\ I_0(X_1) + K_0(X_1)\ I_1(X_1)} \right]$$

$$\epsilon_\gamma = \sqrt{\beta_{ff}} \frac{[I_0(X_1) K_0(X_0) - K_0(X_1) I_0(X_0)]}{[I_0(X_1) K_1(X_0) + I_0(X_1) K_1(X_0)]} \tag{4.80}$$

where,

$$X_1 = \frac{2\sqrt{\epsilon_i}(y_{1D} - w_D/2)}{\ln(k_{\beta D})\ \sqrt{k_{\beta D}}}, \quad X_0 = \frac{2\sqrt{\epsilon_i}(y_{1D} - w_D/2)}{\ln(k_{\beta D})}$$

As $k_{\beta D}$ approaches to 1, X_1 and X_0 approaches to infinity and the modified Bessel functions behaves as below:

$$\lim_{z\to\infty} I_\nu(z)\ \sim \frac{1}{\sqrt{2\pi}} \frac{e^z}{\sqrt{z}} \tag{4.81}$$

$$\lim_{z\to\infty} K_\nu(z)\ \sim \frac{\sqrt{\pi}}{\sqrt{2}} \frac{e^{-z}}{\sqrt{z}} \tag{4.82}$$

Applying the asymptotic relations of Equation (4.81) and Equation (4.82) into Equation (4.80).

$$\epsilon_\gamma = \sqrt{\beta_{ff}}\ \frac{e^{X_1}\ e^{-X_0} - e^{-X_1} e^{X_0}}{e^{X_1}\ e^{-X_0} + e^{-X_1} e^{X_0}} \tag{4.83}$$

Finding the limiting value for the exponent first:

$$\lim_{k_{\beta D}\to 1}(X_1\ - X_0) = \lim_{k_{\beta D}\to 1} \left[2\sqrt{\epsilon_i}(y_{1D} - w_D/2) \left(\frac{1}{\ln(k_{\beta D})\ \sqrt{k_{\beta D}}} - \frac{1}{\ln(k_{\beta D})} \right) \right] \tag{4.84}$$

$$\lim_{k_{\beta D}\to 1}(X_1\ - X_0) = 2\sqrt{\epsilon_i}(y_{1D} - w_D/2) \lim_{k_{\beta D}\to 1} \left[\frac{1 - \sqrt{k_{\beta D}}}{\ln(k_{\beta D})\ \sqrt{k_{\beta D}}} \right] \tag{4.85}$$

Application of L'Hospital's Rule helps to find the limit here. Applying the rule,

$$\lim_{x\to a} \frac{f(x)}{g(x)}\ = \frac{0}{0}\ \Longrightarrow \lim_{x\to a} \frac{f(x)}{g(x)} = \lim_{x\to a} \frac{f'(x)}{g'(x)} \tag{4.86}$$

$$\epsilon_\gamma = \sqrt{\beta_{ff}} \left[\frac{e^{\sqrt{\epsilon_i}\left(y_{1D}-\frac{w_D}{2}\right)} - e^{-\sqrt{\epsilon_i}\left(y_{1D}-\frac{w_D}{2}\right)}}{e^{\sqrt{\epsilon_i}\left(y_{1D}-\frac{w_D}{2}\right)} + e^{-\sqrt{\epsilon_i}\left(y_{1D}-\frac{w_D}{2}\right)}} \right] \tag{4.87}$$

$$\epsilon_\gamma = \sqrt{\beta_{ff}} \tanh\sqrt{\epsilon_i} \left(y_{1D} - \frac{w_D}{2} \right) = \beta_{HF} \tag{4.88}$$

In summary, when $k_{\beta D} \to 1$ and $y_{1D} = y_{2D}$:

$$\epsilon_3 = \beta_o, \quad \epsilon_m = \beta_m, \quad \epsilon_i = \beta_{ff}, \quad \epsilon_\gamma = \beta_{HF} \text{ and } \epsilon_F = \alpha_{HF} \tag{4.89}$$

Therefore, the proposed SIBFF model yields the conventional TADDP model when applied certain modifications and asymptotic conditions. The graphical verification is also presented in the Figure 4.11. The wellbore pressure solution completely matches with the TADDP model when un-fractured region of the SRV and varying branch-fracture permeability condition is disregarded. The necessary data used in the verification is listed in Table 4.4. Therefore, the coherence with the standard model in the literature has increased the confidence to apply the proposed model for practical purposes.

4.4.2 Sensitivity Study

Pressure drop at the wellbore is tested by varying a set of diverse parameters of the presented model such as permeability at the vicinity of fracture plane (k_i), intrinsic matrix permeability (k_β) and subdiffusion exponent of matrix (β). The analysis of sensitive parameters helps to categorize the most influential parameters that should be handled differently in history matching ultimately leading to a quick match. Table 4.5 lists the inputs of the SIBFF model. The Figure 4.12, 4.13 and 4.14 show the sensitivity of permeability field, matrix permeability and subdiffusion exponent respectably.

Effect of k_i on wellbore pressure drop

Branch-fracture permeability field is significantly affected by the permeability at the vicinity of the primary fracture plane. We have learnt from Figure 4.5 of Section 4.3.4 that each different k_i generates a distinct permeability field in branch-fracture

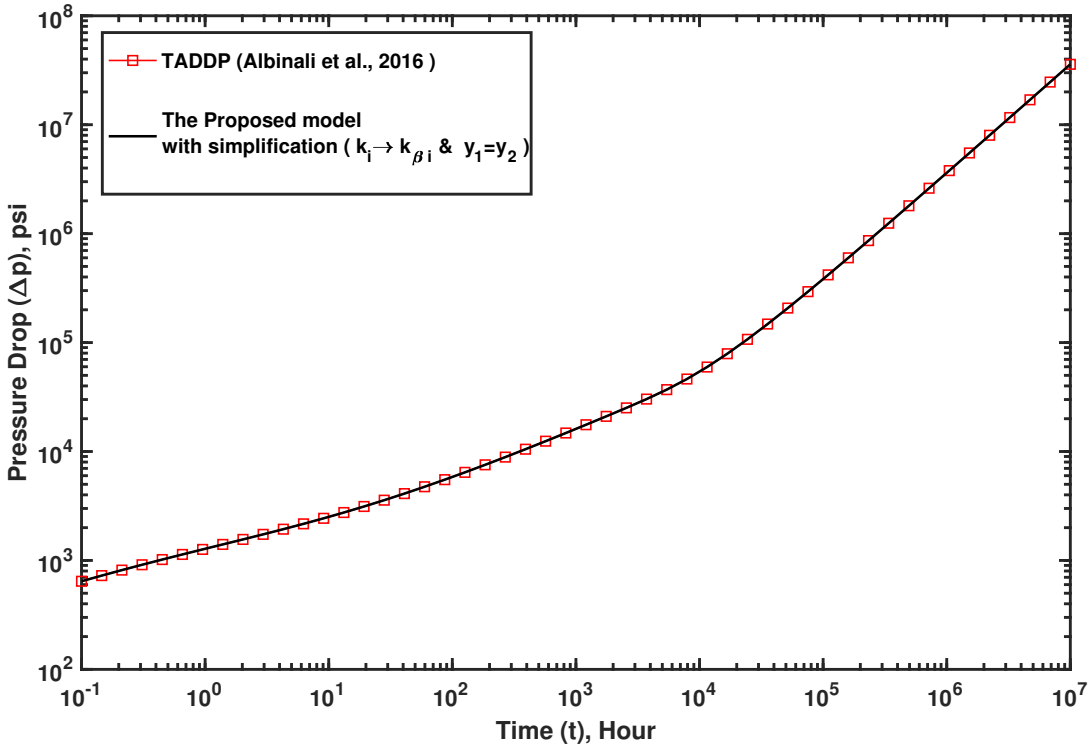

Figure 4.11: Verification of SIBFF model with TADDP model

domain. In the SRV flow domain, branch-fractures are the only transport medium while the SRV matrices acts as a storage only. In order to analyze the effect, we have evaluated the wellbore pressure drop for varying values of k_i and the pressure drop responses are depicted in Figure 4.12.

In Figure 4.12, the wellbore pressure drop responses moves downward with the increase of k_i. As k_i is the highest permeability in the branch-fracture, the value of k_i indicates the performance of of the stimulation job in a distinct formation. As the value of k_i increases, the permeability of the other points in the branch-fracture domain also increases due to the assumption exponential, monotonic behaviour of branch fracture permeability field (Fuentes-Cruz, Gildin, Valkó, et al., 2014). Therefore, as the value of k_i increases, the hindrance to flow in the SRV region decreases. The decrease in flow resistance ultimately results in a decrease in pressure drop (Δp). It is also evident from Figure 4.12 that this highest permeability significantly affects the pressure responses throughout the life of the reservoir with high impact in the early times. Therefore, in order to enhance productivity of an unconventional reser-

Table 4.4: Synthetic data used for the verification with TADDP model (Albinali et al., 2016)

Parameters	Typical values
Matrix Subdiffusion exponent, β	0.8
Hydraulic fracture half-length, x_F, ft	250
Distance to boundary to well, x_2, ft	400
Hydraulic fracture half-spacing, $y_1 = y_2$, ft	140
Pay zone thickness, h, ft	200
Radius of spherical matrix, r_m, ft	0.5
Matrix porosity, ϕ_β,	0.05
Matrix intrinsic permeability, k_β	0.0001
Total matrix compressibility, c_{mt}, psi^{-1}	1×10^{-5}
Average branch fracture aperture, h_f, ft	3×10^{-3}
Branch fracture porosity, ϕ_i	0.56
Branch fracture permeability $k_i \rightarrow k_{\beta i}$, md	0.1
Branch fracture compressibility, c_{fi},psi^{-1}	1×10^{-4}
Hydraulic fracture aperture, w_F, ft	0.01
Hydraulic fracture porosity, ϕ_F	0.38
Hydraulic fracture permeability, k_F	1×10^4
Hydraulic fracture compressibility, c_{tF}, psi^{-1}	5×10^{-4}
Fluid viscosity, μ, cp	0.3
Single fracture flow rate, q_F, stb/day	100

voir, the hydraulic fracturing design should carried out in such a tactic manner so that it creates branch-fractures with high value of k_i.

Effect of intrinsic matrix permeability, k_β

In outer region and USRV of inner region, the matrix is the transport medium. The term k_β is also termed as a phenomenological coefficient as it is a special parameter in the fractional flux law by Raghavan (2011). However, when the subdiffusion exponent equals 1, this phenomenological coefficient turns into the intrinsic permeability of the matrix. From this standpoint, we analyze the effect of k_β on the pressure drop behaviour of the proposed model.

Table 4.5: Synthetic data used for the sensitivity analysis of SIBFF model (Albinali et al., 2016)

Parameters	Typical values
Hydraulic fracture half-length, x_F, ft	250
Distance to boundary to well, x_2, ft	400
Hydraulic fracture half-spacing, y_2, ft	150
Pay zone thickness, h, ft	250
Radius of spherical matrix, r_m, ft	0.5
Matrix porosity, ϕ_β,	0.05
Total matrix compressibility, c_{mt}, psi^{-1}	1×10^{-5}
Average branch fracture aperture, h_f, ft	3×10^{-3}
Branch fracture porosity, ϕ_i	0.56
Branch fracture compressibility, c_{fi},psi^{-1}	1×10^{-4}
Hydraulic fracture aperture, w_F, ft	0.01
Hydraulic fracture porosity, ϕ_F	0.38
Hydraulic fracture compressibility, c_{tF}, psi^{-1}	5×10^{-4}
Fluid viscosity, μ, cp	0.3
Single fracture flow rate, q_F, stb/day	100

From Figure 4.13, two pressure behaviours can be recognized for this impact. The first one exhibits very small decreases of pressure drops with increasing values of k_β at the early times. At intermediate times, the impact of k_β is the highest on pressure drop. In order to focus the pressure drop behaviour (Δp) qualitatively, we tabulated the pressure drops in Table 4.6 at different times of the flow period. At early production, the contribution of fluid from hydraulic fracture and SRV is dominant and the sensitivity of k_F and k_i is significant. Hence, the pressure drop at the early times are more sensitive to k_F and k_i than k_β. On the other hand, at the intermediate times, the depletion effect from the outer region and USRV becomes pronounced.

Effect of subdiffusion exponent, β

The unconventional matrix is disordered, extremely tight and full of various scales of natural microfractures that renders significant hindrance to the flow. According to (Raghavan, 2011), when β is less than 1, subdiffusion prevails over the porous

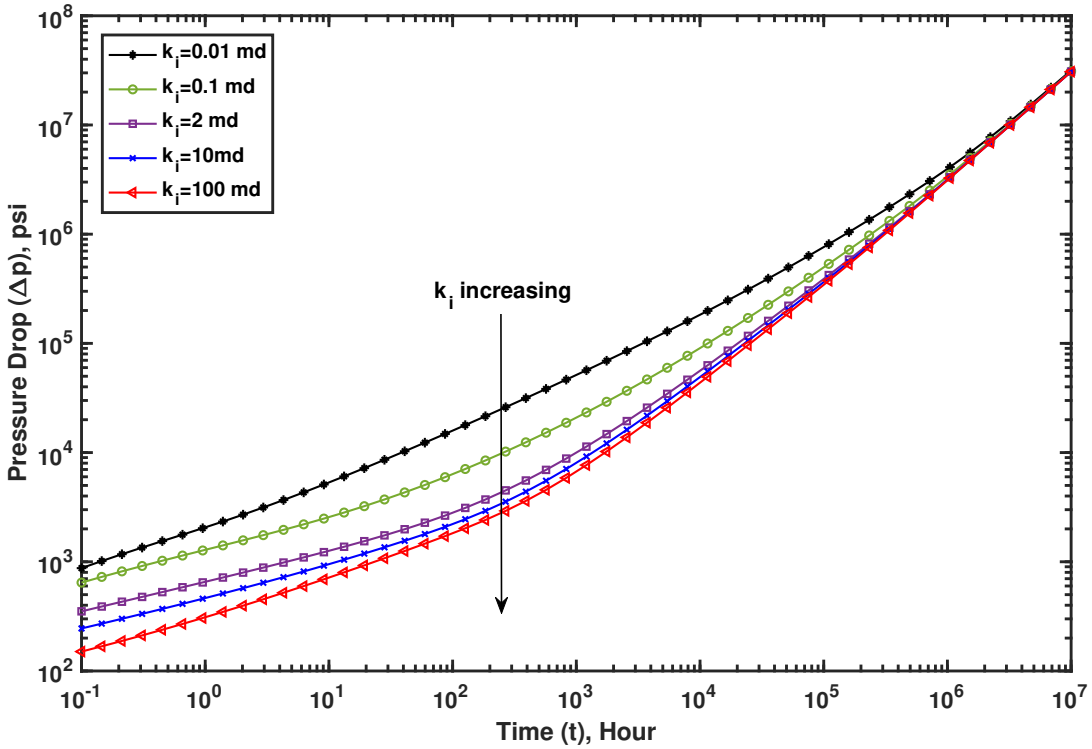

Figure 4.12: Effect of branch-fracture permeability at the vicinity of fracture plane

medium. Figure 4.14 exhibits the pressure responses of varying values of β.

As the impact of hydraulic fracture and k_i of SRV is pronounced at the early times of the flow period, the effect of subdiffusion is small. However, at intermediate and late times, the severity of subdiffusion is greatly increased due to the delay of fluid contribution into the production. At late times, as the value of β increases, the hindrance to flow decreases and the diffusion gets closer to the normal diffusion. The decrease in hindrance to flow in unconventional matrices ultimately results in a decrease in pressure drop (Δp).

4.4.3 Rate Transient Solution

This section presents variable rate solution of the SIBFF model while the bottom-hole pressure at the horizontal well are kept constant. The field data analysis in the next section requires constant bottomhole pressure solution for the diffusivity equations of the SIBFF model. The semi-analytical solution derived in Section 4.3 represent the

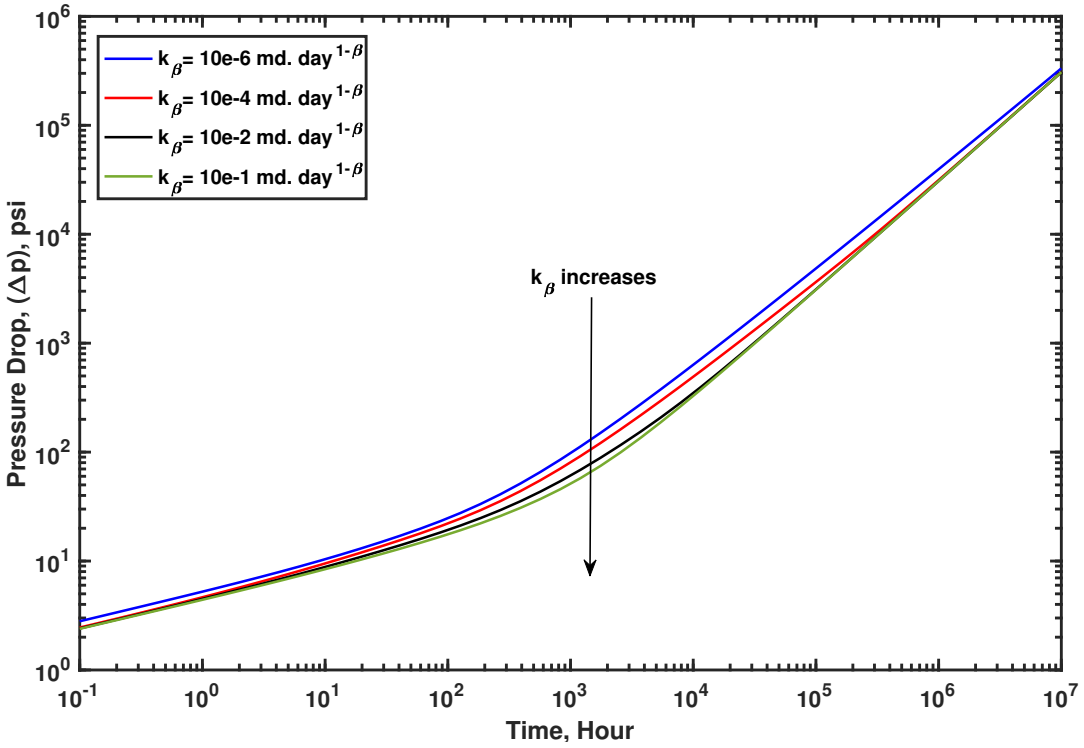

Figure 4.13: Effect of intrinsic matrix permeability

solution for constant rate condition. According to Duhamel's superposition theorem, the constant rate and constant pressure solutions to the diffusivity equations of fluid flow through porous media are coupled in Laplace domain as (Van Everdingen, Hurst, et al., 1949),

$$\overline{p}_D \overline{q}_D = \frac{1}{s^2} \tag{4.90}$$

where $\overline{p}_D$ is the dimensionless wellbore pressure for the constant rate solution and $\overline{q}_D$ is the dimensionless flow rate for the constant pressure solution in the Laplace domain. This is one of the most quintessential relations of reservoir engineering that are frequently used to switch back and forth to the solution of constant pressure inner boundary condition.

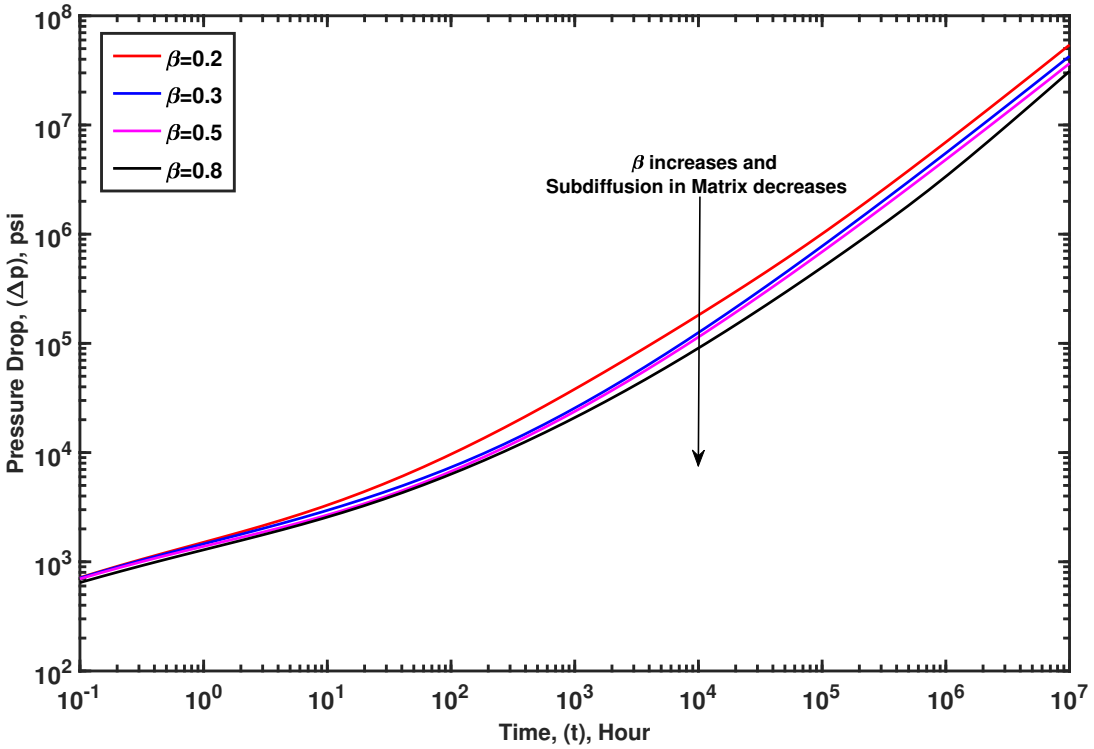

Figure 4.14: Effect of subdiffusion exponenet

4.4.4 Field Application

This section presents production history matching of a multifractured horizontal well with the SIBFF model. The well was drilled in Niobrara Shale formation in Weld County, Colorado with a horizontal length of 3885 ft and 14 fracture stages. The neccessary parameters for initializing the SIBFF model for the history match was adopted from Albinali et al. (2016) and listed in Table 4.7. As of 2014(EIA), this formation contains 0.512 billion barrels of oil, gas and gas condensate with TOC ranging from 2 to 8 weight % (Sonnenberg, 2011). Albinali et al. (2016) acquired the monthly production data (such as production volumes, number of production days and oil API) and the other well completion data from Colorado Oil and Gas Conservation Commission (COGCC) website. The data contains production history of 3.25 years from October 2012 to January 2016. The constrained parameters that are to be determined from the history match are as follows:

- ☐ Hydraulic fracture half-length, x_F

Table 4.6: Effect of k_β on the pressure behaviour of the proposed model

k_β, md.day$^{1-\beta}$	Pressure Drop (Δp), psi			
	t= 100 hrs	t= 1000 hrs	t= 10000 hrs	t= 100000 hrs
10×10^{-6}	25.30	98.67	673.08	5106.48
10×10^{-4}	22.74	79.75	515.78	3810.25
10×10^{-2}	19.39	61.11	374.74	3247.80
10×10^{-1}	17.90	50.72	345.98	3425.40

☐ Branch fracture permeability at the vicinity of primary fracture plane, k_i

☐ Branch fracture permeability at $y = y_1$, $k_{\beta i}$

☐ Subdiffusion exponent, β

☐ Matrix intrinsic permeability, k_β

☐ Average permeability in the x-direction, $\overline{k_x}$

After initialization of the SIBFF model with that data summarized in Table 4.7, the dimensionless flowrate values, q_D are computed for a required set of dimensionless time values, t_D using Gaver-Wynn-Rho Laplace inversion algorithm. From the definition of the dimensionless q_D and t_D, the flow rate and time are computed and compared against the field data. In the sensitivity analysis of type curves for SIBFF model, we observe that production performance is most influenced by hydraulic fracture permeability (k_F) and branch fracture permeability field (k_i and k_β) in the early and intermediate time period. These parameters are therefore carefully adjusted to obtain the early trend of the production behaviour. Through the adjustment of most influential parameters, such as branch fracture permeabilities (k_i and k_β), hydraulic fracture half-length (x_F), effective SRV width (y_1) and subdiffusion parameter (β), the optimum history match is obtained and presented in figure 4.15.

The model match with the Niobrara field data results in determination of the constrained parameters. The matched parameters are listed in 4.8. The realistic determination of these parameters is always a difficult job with a number of uncertainties. The model match quantifies the matrix permeability as 0.001. Cho et al. (2016) also determined the matrix permeability to be 0.001 md from a core analysis of Niobrara formation. The proposed semi-analytical model has shown a good agreement with the

Table 4.7: Model initialization with typical values for a horizontal well in Niobrara Field (Albinali et al., 2016)

Parameters	Typical values
Initial reservoir pressure, p_i, psi	4000
Flowing bottomhole pressure, p_{wf}, psi	800
Number of hydraulic fracture stages, n_F	14
Horizontal lateral length, ft	3885
Perforated interval length, ft	3417
Distance to boundary to well, x_2, ft	400
Hydraulic fracture half-spacing, y_2, ft	122.5
Pay zone thickness, h, ft	200
Radius of spherical matrix, r_m, ft	0.5
Matrix porosity, ϕ_β,	0.02
Total matrix compressibility, c_{mt}, psi^{-1}	1×10^{-5}
Branch fracture porosity, ϕ_i	0.6
Average branch fracture aperture, h_f, ft	3×10^{-3}
Branch fracture compressibility, c_{fi},psi^{-1}	1×10^{-4}
Hydraulic fracture porosity, ϕ_F	0.38
Hydraulic fracture permeability, k_F	5×10^4
Hydraulic fracture compressibility, c_{tF}, psi^{-1}	1×10^{-5}
Hydraulic fracture aperture, w_F, ft	0.01
Fluid viscosity, μ, cp	0.5

Niobrara field data. The model match characterizes the SRV region with quantifying the branch fracture permeability field and it's effective width. This validates that the SIBFF model can serve as an analytical tool for SRV region characterization, stimulation job plan, production evaluation and prediction of multi-fractured unconventional reservoirs.

4.5 Conclusion

In this Chapter, an upgraded semi-analytical model for the analysis of production data with variable rate and wellbore pressure for multifractured horizontal wells in unconventional reservoirs is developed, which accounts for branch-fracture perme-

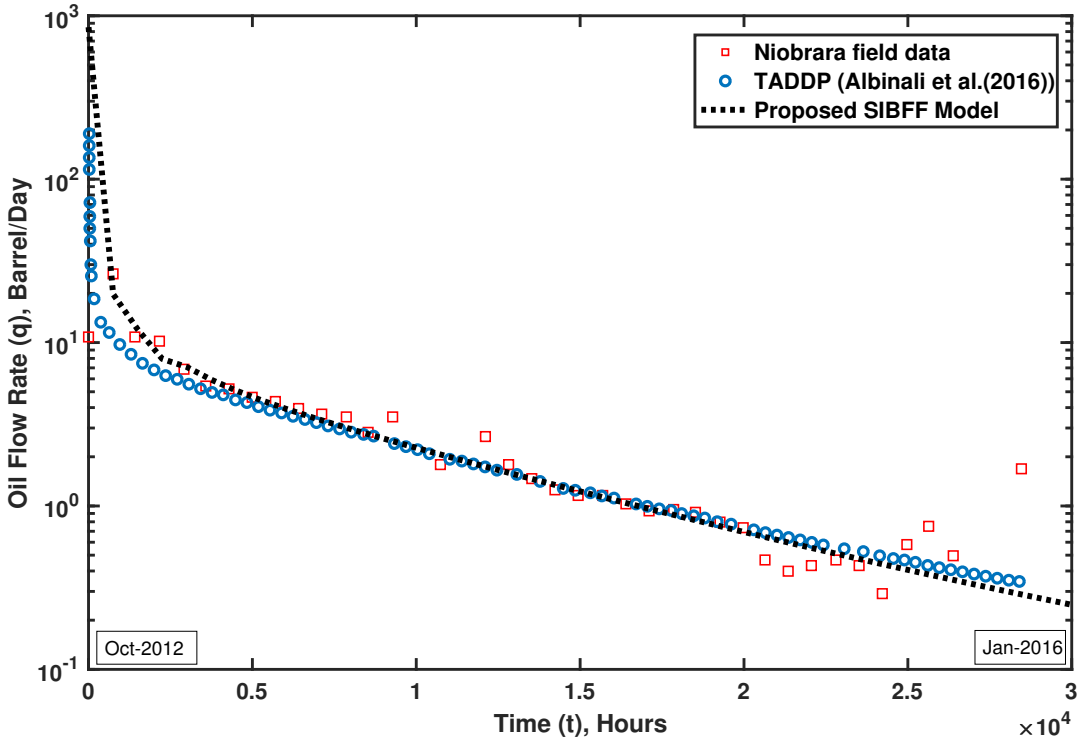

Figure 4.15: History matching results with the proposed SIBFF model

ability field, subdiffusive fluid transport in matrix, and USRV region. Based on the analysis of the proposed model, the following conclusions can be drawn:

- ☐ The standard models for unconventional reservoirs are reviewed and compared to the new features of the presented model. Advanced analytical methods are employed to handle the complexity of the mathematical model introduced by the spatial permeability function in SRV.

- ☐ The proposed SIBFF model generalizes the standard models with uniform fracture permeability and normal diffusion. The solution of this model was accurately verified with a standard model, the TADDP model.

- ☐ The presented SIBFF model can be applied to characterize unconventional fractured reservoirs considering several flow regions: Outer reservoir, Inner reservoir and Hydraulic fracture with finite conductivity.

- ☐ Wellbore pressure is highly sensitive to the branch-fracture permeability field

Table 4.8: Values of the constrained parameters determined from the history matching

Parameters	Matched values
Hydraulic fracture half-length, x_F, ft	265
Branch fracture permeability at the vicinity of primary fracture plane, k_i, md	0.7
Branch fracture permeability at $y = y_1$, $k_{\beta i}$, md	0.013
Subdiffusion exponent, β	0.5
Matrix intrinsic permeability, k_β	0.001
Average permeability in the x-direction, $\overline{k_x}$, md	0.17234
Effective SRV width, y_1, ft	117

and it affects the production behaviour throughout the whole life of an unconventional reservoir. The study also bolsters the fact that generating high permeability complex branch-fractures should significantly increase the production rates.

- Results of history matching for a Niobrara Shale well data for 39 months of production validates the applicability and predictability of the SIBFF model. The new semi-analytical model provides a mathematically-efficient tool for characterization, production evaluation and forecast for multifractured unconventional reservoirs.

Chapter 5

Unlocking the Heterogeneity Using Fractal Theory and Subdiffusion

5.1 Introduction

In the new era of energy exploitation, multi-fractured horizontal well technology have quickly transformed ultra-low unconventional resources sector by introducing a economic completion technology. The enhancement of the extent of induced permeability region in these reservoirs is the first job in the planning for the development of the unconventional reservoirs. Drilling a long and lateral well with multiple stimulation stages is regarded as the most effective production technique to facilitate the economic recovery from these reservoirs. In the case of ultralow unconventional reservoirs, the effect of outer reservoir is neglected as it has negligible impact in the production from the inner reservoir (Mayerhofer et al., 2006). Therefore, the drainage area of the reservoir can necessarily be assumed to be confined only in the inner reservoir with stimulated and unstimulated reservoir volume. The stimulation job using hydraulic fracturing generates a complex fracture network around a primary fracture plane and enhances total reservoir contact area ultimately improving recovery (Zhou, Banerjee, Poe, Spath, & Thambynayagam, 2013). In order to unlock the heterogeneity of various scales, it is critical to employ the most realistic model that describe the flow process and accounts for the complex interplay of matrix and fractures. The region of enhanced permeability around the primary fracture plane, often referred to as the Stimulated Reservoir Volume (SRV), is an important component in characterization

of a stimulated reservoir. Alongside SRV, a hydraulically stimulated reservoir consists of hydraulic fracture, unstimulated reservoir volume (USRV) and outer reservoir. Anderson et al. (2010) also showed that the outer reservoir plays an insignificant role in terms of a 20-year estimated ultimate recovery when the matrix permeability is below 10 nano Darcy. The USRVs are the non-affected region where no branch fractures is created from the primary fracture plane and the permeability in that region remains in nano-Darcy level (Fan & Ettehadtavakkol, 2017b).

The SRV region is composed of branch fractures, the reactivated natural fractures and matrix with ultralow permeability. The seminal work of Warren and Root (1963) has assumed the fracture continuum of a fractured media as a homogeneous medium of Euclidean geometry. Chang and Yortsos (1990) investigated a number of conventional models on describing pressure transient behavior of fractured media and outlined three premises on which those models are founded.

- Fractured media contains two media with two distinct scale of conductivity and storage capacity

- The fracture network is a Euclidean object which is embedded in another Euclidean object, matrix.

- There is no connectivity in the matrix. It only acts as a storage of fluid and does not produce to the well. Only perfectly connected fractures produce to well.

Ozkan et al. (2009) developed a trilinear model that idealizes the SRV as a vertical stack of matrix and uniform fracture slabs honouring these premises. Yuan et al. (2015) extended the idea of the trilinear model by subdividing the SRV into two regions with different permeability and fracture densities.

In order to account for the conductive potential of the matrix in fractured media, Al-Ghamdi and Ershaghi (1996) developed a triple porosity model incorporating the inflow from the matrix to the well. Ezulike and Dehghanpour (2014) suggested a simultaneous depletion model which also relaxes the the first premise and the matrix contributes to the both, natural fractures and hydraulic fractures. However, recognizing the need for further enhancement in the SRV categorization, (Chang & Yortsos,

1990) applied fractal theory to define the systems exhibiting a large number of different scales, poor connectivity and disordered spatial distribution. They idealized the SRV as fractal fracture network embedded in a Euclidean matrix where the fracture properties are scale dependent. Their model results in the following power-law expressions for porosity and permeability distribution, respectively:

$$\phi(r) = \frac{AV_s}{G} r^{D-d} \tag{5.1}$$

$$k(r) = \frac{AV_s m}{G} r^{D-d-\theta} \tag{5.2}$$

where D is the fractal dimension or Hausdorff dimension; d is the Euclidean dimension ($d = 2$ for planes, $d = 3$ for volumes); θ is the connectivity index, also referred to as tortuosity index; r is the radius from the centre of the wellbore and ϕ , k are the posoity and permeability respectably. Later,J. Acuna and Yortsos (1991) verified this hypothesis using numerical simulations for 2D fracture networks. Cossio, Moridis, Blasingame, et al. (2013) simplified the fractal porosity/permeability relationship and applied the relation in cartesian coordinates making it possible to be used in horizontal well where fluid flow is almost linear. The trilinear model of Ozkan et al. (2009) was upgraded by Wang, Shahvali, and Su (2015); Wang, Su, Sheng, Cossio, and Shang (2015) incorporating fractal distribution of porosity and permeability in the SRV under pseudo-steady state flow conditions. Fan and Ettehadtavakkol (2017b) developed a semi-analytical solution for shale gas flow in fractal reservoirs and presented a detailed workflow to evaluate induced fractures' porosity/permeability when only microseismic data of induced fracture density is available.

The aforementioned models captures the diffusion phenomenon in the matrix continuum using classical diffusivity equation and assumed the matrix as a well connected , continuous and well-distributed medium in the reservoir system. However, the above fractal models incorporated the deviation from classic diffusion in SRV fractures considering the subdffusion as a consequence of the presence the highly disordered geometry only (Holy, 2016). A number of authors have investigated the importance of considering other reservoir properties of different scales and suggested that different scale dependent transport mechanisms should be considered in the modelling of fluid flow in unconventional reservoirs (Javadpour et al., 2007, 2007; Akkutlu et al., 2012).

Metzler et al. (1994); Park et al. (2000) presented a generalized fractal diffusivity equation that accounts for temporal dependencies on fluid flux in the form of a time fractional derivative of pressure gradients. Raghavan (2011) upgraded the time fractional model and revealed that the application of fractional constitutive flux law is inherent in the nature of the unconventional fractured reservoirs that exhibits a number of scales in the form of obstacles and channels as well as induced changes affected by the stimulation job. In the light of the above literatures, it can conclusively stated that the factors influencing the production most are the fractal characteristics of the complex branch fractures and temporal dependencies in the matrix media of SRV and USRV. An extensive study should be done to elicit a comprehensive set of features from the characterization process of unconventional reservoirs.

The effect of subdiffusive fluid transport in ultralow matrix is more pronounced than that in conventional, high permeability matrix. Also, the fractal fracture network generated by the stimulation job effectively captures the heterogeneity of fracture continuum in a dual-porosity idealization of SRV. This study couples subdiffusive fluid transport and fractal branch-fracture permeability field into a new semi-analytical flow model in an endeavour to better characterize the SRV and USRV of ultralow permeability reservoir. Although, all the reported fractal models assumed fluid transfer from USRV matrix to SRV matrix which is unrealistic from the reservoir engineering point of view, this study considers fluid influx from the USRV matrix to the fractal branch fractures and investigates the impact of USRV on the production. Table 5.1 compares the proposed fractal branch-fracture model with the existing standard models for fluid flow in multi-fractured reservoir. The generated solution in this study captures heterogeneity of matrix in terms of subdiffusion exponent and accounts for the variation of permeability and porosity in terms of fractal dimension and connectivity index and thus can be employed for pressure and rate transient analysis of unconventional reservoirs with ultralow permeability.

Table 5.1: Feature comparison of the proposed model with the other standard semi-analytical models

Model Features	Models					
	Ozkan et al. (2009)	Cossio et al. (2013)	Wang, Shahvali, and Su (2015)	Fan and Ettehadtavakkol (2017a)	Fan and Ettehadtavakkol (2017b)	Fractal Branch Fracture Model
1.SRV idealization	Dual porosity	Single porosity	Dual porosity	Dual porosity	Dual porosity	*Dual porosity*
2.Diffusion in SRV matrix	Classical	N/A	Classical	Classical	Classical	*Subdiffusion*
3.Fluid Transfer from SRV matrix to fracture	Transient	N/A	Pseudo-steady	Transient	Transient	*Transient*
4.SRV matrix blocks	Slab	N/A	Sugar-cube	Slab	Slab	*Spherical matrix*
5.USRV idealization	Not considered	Not considered	Not considered	Dual porosity	Single porosity	*Single porosity*
6.Diffusion in USRV	N/A	N/A	N/A	Classical	Classical	*Subdiffusion*
7.Flow regime from USRV to branch fracture	N/A	N/A	N/A	Not considered	Not considered	*Considered (Transient)*

5.2 Fractal Distribution of Porosity and Permeability

Naturally occurring fractured porous media exhibits fractal behaviour in its properties (Barton & La Pointe, 2012). In order to describe the properties of porous media, Chang and Yortsos (1990) carried out an investigation for the fluid flow across a cylindrical differential shell that contains a fracture network with fractal dimension. The fractal network was necessarily embedded in a Euclidean matrix. They came up with power law distribution of porosity and permeability. The derived relations are stated in equation (5.2) and (5.2). J. A. Acuna and Yortsos (1995) simplified the relations and proposed in a different way, these are

$$\phi\left(r\right) = \phi_0 \left(\frac{r}{r_0}\right)^{D-d} \tag{5.3}$$

$$k\left(r\right) = k_0 \left(\frac{r}{r_0}\right)^{D-\theta-d} \tag{5.4}$$

where k_0, ϕ_0 and r_0 are permeability, porosity and radius, respectively. These relations are suitable for simulating fractal flow in radial geometry. Cossio et al. (2013) later modified the relations and made them possible to apply in linear geometry. The rectangular geometry is the centre of concern for us, because the theoretical and lab-

oratory analysis show that the dominant flow in hydraulically stimulated reservoir is linear flow. Therefore, fractal porosity/permeability relations in cartesian coordinates takes the following form,

$$\phi(x) = \phi_0 \left(\frac{x}{x_w}\right)^{D-d} \tag{5.5}$$

$$k(x) = k_0 \left(\frac{x}{x_w}\right)^{D-\theta-d} \tag{5.6}$$

where, k_w, ϕ_w and x_w are the permeability , porosity and the distance from a specified point in a fractal reservoir defined in cartesian coordinate. A handful of studies have been carried out to implement the fractal distribution of porosity/permeability in multifractured flow modelling (Fan & Ettehadtavakkol, 2017a; Wang, Shahvali, & Su, 2015; Fan & Ettehadtavakkol, 2017b). The relations applied to the geometry of rectangular multi-fractured reservoirs are given as,

$$k(y) = k_i \left(\frac{y}{w_{FH}}\right)^{H-E-\theta} \tag{5.7}$$

$$\phi(y) = \phi_i \left(\frac{y}{w_{FH}}\right)^{H-E} \tag{5.8}$$

where, k_i and ϕ_i the permeability and porosity at the distance of w_{FH}; $_{FH}$ is the half-width of the primary fracture plane. H is the Hausdorff dimension or fractal dimension and θ is the tortuosity index or connectivity index. These relations have been employed in this study to define the distribution of porosity and permeability of branch-fracture in SRV. The assumption of fluid influx from USRV to SRV matrix provided an ease in the mathematical formulation of previous models. However, unlike the previous analytical models, the presented model takes the fluid influx directly from the USRV to the fractal network into account. The analytical complexities has been carefully resolved by applying Bessel functions and Laplace transformations.

The fractal dimension H and the tortuosity index θ have a significant impact on the distribution of the meduim properties. Figure 5.1 shows a branch fracture permeability field and the effect of k_i on the distribution of the fields.
The dimension H describes how rough, irregular and disordered the object is and the tortuosity index θ characterizes diffusion process in that medium. Higher values of

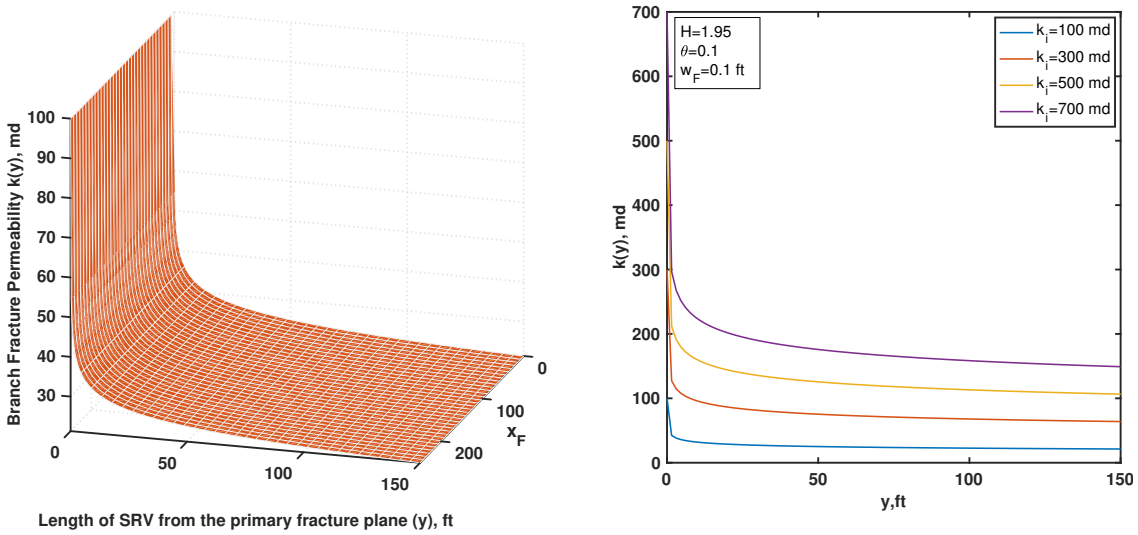

Figure 5.1: Fractal branch-fracture permeability field (left); The variation of fields in terms of different k_i (right)

θ indicate that significant hindrance would be experience by the fluid if a pressure differential exists in that media. This geometric property indicate classical random walk diffusion when θ equals to zero and more general continuous walk diffusion when θ is greater than zero(Cossio et al., 2013). The exact physical meaning and connection between θ and H may be identified through exhaustive investigation through mathematics and Fractal theory, which is beyond the objective of this study.

Figure 5.2 presents the impact of the fractal dimension and the tortuosity index in the branch fracture permeability field. The idea behind the properties distribution equation is that the branch-fracture with fractal dimension is embedded in a medium with dimension 2 (Euclidean dimension). As the value of H with a fixed θ decreases from the embedded dimension E, the network becomes more complex and irregular ultimately inducing a gradual decrease in permeability. However, when the value of H becomes larger than the embedded dimension E, it starts to behave like a piece of volume rather than an area with dimension 2 and enhances the permeability of the field. The figure 5.2 shows a gradually-increasing permeability field when H equals 2.1. On the other hand, as the value of θ increases from 0, the permeability field exhibit greater hindrance to the flow and a significant decrease in the trends of permeability fields.

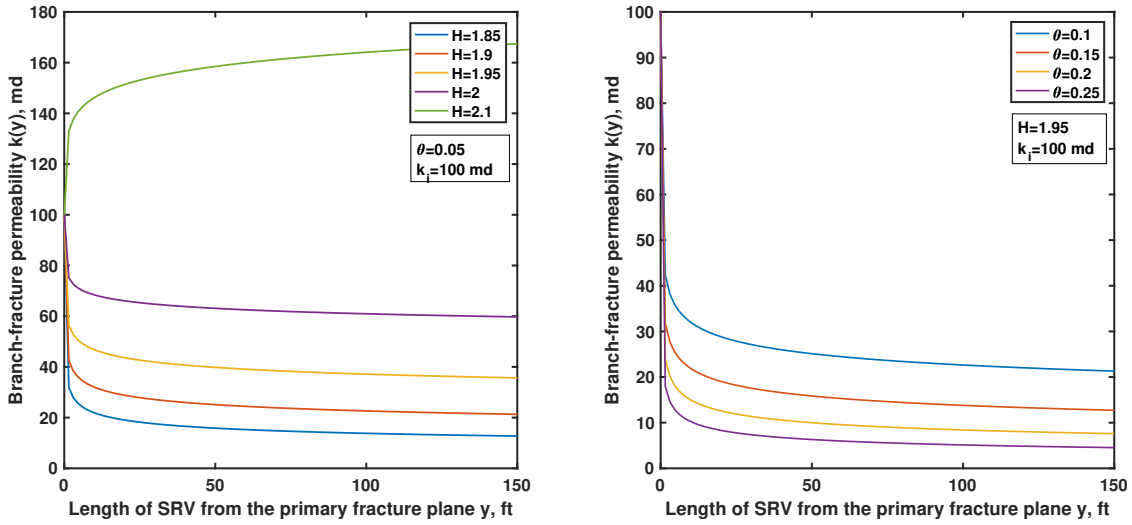

Figure 5.2: Effect of fractal dimension (left) and tortuosity index (right) on branch-fracture permeability

5.3 Model Description and Solution

This section presents a fractal branch-fracture model coupling two important concepts in the modelling of heterogenous media. Figure 5.3 illustrates the development and idealization of the geometry of fractal-branch fracture flow model. The branch-fractures with fractal dimension H are embedded in the matrix with Euclidean dimension E. In this model, we assume that the effect of outer reservoir is negligible due to the extreme low permeability of unconventional matrix. The semi-analytical solution is based on the following assumptions:

- The reservoir is rectangular with closed boundaries and with a fractured horizontal well in the center of the reservoir.
- The formation permeability is so low that the effect of outer reservoir can be neglected.
- The primary hydraulic fractures are transverse, fully-penetrated and finitely conductive in nature.
- Multiple transverse fracture interaction is modelled using symmetry with no-flow boundaries

- The fluid is single phase oil or gas.

- The matrix does not produce to the well

- Pressure loss inside the horizontal well is negligible

The symmetry element of the multifractured horizontal well (illustrated in Figure 5.3) is composed of three flow regions: unstimulated reservoir volume (USRV), stimulated reservoir volume (SRV) and a primary hydraulic fracture. In the derivation of the fractal branch fracture flow model, we exploit the Darcy's law and fractional flux law to define normal and subdiffusion, respectably.

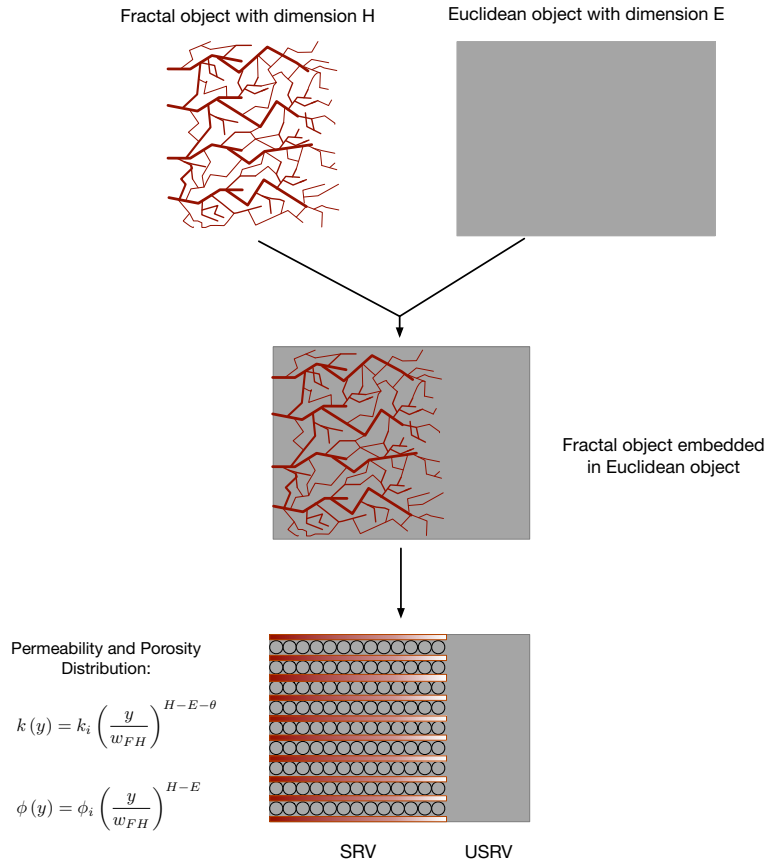

Figure 5.3: Idealization of the fractal branch fracture property distribution in fractured reservoir; Branch-fractures with fractal dimension and matrix with euclidean dimension (Top); Branch-fractures embedded in matrix (Middle); Symmetry element of the multifractured horizontal well with spherical matrix and slabs of branch-fractures (Bottom)

The mass balance or continuity equation with a source which continuously feeds influx of fluid into the representative elementary volume, could be written as,

$$\nabla \cdot (\rho \vec{v}) + \dot{Q_m} = -\frac{\partial (\phi \rho)}{\partial t} \tag{5.9}$$

where ρ =fluid density, $\vec{v}$ =superficial fluid velocity, ϕ = porosity of the medium and $\dot{Q_m}$ denotes the source term from the contiguous fracture/matrix segment representing the influx of mass into the control volume for a time interval of dt. Expanding the equation (5.9) and introducing the concept of isothermal compressibility,

$$\rho (\nabla \cdot \vec{v}) + \vec{v} \cdot (\nabla \rho) + \rho \dot{Q} = -\rho \phi (y) c_t \frac{\partial p}{\partial t} \tag{5.10}$$

$\vec{v} \cdot (\nabla \rho)$ term in equation (5.10) can be neglected for the slightly compressible fluid. The equation (5.10) now reduces to,

$$\rho (\nabla \cdot \vec{v}) + \rho \dot{Q} = -\rho \phi (y) c_t \frac{\partial p}{\partial t} \tag{5.11}$$

The equation (5.11) presents a basic diffusivity equation for fluid flow in porous media. The definition of velocity term ($\vec{v}$) in equation (5.11) varies with the assumption of the diffusion characteristics in the medium of interest. For normal or classical diffusion, Darcy's law defines the fluid transport. Darcy's law:

$$\vec{v_n} = -\frac{k}{\mu} (\nabla p) \tag{5.12}$$

As the dominant fluid flow in unconventional matrix conituum is sub-diffusion, a fractional velocity term should be used in the 5.11. Assuming a Continuous-Tine-Random-Walk process in the particle displacement of the diffusion in porous media, a fractional velocity equation incorporating subdiffusion is given by (Fomin et al., 2011; C. Chen & Raghavan, 2015; Raghavan, 2011),

$$\vec{v_s} = -\frac{k_\beta}{\mu} \frac{\partial^{1-\beta}}{\partial t^{1-\beta}} \frac{\partial p}{\partial y} \tag{5.13}$$

The following segments discuss the fluid transport and governing diffusivity equations for each flow regions in detail.

Table 5.2: Scaled and dimensionless variables used in the formulation of Fractal Branch-fracture Flow model

Dimensionless and Scaled Variables	
Dimensionless length in the y-direction	$y_D = \frac{y}{x_F}$
Dimensionless radius	$r_D = \frac{r}{x_F}$
Scaled pressure	$p_D = \frac{2\pi k_i h_{ft}(p-p_i)}{qB\mu} = \frac{2\pi k_i h_{ft}}{qB\mu}(\Delta p)$
Scaled time	$t_D = \frac{k_i t}{(\phi\mu c_t)_i} x_F^2 = \left(\frac{\eta_i}{x_F^2}\right) t$
Scaled flowrate	$q_D = \frac{qB\mu}{2\pi k_i h_{ft}(p-p_i)} = \frac{qB\mu}{2\pi k_i h_{ft}(\Delta p)}$
Dimensionless diffusivity	$\eta_D = \frac{\eta}{\eta_i}$
Hydraulic fracture conductivity	$C_{FD} = \frac{k_F w_F h}{k_i x_F h_{ft}}$
Bulk permeability at $y = y_1$	$\tilde{k}_1 = \frac{k_\beta h_{ft}}{h}$

5.3.1 Transport in USRV

USRV region contains inherent formation characteristics and extends from the no-flow region to the boundary of the SRV region. We assume that the pre-existing natural fractures and ultralow unconventional matrix creates a flowfield which is non-gaussian and could be best described by subdiffusion phenomena. The governing diffusivity equation in USRV can be derived from equation (5.11) and (5.13),

$$\frac{\partial}{\partial x}\left(\frac{k_\beta}{\mu}\frac{\partial^{1-\beta}}{\partial t^{1-\beta}}\frac{\partial \Delta p_u}{\partial x}\right) = (\phi c_t)\frac{\partial \Delta p_u}{\partial t} \tag{5.14}$$

☐ Initial condition (Pressure difference Δp_u at $t = 0$):

$$\Delta p_u|_{t=0} = 0 \tag{5.15}$$

☐ Boundary condition 1 (No flow boundary at $y = y_2$):

$$\left.\frac{\partial \Delta p_u}{\partial y}\right|_{y=y_2} = 0 \tag{5.16}$$

☐ Boundary condition 2 (Pressure continuity at the interface of SR branch-fracture and SRV):

$$\left(\overline{p}_i\right)|_{y=y_1} = \left(\overline{p}_u\right)|_{y=y_1} \tag{5.17}$$

The diffusivity equation in (5.14) is solved for the initial and boundary conditions in equation (5.15), (5.16) and (5.17) by applying Laplace transform. The derived pressure solution for USRV is,

$$\left.\frac{\partial \overline{p}_{uD}}{\partial y_D}\right|_{y_D=y_{1D}} = -\left.\overline{p}_{iD}\right|_{y_D=y_{1D}} \sqrt{\epsilon_u}\tanh\left[\sqrt{\epsilon_u}\left(y_{2D}-y_{1D}\right)\right] \tag{5.18}$$

5.3.2 Transport in SRV

The SRV flow region is composed of repetitive matrix medium and fractal branch-fracture slabs. Unlike all the other fractal flow models, we assume fluid flows directly to the SRV branch-fractures and there is no flow transfer from USRV to SRV matrix. Fluid flow in SRV fractures consists of flux from matrix medium, total flow from USRV and the flow from itself. The flow in the fractal branch-fracture is assumed to be one-dimensional and perpendicular to the primary fracture plane.

Transport in Spherical Matrix

The matrix medium in SRV is assumed to be composed of repetitive array of spherical matrix. The governing diffusivity equation for spherical matrix can be written as,

$$\frac{1}{r^2}\frac{\partial}{\partial r}\left(r^2\frac{k_\beta}{\mu}\frac{\partial^{1-\beta}}{\partial t^{1-\beta}}\frac{\partial \Delta p_m}{\partial r}\right) = \left(\phi c_t\right)_\beta \frac{\partial \Delta p_m}{\partial t} \tag{5.19}$$

The diffusivity equation (eq. (5.19)) is subjected to the following boundary conditions,

☐ Boundary condition 1

$$\begin{aligned} \Delta p_m\left(r=0,t\right) &= 0 \\ \overline{M_D}\left(r_D=0,\ s\right) &= 0 \end{aligned} \tag{5.20}$$

☐ Boundary condition 2 (Pressure continuity at the interface of spherical matrix

and branch-fracture medium)

$$\overline{p_{mD}}|_{r_D=r_{mD}} = \overline{(p_{iD})}\Big|_{r_D=r_{mD}} \tag{5.21}$$

The diffusivity equation in (5.19) is solved for the boundary conditions in equation (5.40) and (5.41) by applying Laplace transform. The derived pressure solution for SRV spherical matrix is,

$$\overline{p}_{mD} = \frac{r_{mD}}{r_D} \frac{\sinh\left(\sqrt{\epsilon_m}\, r_D\right)}{\sinh\left(\sqrt{\epsilon_m}\, r_{mD}\right)} \; (\overline{p}_{iD})|_{r_D=r_{mD}} \tag{5.22}$$

Transport in Fractal Branch-fracture

The fluid transport in the branch-fractures is sensitive to the variation of permeability and porosity. The distribution of porosity and permeability is given in equation (5.7) and (5.8). The diffusivity equation for branch-fracture with matrix medium as a fluid source can be derived from (5.11) and (5.12):

$$\frac{\partial}{\partial y}\left[\frac{k\,(y)}{\mu}\frac{\partial \Delta p_i}{\partial y}\right] + \dot{Q} = \phi\,(y)\, c_t \frac{\partial \Delta p_i}{\partial t} \tag{5.23}$$

Where $\dot{Q}$ accounts for the influx of fluid from the array of spherical matrix. Substituting (5.7) and (5.8) in (5.23):

$$\frac{k_i}{\mu}\left(\frac{y}{w_{FH}}\right)^{H-E-\theta}\left[\frac{H-E-\theta}{y}\frac{\partial \Delta p_i}{\partial y} + \frac{\partial^2 \Delta p_i}{\partial y^2}\right] + \dot{Q} = \phi_i \left(\frac{y}{w_{FH}}\right)^{H-E} c_t \frac{\partial \Delta p_i}{\partial t} \tag{5.24}$$

According to de Swaan O et al. (1976), the matrix source term should be the ratio of the total flux across the surface of a spherical matrix to the half of the fracture volume envelope around each sphere. Therefore, the source term $\dot{Q}$ that accounts for matrix influx can be written as:

$$\dot{Q} = -\frac{2k_\beta}{\mu h_f}\frac{\partial^{1-\beta}}{\partial t^{1-\beta}} \left.\frac{\partial \Delta p_m}{\partial r}\right|_{r=r_m} \left(\frac{y}{w_{FH}}\right)^{H-E} \tag{5.25}$$

Substituting equation (5.25) in equation 5.24:

$$\frac{k_i}{\mu}\left[\frac{H-E-\theta}{y}\frac{\partial \Delta p_i}{\partial y}+\frac{\partial^2 \Delta p_i}{\partial y^2}\right]-\frac{2k_\beta}{\mu h_f}\frac{\partial^{1-\beta}}{\partial t^{1-\beta}}\left.\frac{\partial \Delta p_m}{\partial r}\right|_{r=r_m}\left(\frac{y}{w_{FH}}\right)^\theta = \phi_i\left(\frac{y}{w_{FH}}\right)^\theta c_t\frac{\partial \Delta p_i}{\partial t} \tag{5.26}$$

Transforming the equation (5.26) into dimensionless form utilizing the definition of dimensionless variables listed in Table 5.2,

$$\left[\frac{H-E-\theta}{y_D}\frac{\partial p_{iD}}{\partial y_D}+\frac{\partial^2 p_{iD}}{\partial y_D^2}\right]-\frac{2k_\beta}{h_{fD}k_i}\left(\frac{\eta_i}{x_F^2}\right)^{1-\beta}\frac{\partial^{1-\beta}}{\partial t_D^{1-\beta}}\left.\frac{\partial p_{mD}}{\partial r_D}\right|_{r_D=r_{mD}}\left(\frac{y_D}{w_{HD}}\right)^\theta = \left(\frac{y}{w_{HD}}\right)^\theta\frac{\partial p_{iD}}{\partial t_D} \tag{5.27}$$

Taking Laplace transform of the both sides of equation (5.27) yields,

$$\left[\frac{H-E-\theta}{y_D}\frac{\partial \overline{p}_{iD}}{\partial y_D}+\frac{\partial^2 \overline{p}_{iD}}{\partial y_D^2}\right]-\frac{2k_\beta}{h_{fD}k_i}\left(\frac{\eta_i}{x_F^2}\right)^{1-\beta}\left.\frac{\partial \overline{p}_{mD}}{\partial r_D}\right|_{r_D=r_{mD}}s^{1-\beta}\left(\frac{y_D}{w_{HD}}\right)^\theta = \left(\frac{y}{w_{HD}}\right)^\theta s\overline{p}_{iD} \tag{5.28}$$

From the pressure solution for spherical matrix given in (5.22), we can derive,

$$\left.\frac{\partial \overline{p}_{mD}}{\partial r_D}\right|_{r_D=r_{mD}} = \frac{\overline{p}_{iD}|_{r_D=r_{mD}}}{r_{mD}}\left[r_{mD}\sqrt{\epsilon_m}\coth\left(\sqrt{\epsilon_m}\right)-1\right] \tag{5.29}$$

Substituting equation 5.29 in the equation 5.28 and identifying the terms that are independent of y_D and lumping them into as a function of s variable,

$$\left[\frac{H-E-\theta}{y_D}\frac{\partial \overline{p}_{iD}}{\partial y_D}+\frac{\partial^2 \overline{p}_{iD}}{\partial y_D^2}\right]-\epsilon_i y_D^\theta \overline{p}_{iD}=0 \tag{5.30}$$

The equation 5.30 is the general form of the double porosity fractal diffusivity equation. Where,

$$\epsilon_i = \frac{2k_\beta}{h_{fD}k_i r_{mD}}\left(\frac{\eta_i}{x_F^2}s\right)^{1-\beta}\left(\frac{1}{w_{HD}}\right)^\theta\left[r_{mD}\sqrt{\epsilon_m}\coth\left(\sqrt{\epsilon_m}\right)-1\right] \tag{5.31}$$

The equation 5.30 is analogous to the general form of the modified Bessel equation. The general solution can be obtained in terms of modified Bessel functions, K_ν and I_ν.

$$\overline{p}_{iD} = y_D^a \left[C_1 I_\nu \left(b y_D^c \right) + C_2 K_\nu \left(b y_D^c \right) \right] \tag{5.32}$$

In the equation 5.32, a, b and c are the lumped parameter of θ, H and ϵ_i and C_1 and C_2 are the constants to be determined from the boundary conditions.

$$a = \left(\frac{\theta + 3 - H}{2} \right) \qquad b = \left(\frac{2\sqrt{\epsilon_i}}{\theta + 2} \right)$$
$$c = \left(\frac{\theta + 2}{2} \right) \qquad \nu = \left(\frac{\theta + 3 - H}{\theta + 2} \right)$$

- Boundary condition 1 (Flux continuity at the interface of SRV branch fracture and USRV)

$$q_i|_{y=y_1} = q_u|_{y=y_1} \tag{5.33}$$

- Boundary condition 2 (Pressure continuity at the interface of SRV branch-fracture and primary hydraulic fracture)

$$\Delta p_i|_{y=w_F/2} = \Delta p_F|_{y=w_F/2} \tag{5.34}$$

Applying the fractional flux law stated in equation (5.13) into equation (5.33) results in,

$$\left. \frac{\partial \overline{p}_{iD}}{\partial y_D} \right|_{y_D = y_{1D}} = \frac{k_\beta}{\tilde{k}_1} \left(\frac{\eta_i}{x_F^2} s \right)^{1-\beta} \left. \frac{\partial \overline{p}_{uD}}{\partial y_D} \right|_{y_D = y_{1D}} \tag{5.35}$$

where, k_1 represents the intrinsic branch-fracture permeability evaluated at $y = y_1$

$$\tilde{k}_1 = k_i \left(\frac{y_1}{w_{FH}} \right)^{H-E-\theta} \tag{5.36}$$

Recalling the pressure solution for USRV given in (**??**),

$$\left. \frac{\partial \overline{p}_{uD}}{\partial y_D} \right|_{y_D = y_{D1}} = - \left. p_{iD} \right|_{y_D = y_{D1}} \sqrt{\epsilon_u} \tanh \left[\sqrt{\epsilon_u} \left(y_{2D} - y_{1D} \right) \right] \tag{5.37}$$

In the equation (5.37), ϵ_u contains USRV attributes.

$$\epsilon_u = \left(\frac{x_F^2}{\eta_\beta}\right)\left(\frac{\eta_i}{x_F^2}\right)^\beta s^\beta \tag{5.38}$$

Differentiating the equation (5.32) and evaluating at $y_D = y_{1D}$,

$$\left.\frac{\partial \overline{p}_{iD}}{\partial y_D}\right|_{y_D=y_{1D}} = \sqrt{\epsilon_i} y_{1D}^{a+c-1}\left[C_1 I_{\nu-1}\left(b y_{1D}^c\right) - C_2 K_{\nu-1}\left(b y_{1D}^c\right)\right] \tag{5.39}$$

Substituting the equations (5.39) and 5.37 in the equation (5.35),

$$\begin{aligned} -\frac{k_\beta}{\tilde{k}_1\sqrt{\epsilon_u}}\left(\frac{\eta_i}{x_F^2}s\right)^{1-\beta} &\tanh\left\{\sqrt{\epsilon_u}\left(y_{2D}-y_{1D}\right)\right\}\overline{p}_{iD}\big|_{y_D=y_{1D}} \\ &= \sqrt{\epsilon_i} y_{1D}^{a+c-1}\left[C_1 I_{\nu-1}\left(b y_{1D}^c\right) - C_2 K_{\nu-1}\left(b y_{1D}^c\right)\right] \end{aligned} \tag{5.40}$$

Identifying parameters that remain constant and lumping them into a single parameter, ϵ_α

$$\epsilon_\alpha\, \overline{p}_{iD}\big|_{y_D=y_{1D}} = \left[C_2 K_{\nu-1}\left(b y_{1D}^c\right) - C_1 I_{\nu-1}\left(b y_{1D}^c\right)\right] \tag{5.41}$$

Where,

$$\epsilon_\alpha = \left[\frac{k_\beta}{\tilde{k}_1\sqrt{\epsilon_u}}\left(\frac{\eta_i}{x_F^2}s\right)^{1-\beta}\tanh\left\{\sqrt{\epsilon_u}\left(y_{2D}-y_{1D}\right)\right\}\right] \tag{5.42}$$

Now we recall the general solution (eq. (5.32)) to the fracture diffusivity equation. Evaluating the equation (5.32) at $y_D = y_{1D}$ yields,

$$\bar{p}_{iD}\big|_{y_D=y_{1D}} = y_{1D}^a\left[C_1 I_\nu\left(b y_{1D}^c\right) + C_2 K_\nu\left(b y_{1D}^c\right)\right] \tag{5.43}$$

Rearranging the equation (5.43) and evaluating for C_1,

$$C_1 = \frac{\overline{p}_{iD}\big|_{y_D=y_{1D}}}{y_{1D}^a I_\nu\left(b y_{1D}^c\right)} - \frac{K_\nu\left(b y_{1D}^c\right)}{I_\nu\left(b y_{1D}^c\right)} C_2 \tag{5.44}$$

From equation (5.41) and (5.44), we solve for C_2,

$$C_2 = \left[\frac{\epsilon_\alpha y_{1D}^a I_\nu\left(b y_{1D}^c\right) + I_{\nu-1}\left(b y_{1D}^c\right)}{K_{\nu-1}\left(b y_{1D}^c\right) I_\nu\left(b y_{1D}^c\right) + K_\nu\left(b y_{1D}^c\right) I_{\nu-1}\left(b y_{1D}^c\right)}\right]\overline{p}_{iD}\big|_{y_D=y_{1D}} \tag{5.45}$$

Identifying constants in equation (5.44) and (5.45) and letting

$$A = \left[\frac{\epsilon_\alpha y_{1D}^a I_\nu\left(by_{1D}^c\right) + I_{\nu-1}\left(by_{1D}^c\right)}{K_{\nu-1}\left(by_1 D^c\right) I_\nu\left(by_{1D}^c\right) + K_\nu\left(by_{1D}^c\right) I_{\nu-1}\left(by_{1D}^c\right)}\right] \tag{5.46}$$

$$B = \left[\frac{1}{y_{1D}^a I_\nu\left(by_{1D}^c\right)} - \frac{K_\nu\left(by_{1D}^c\right)}{I_\nu\left(by_{1D}^c\right)} A\right] \tag{5.47}$$

Substituting A and B in equation (5.44) and (5.45) results in,

$$C_2 = A\,\overline{p}_{iD}|_{y_D=y_{1D}} \qquad\qquad C_1 = B\,\overline{p}_{iD}|_{y_D=y_{1D}}$$

The integration constants C_1 and C_2 were carefully written in terms of $\overline{p}_{iD}|_{y_D=y_{1D}}$ to facilitate the solution. Now, writing the general solution equation (5.33) in terms of $\overline{p}_{iD}|_{y_D=y_{1D}}$,

$$\overline{p}_{iD} = y_D^a\left[BI_\nu\left(by_D^c\right) + AK_\nu\left(by_D^c\right)\right] \tag{5.48}$$

Applying the 2$^{\text{nd}}$ boundary condition from equation (5.34) in equation (5.48), we obtain the pressure solution for the fluid transport in branch-fracture network.

$$\overline{p}_{iD} = \frac{y_D^a\left[BI_\nu\left(by_D^c\right) + AK_\nu\left(by_D^c\right)\right]}{\left(\frac{w_D}{2}\right)^a\left[BI_\nu\left\{b\left(\frac{w_D}{2}\right)^c\right\} + AK_\nu\left\{b\left(\frac{w_D}{2}\right)^c\right\}\right]} \tag{5.49}$$

Now, we derive the derivative of equation (5.49) and evaluate it at $y_D = w_D/2$. We will need this result to derive the final wellbore solution in primary fracture flow region.

$$\frac{\partial\overline{p}_{iD}}{\partial y_D} = \sqrt{\epsilon_i}\left(\frac{w_D}{2}\right)^{c-1}\left[\frac{D\ I_{\nu-1}\left(X_0\right) - C\ K_{\nu-1}\left(X_0\right)}{D\ I_\nu\left(X_0\right) + C\ K_\nu\left(X_0\right)}\right](\overline{p_{FD}})|_{y_D=w_D/2} \tag{5.50}$$

Here, the argument, X_0, in the Bessel functions I and K is,

$$X_0 = b\left(\frac{w_D}{2}\right)^c \tag{5.51}$$

Identifying the constants and lumping into a single term,

$$\epsilon_\gamma = \sqrt{\epsilon_i}\left(\frac{w_D}{2}\right)^{c-1}\left[\frac{D\ I_{\nu-1}(X_0) - C\ K_{\nu-1}(X_0)}{D\ I_\nu(X_0) + C\ K_\nu(X_0)}\right] \tag{5.52}$$

The equation (5.50) reduces to:

$$\frac{\partial \overline{p}_{iD}}{\partial y_D} = \epsilon_\gamma\ (\overline{p_{FD}})|_{y_D = w_D/2} \tag{5.53}$$

Therefore, the equation (5.53) is ready to be coupled with the pressure solution of primary hydraulic fracture. In this equation ϵ_γ carries all the transport information from SRV matrix, branch-fracture and USRV to the hydraulic fracture pressure solution.

5.3.3 Transport in Primary Hydraulic Fracture

In this study, primary hydraulic fracture is idealized as a vertical slab intersecting the horizontal wellbore. This medium is well connected and provides less hindrance to flow. Therefore, the diffusion phenomena can be defined by using classical diffusion formula. Fluid flows linearly from fractal branch-fracture network to hydraulic fracture in the y-direction, then flows along the x-direction to the wellbore. Flow inside the hydraulic fracture is also assumed linear. The Governing diffusivity equation for hydraulic fracture flow region can be written as,

$$\frac{\partial}{\partial x}\left(\frac{k_F}{\mu}\frac{\partial \Delta p_F}{\partial x}\right) + \frac{\partial}{\partial y}\left(\frac{k_F}{\mu}\frac{\partial \Delta p_F}{\partial y}\right) = (\phi c_t)_F \frac{\partial \Delta p_F}{\partial t} \tag{5.54}$$

- ☐ Boundary condition 1 (Flux continuity at the interface of fractal branch-fracture and primary fracture region)

$$(q_F)|_{y=w_F/2} = (q_i)|_{y=w_F/2} \tag{5.55}$$

- ☐ Boundary condition 2 (Flux continuity at the interface of primary fracture plane and the wellbore)

$$\left(\frac{Bq_f}{4}\right)\Big|_{x=0} = (q_F)|_{x=0} \tag{5.56}$$

- ☐ Boundary condition 3 (No flow boundary at $x = x_1$)

$$\left(\frac{\partial \Delta p_F}{\partial x}\right)\Big|_{x=x_1} = 0 \tag{5.57}$$

Utilizing the flux continuity condition stated in (5.55), the effect from the fractal branch-fracture, Spherical matrix and USRV is incorporated to the hydraulic fracture diffusivity equation. Finally, utilizing boundary condition 2 and 3, we obtain the following wellbore pressure solution,

$$\overline{p}_{WD} = \frac{\pi}{s\ C_{FD}\ \sqrt{\epsilon_F}\tanh\left[\sqrt{\epsilon_F}\ \right]} \tag{5.58}$$

The equation (5.58) presents the constant rate solution for the buttomhole pressure of the fractal-branch fracture flow model in Laplace domain. It should be noted that the term ϵ_F carries the fluid depletion information from all the flow regions. The pressure solution terms for the regions other than hydraulic fracture are nested in ϵ_F. The full solution with all the model functions are summarized below,

$$\overline{p}_{WD} = \frac{\pi}{s\ C_{FD}\ \sqrt{\epsilon_F}\tanh\left[\sqrt{\epsilon_F}\ \right]}$$

$$\epsilon_F = \frac{s}{\eta_{FD}} - \frac{2}{C_{FD}}\epsilon_\gamma$$

$$\epsilon_\gamma = \sqrt{\epsilon_i}\left(\frac{w_D}{2}\right)^{c-1}\left[\frac{D\ I_{\nu-1}\left(X_0\right) - C\ K_{\nu-1}\left(X_0\right)}{D\ I_\nu\left(X_0\right) + C\ K_\nu\left(X_0\right)}\right]$$

$$A = \left[\frac{\epsilon_\alpha y_{1D}^a I_\nu\left(by_{1D}^c\right) + I_{\nu-1}\left(by_{1D}^c\right)}{K_{\nu-1}\left(by_1 D^c\right) I_\nu\left(by_{1D}^c\right) + K_\nu\left(by_{1D}^c\right) I_{\nu-1}\left(by_{1D}^c\right)}\right]$$

$$B = \left[\frac{1}{y_{1D}^a I_\nu\left(by_{1D}^c\right)} - \frac{K_\nu\left(by_{1D}^c\right)}{I_\nu\left(by_{1D}^c\right)}A\right]$$

$$\epsilon_\alpha = \left[\frac{k_\beta}{\tilde{k}_1\sqrt{\epsilon_u}}\left(\frac{\eta_i}{x_F^2}s\right)^{1-\beta}\tanh\left\{\sqrt{\epsilon_u}\left(y_{2D} - y_{1D}\right)\right\}\right]$$

$$\epsilon_i = \frac{2k_\beta}{h_{fD}k_i r_{mD}}\left(\frac{\eta_i}{x_F^2}s\right)^{1-\beta}\left(\frac{1}{w_{HD}}\right)^\theta\left[r_{mD}\sqrt{\epsilon_m}\coth\left(\sqrt{\epsilon_m}\right) - 1\right]$$

$$\epsilon_u = \left(\frac{x_F^2}{\eta_\beta}\right)\left(\frac{\eta_i}{x_F^2}\right)^\beta s^\beta$$

$$\epsilon_m = \left(\frac{x_F^2}{\eta_\beta}\right)\left(\frac{\eta_i}{x_F^2}\right)^\beta s^\beta$$

A computational code for the developed model equations was written in MATLAB and the model solution in real domain is obtained applying the multiprecision Gaver-Wynn-Rho algorithm in a symbolic environment to avoid the round-off error. In the subsequent segments, the analysis of the derived solution is presented.

5.4 Results and Field Applications

Horizontal well performance in a unconventional reservoir is governed by a numerous physical parameters as presented in the fractal model. The accurate computation of

these parameters always poses challenge to the engineers. Some of these parameters exhibits significant influence in the field scale observation and some presents negligible impact on production. A comprehensive sensitivity analysis of these important parameters is presented in this section. Finally, in order to validate the applicability of the presented model, the simulated response is matched with data from a well in the Eagle Ford Shale. The match and the evaluation of the constrained parameters is also presented in this section.

5.4.1 Sensitivity of Important Parameters

Effect of Fractal Dimension

We have learnt from the Section 5.2 that the branch-fractture permeability field is significantly affected by the fractal dimension H. Each different fractal dimension generates a distinct permeability field provided that the connectivity index θ is constant. The branch-fractures are the only flowing path in the SRV flow region. We have evaluated the pressure drop at the wellbore for fractal dimensions starting from 2 with an increment of 0.2. Figure 5.4 exhibits pressure responses of this model affected by fractal dimension H. As shown in Figure 5.2, the induced permeability field becomes more stimulated and enhanced when the fractal dimension is larger.

In Figure 5.4, the wellbore pressure drop (Δp) curves moves downward with the increase of the fractal dimension. As the value of H increases, the permeability of each point in the SRV fractures increases and subsequently hindrance to flow in SRV region decreases. The decrease in hindrance to flow in SRV region ultimately results in a decrease in pressure drop (Δp). In addition, the impact of fractal dimension on pressure response is evident throughout the entire production period. It also can be observed from the Figure 5.4, the impact of H is smaller at early times due to the fact that the early time flow is dominantly affected by the hydraulic fracture conductivity. However, the late time production is greatly affected by the variation of fractal dimension.

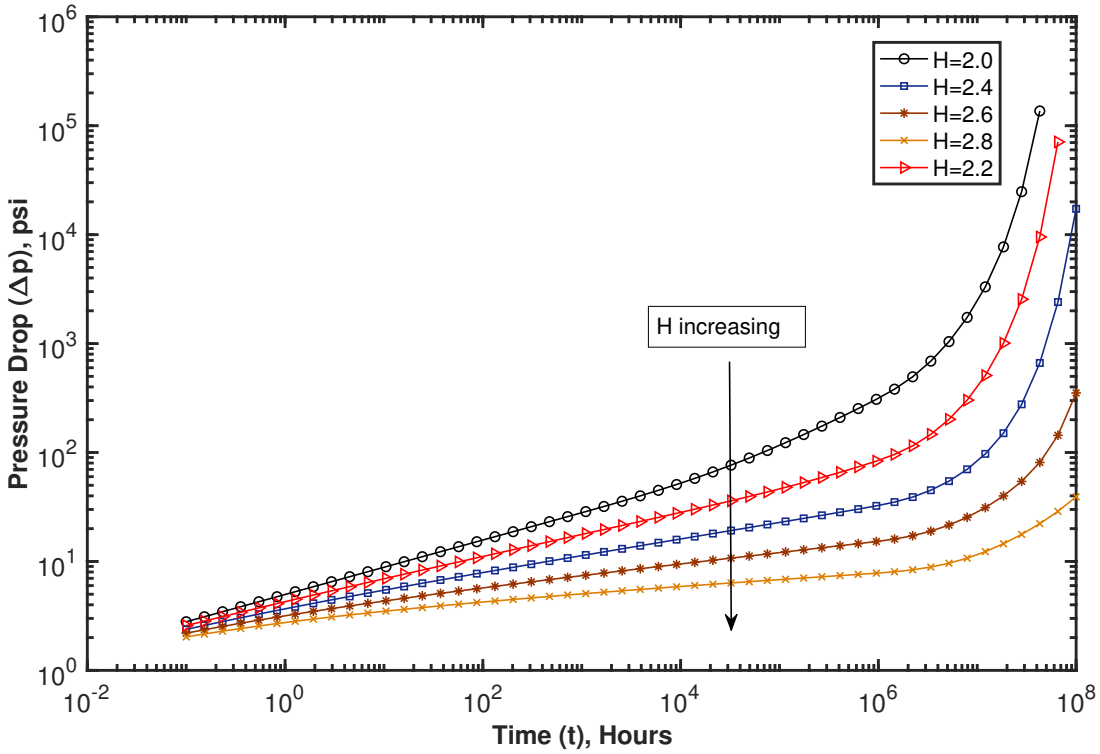

Figure 5.4: Effect of fractal dimension on the pressure drop behaviour

Effect of Tortuosity Index

Fractal theory suggests, fractal dimension shows how complex a branch-fracture network is, whereas the tortuosity index exhibits how well-connected a given fractal object is. Therefore, H and θ are independent and are unique of branch-fracture physical properties. The Figure 5.2 in section 5.2 illustrate the impact of tortuosity index on branch-fracture permeability field. It can be observed that the increase of θ induces the average decrease in induced fracture permeability. When $\theta = 0$, the diffusion process in the fractures is normal and the permeability field is only affected by the fractal dimension H. The impact of θ on the pressure drop responses (Δp) is presented in Figure 5.5.

In Figure 5.5, the pressure response curves move upward with the increase of θ. The increase of tortuosity index reflects the hindrance that the reservoir fluid is subjected to. In the curves with higher value of θ, two slopes are evident throughout the flowing period. These two slopes represents two characteristic flow regimes in the

reservoir. In early production times, the hydraulic fracture linear flow and HF-SRV bilinear flow is dominant. In addition, the impact of θ is more pronounced in the middle times of the production period.

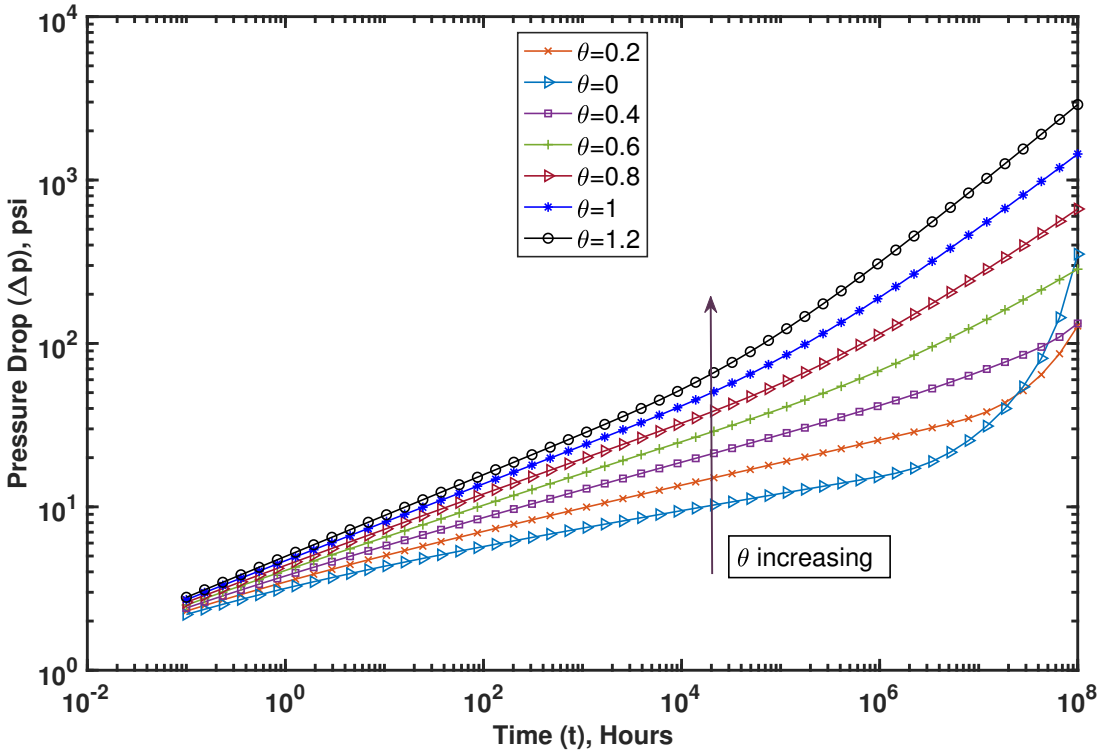

Figure 5.5: Effect of tortuosity index on the pressure drop behaviour

5.4.2 Analysis of Field Data

The presented fractal model was run to match the production history of an Eagle Ford shale well. The Eagle Ford is composed of organic-rich calcaerous mudstones and marls with payzone thickness ranging from 50 to 350 feet (Curnow, 2015). The monthly production data, pressure data, reservoir properties data and other important inputs are adopted from Albinali et al. (2016); Curnow (2015) and listed in Table 5.3. The well produces from three horizontal laterals. The monthly production rates were normalized based on the following premises: (i)Each lateral produces 33.3% of the total production, (ii) The properties of all hydraulic fractures are same and shares the stimulation efficiency and (iii)Average fracture spacing is based on the laterals stimulation design

Table 5.3: Model initialization with typical values for a horizontal well in Eagle Ford Shale (Curnow, 2015; Albinali et al., 2016)

Parameters	Typical values
Initial reservoir pressure, p_i, psi	5375
Flowing bottomhole pressure, p_{wf}, psi	800
Hydraulic fracture half-spacing, y_2, ft	170
Pay zone thickness, h, ft	150
Radius of spherical matrix, r_m, ft	0.5
Matrix porosity, ϕ_β,	0.1
Matrix permeability,k_β, md	0.0001
Total matrix compressibility, c_{mt}, psi^{-1}	1×10^{-5}
Average branch fracture aperture, h_f, ft	3×10^{-3}
Branch fracture compressibility, c_{fi},psi^{-1}	1×10^{-4}
Hydraulic fracture porosity, ϕ_F	0.38
Hydraulic fracture permeability, k_F	5×10^4
Hydraulic fracture compressibility, c_{tF}, psi^{-1}	1×10^{-5}
Hydraulic fracture aperture, w_F, ft	0.01
Fluid viscosity, μ, cp	0.5

First, the presented model is initialized with the measured data listed in Table 5.3. Some of these data are estimates of established models. The following parameters have been considered as constrained parameters that are to be evaluated from the match. The parameters are,

- ☐ Hydraulic fracture half-length, x_F
- ☐ Branch fracture permeability at the vicinity of primary fracture plane, k_i
- ☐ Branch fracture porosity at the vicinity of primary fracture plane, ϕ_i
- ☐ Fractal dimension of the branch-fracture network, H
- ☐ Tortuosity index, θ
- ☐ Matrix intrinsic permeability, k_β

The results of the production history matching for 39 months from October 2012 to January 2016 are presented in Figure 5.6. The knowledge from the sensitivity analysis was utilized to match the field data with the model response. The model shows convincing agreement with the field data. The evaluated fitting parameters are listed in Table 5.4.

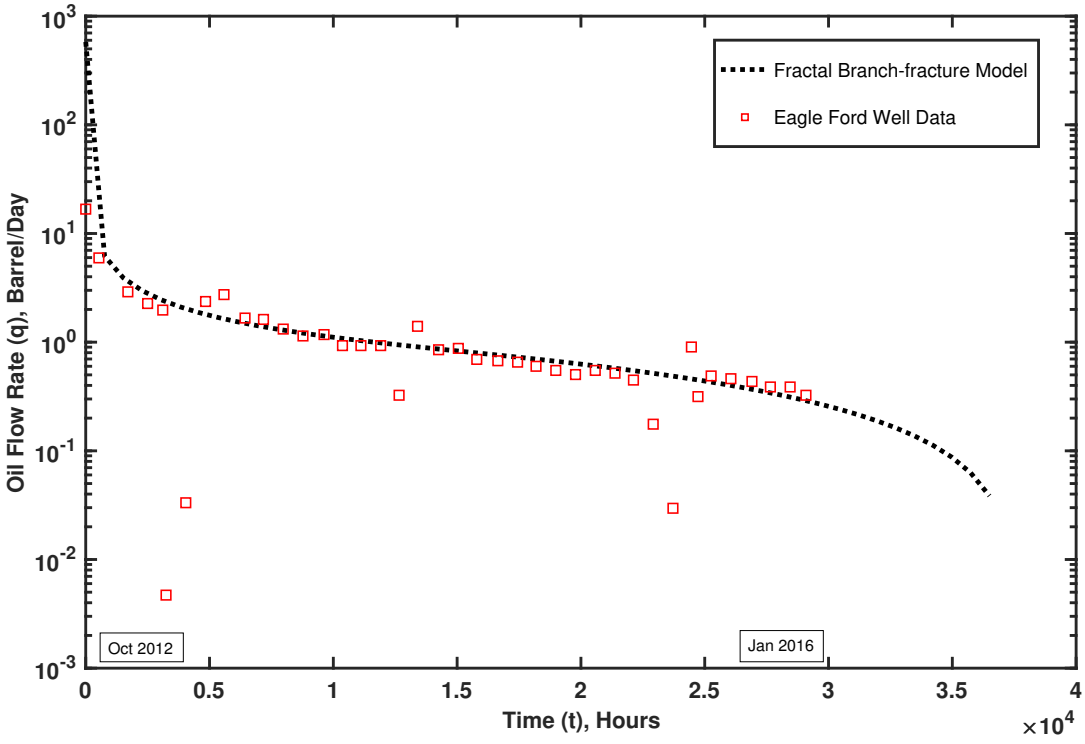

Figure 5.6: History matching results with the proposed fractal branch-fracture flow model

One of the most interesting features of this model is that it can glean important information about the SRV with providing k_i, H, θ and β. From the values of k_i, ϕ_i H and θ, the predicted branch-fracture permeability/porosity field is generated. Figure 5.7 presents the permeability and porosity field predicted by the proposed model.

A number of conclusions can be drawn from values evaluated by the model. An ineffective fracture network was generated by the stimulation job and the fracture. The fractures are extremely tortuous and provide significant hindrance to the flow. The fracturing job failed to reactivate the existing natural fractures and/or to generate new branch-fractures ultimately increasing the tortuosity index (θ=0.34) and decreas-

Table 5.4: Values of the constrained parameters determined from the history matching

Parameters	Matched values
Hydraulic fracture half-length, x_F, ft	540
Branch fracture permeability at the vicinity of primary fracture plane, k_i, md	0.1
Branch fracture porosity at the vicinity of primary fracture plane, ϕ_i	0.6
Tortuosity index, θ	0.34
Fractal dimension of the branch-fracture network, H	1.78
Matrix subdiffusion exponent, β	0.7
Effective SRV width, y_1, ft	140

ing fractal dimension (H=1.78). The stimulation job also failed to make the fractures traverse the total distance between fractures. Curnow (2015) also suggested that SRV has extremely low permeability by analyzing geo-mechanical effects in SRV. Albinali et al. (2016) matched the Eagle Ford well data with TADDP model and concluded that induced fractures have diffusion exponent of 0.2 which translates to significant hindrance to flow. The solution therefore is in good agreement with the existing standard models. The application of the presented model also revealed some important features of the SRV, which, to the best of our knowledge, was not investigated before with the Eagle Ford Shale well. The model match shows that effective SRV width is 140 feet whereas the half-spacing between two hydraulic fractures was considered 170 feet during stimulation. Therefore, there exists a region of width of 30 ft where the stimulation job did not generate any fracture network. Most of the trilinear models did not account for the USRV regions in a stimulated reservoirs. Neglecting the USRV may lead a forecast error as it posses entirely different characteristics from SRV. The width of effective SRV also indicates the efficacy of the fracturing design and could be accounted for in the next completion design. On the other hand, the matrix sub-diffusion exponent of 0.7 indicates the matrix provide less conductivity to the fluid flow. In order to achieve economic production rates in this formation, massive stimulation is required.

The possible further applications of the result generated by the proposed model

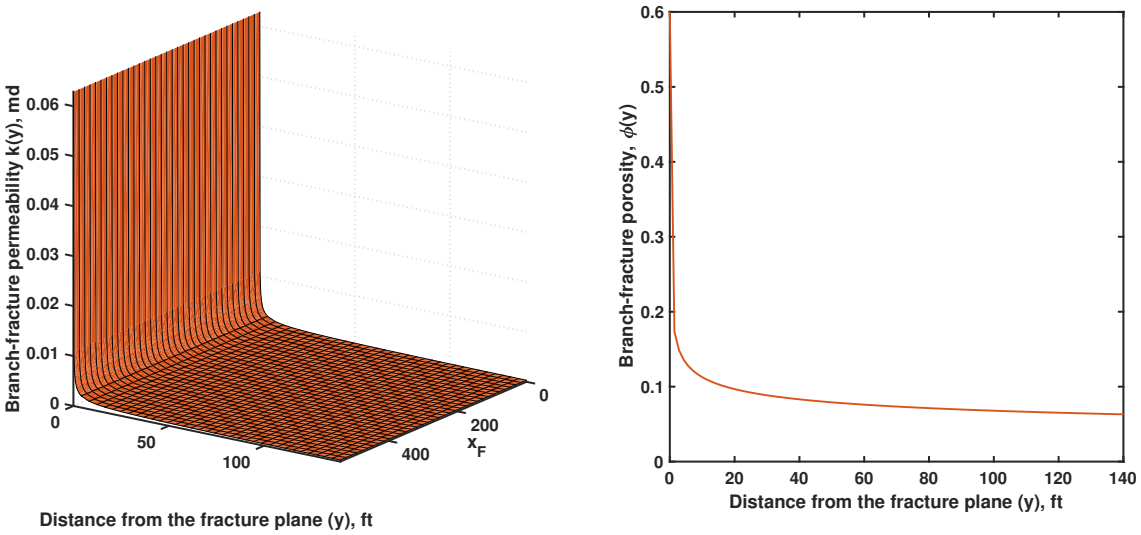

Figure 5.7: Branch-fracture peremability field (left); Branch-fracture porosity distribution (right)

can be summarized as:

- The porosity/permeability distribution can be taken as input to build a robust numerical simulator
- The values of k_i, H, θ and y_1 can be taken into account to make an investment plan for re-fracturing a existing well and/or completing a new well in the same formation
- The permeability field can be utilized to design completion plan in terms of optimum SRV width
- The optimum half-fracture spacing can be computed from the field and width
- The effective width can be utilized in the determination of injection fluid velocity so that the induced fractures can traverse the whole distance between fractures

5.5 Conclusion

In this Chapter, an upgraded fractal model for the analysis of production data with variable rate and borehole pressure for multifractured horizontal wells in ultralow

unconventional reservoirs is developed, which takes subdiffusive fluid transport snd USRV-branch-fracture flow into consideration.

The following conclusions are derived from the development and analysis of the fractal branch-fracture flow model:

- The novel fractal reservoir model, Fractal Branch-fracture model, idealizes the heterogeneity of ultralow multi-fractured reservoir by applying fractal characteristics of medium and subdiffusive behaviour of matrix. The availability of enough micro seismic data makes this model more efficient in determining other important properties of SRV and USRV.

- The proposed semi-analytical model incorporates the hindrance to flow in SRV by fractal characteristics of the medium and honours the physics of fluid flow in SRV by taking the flow from the USRV to branch fractures into account. The coupling of subdiffusion in the matrix enables the proposed fractal model to deliver comprehensive physical and flow characteristics of unconventional reservoirs.

- The proposed model confines its drainage region in the inner reservoir only as the ultra-low unconventional reservoir shows insignificant impact of outer reservoir on production behaviour. Hence, the number of constrained parameters to be evaluated decreases and evaluating more parameters regarding the SRV becomes feasible.

- The robustness of the semi-analytical model was tested, and the predictability of the fractal model was validated by matching 39 months of production history from Eagle Ford field data. The history matching shows excellent agreement during early, intermediate and late time production ultimately bolstering the basis of the model. The history matching with field data also provides important parameters such as SRV width, Matrix permeability and Fractal permeability field.

- The variability of diffusion phenomena as a result of geometric and temporal consequence was carefully characterized by the Fractal branch-fracture model

and therefore this model provides a solid tool to investigate and forecast performance of multifractured unconventional reservoirs.

Chapter 6

Conclusions and Future Research

In this research, the effect of branch-fracture permeability field and subdiffusion on the well performance of multifractured unconventional reservoirs were investigated.

This thesis presents two semi-analytical models for two distinct types of unconventional fractured reservoirs. In addition, an assessment of the widely used inverse Laplace methods was carried out to establish confidence in applying those methods in the solution of flow problems of fractured media. The novelty of the proposed models, findings of the research and the recommended future research works are discussed in the following sections.

Novel Features of the Proposed Models

- The proposed SIBFF model enables extracting more detailed information of the SRV such as branch-fracture permeability field, the size of the SRV and subdiffuisive characteristics of SRV matrix. The dimension of the outer reservoir can also be extracted from the production data interpretation. The comprehensive data extracted by matching the previous production history help evaluate and predict stimulation efficiency.

- The proposed fractal model for ultralow permeability reservoirs incorporates the hindrance to flow in SRV branch-fractures by fractal characteristics of the medium and honors the physics of fluid flow by taking USRV-fracture flow into account. Fluid flow from USRV matrix to SRV matrix is not realistic as assumed by the previous fractal models.

Conclusion

The following major conclusions are made by the work presented in this thesis:

- ☐ The proposed SIBFF model generalizes the standard models with uniform fracture permeability and normal diffusion. The solution of this model was accurately verified with a standard model, the TADDP model.

- ☐ Wellbore pressure drop is highly sensitive to the branch-fracture permeability field and it affects the production behaviour throughout the whole life of an unconventional reservoir. The generation of permeability field with high k_i and more complexity significantly enhances the production.

- ☐ History match of production data from Niobrara Field with the proposed SIBFF model gleans important physical parameters of SRV (y_1, k_i, $k_{\beta i}$ and β), USRV and outer reservoir.

- ☐ The proposed fractal model for ultralow permeability reservoirs couples temporal subdiffusion phenomena and fractal porosity/permeability distribution. The porosity and permeability distribution of branch-fractures, SRV width of the reservoir of Eagle Ford field was extracted from the production history match with the presented model. The parameters (High θ and low H) indicate that the stimulation job failed to generate effective network of branch-fractures.

- ☐ The parameters determined by applying the proposed models helps to evaluate efficiency of stimulation job, necessity of refracturing and the velocity of fracturing fluid.

Possible Future Research

The following approaches and measures to enhancement of the proposed two models can be employed to improve the performance,

* The semi-analytical solution derived in this work assumes that the horizontal well is intercepted by transverse hydraulic fracture. Extensions of the proposed models can be derived using non-planar non-uniform hydraulic fractures.

* The branch-fracture aperture is sensitive to the variation of the effective stress. The possible changes to the aperture, porosity and permeability for the variation of effective stress can be accounted for to obtain more realistic picture of the unconventional fractured reservoirs

Nomenclature

β	Subdiffusion exponent
ϵ	Model functions
η	Diffusivity
μ	Viscosity, cp
ν	The order of Bessel funcion
ϕ	Porosity
θ	Tortuosity index
$\tilde{k}$	Bulk permeability, md
B	Formation volume factor, rb/stb
c_t	Total compressibility, psi^{-1}
c_{mt}	total matrix compressibility, psi^{-1}
c_{tF}	Hydraulic fracture total compressibility, psi^{-1}
H	Hausdorff Fractal dimension
h	Reservoir thickness, ft
h_f	Branch-fracture aperture, ft
h_{ft}	Total branch-fracture fracture thickness
I	Modified Bessel function of the first kind

K	Modified Bessel function of the first kind
k	Permeability, md
k_i	Branch-fracture permeability at the vicinity of hydraulic fracture
k_β	Phenomenological constant
n_f	Number of branch-fractures
p	pressure
q_F	Single fracture flowrate, stb/day
r	Radius, ft
r_m	Radius of matrix, ft
s	Laplace variable
t_D	Dimensionless time
x	Distance in the x-direction, ft
x_F	Fracture half length, ft
y	Distance in the y-direction, ft
z	Distance in the z-direction, ft

References

Abate, J., & Valkó, P. P. (2004). Multi-precision laplace transform inversion. *International Journal for Numerical Methods in Engineering*, *60*(5), 979–993.

Abate, J., & Whitt, W. (1995). Numerical inversion of laplace transforms of probability distributions. *ORSA Journal on computing*, *7*(1), 36–43.

Acuna, J., & Yortsos, Y. (1991). Numerical construction and flow simulation in networks of fractures using fractal geometry. In *Spe annual technical conference and exhibition.*

Acuna, J. A., & Yortsos, Y. C. (1995). Application of fractal geometry to the study of networks of fractures and their pressure transient. *Water Resources Research*, *31*(3), 527–540.

Akkutlu, I. Y., Fathi, E., et al. (2012). Multiscale gas transport in shales with local kerogen heterogeneities. *SPE journal*, *17*(04), 1–002.

Albinali, A. (2016). *Analytical Solution for Anomalous Diffusion in Fractured Nano-Porous Reservoirs* (Unpublished doctoral dissertation). Colorado School of Mines.

Albinali, A., Ozkan, E., et al. (2016). Anomalous diffusion approach and field application for fractured nano-porous reservoirs. In *Spe annual technical conference and exhibition.*

Al-Ghamdi, A., & Ershaghi, I. (1996). Pressure transient analysis of dually fractured reservoirs. *Spe Journal*, *1*(01), 93–100.

Anderson, D. M., Nobakht, M., Moghadam, S., & Mattar, L. (2010). Analysis of production data from fractured shale gas wells. In *Spe unconventional gas*

conference.

Arps, J. J., et al. (1945). Analysis of decline curves. *Transactions of the AIME*, *160*(01), 228–247.

Barenblatt, G. I. (1962). The mathematical theory of equilibrium cracks in brittle fracture. In *Advances in applied mechanics* (Vol. 7, pp. 55–129). Elsevier.

Barton, C. C., & La Pointe, P. R. (2012). *Fractals in petroleum geology and earth processes*. Springer Science & Business Media.

Beier, R. A., et al. (1994). Pressure transient model of a vertically fractured well in a fractal reservoir. *SPE Formation Evaluation*, *9*(02), 122–128.

Bowman, F. (2012). *Introduction to bessel functions*. Courier Corporation.

Camacho Velazquez, R., Fuentes-Cruz, G., Vasquez-Cruz, M. A., et al. (2006). Decline curve analysis of fractured reservoirs with fractal geometry. In *International oil conference and exhibition in mexico.*

Caputo, M. (1998). 3-dimensional physically consistent diffusion in anisotropic media with memory. *Atti della Accademia Nazionale dei Lincei. Classe di Scienze Fisiche, Matematiche e Naturali. Rendiconti Lincei. Matematica e Applicazioni*, *9*(2), 131–143.

Chang, J., & Yortsos, Y. C. (1990). Pressure transient analysis of fractal reservoirs. *SPE Formation Evaluation*, *5*(01), 31–38.

Chen, C., & Raghavan, R. (2015). Transient flow in a linear reservoir for space–time fractional diffusion. *Journal of Petroleum Science and Engineering*, *128*, 194–202.

Chen, C.-C., et al. (1996). An approach to handle discontinuities by the stehfest algorithm. *SPE Journal*, *1*(04), 363–368.

Cho, Y., Eker, E., Uzun, I., Yin, X., Kazemi, H., et al. (2016). Rock characterization in unconventional reservoirs: A comparative study of bakken, eagle ford, and niobrara formations. In *Spe low perm symposium.*

Cossio, M., Moridis, G., Blasingame, T. A., et al. (2013). A semianalytic solution

for flow in finite-conductivity vertical fractures by use of fractal theory. *Spe Journal*, *18*(01), 83–96.

Curnow, J. S. (2015). *Coupled geomechanics and fluid flow model for production optimization in naturally fractured shale reservoirs*. Colorado School of Mines.

Davies, B., & Martin, B. (1979). Numerical inversion of the laplace transform: a survey and comparison of methods. *Journal of computational physics*, *33*(1), 1–32.

de Swaan O, A., et al. (1976). Analytic solutions for determining naturally fractured reservoir properties by well testing. *Society of Petroleum Engineers Journal*, *16*(03), 117–122.

Ezulike, D. O., & Dehghanpour, H. (2014). A model for simultaneous matrix depletion into natural and hydraulic fracture networks. *Journal of Natural Gas Science and Engineering*, *16*, 57–69.

Fan, D., & Ettehadtavakkol, A. (2017a). Analytical model of gas transport in heterogeneous hydraulically-fractured organic-rich shale media. *Fuel*, *207*, 625–640.

Fan, D., & Ettehadtavakkol, A. (2017b). Semi-analytical modeling of shale gas flow through fractal induced fracture networks with microseismic data. *Fuel*, *193*, 444–459.

Finjord, J., Aadnoy, B., et al. (1989). Effects of the quadratic gradient term in steady-state and semisteady-state solutions for reservoir pressure. *SPE Formation Evaluation*, *4*(03), 413–417.

Fomin, S., Chugunov, V., & Hashida, T. (2011). Mathematical modeling of anomalous diffusion in porous media. *Fract. Differ. Calc*, *1*(1), 1–28.

Fuentes-Cruz, G., Gildin, E., & Valkó, P. P. (2014). On the analysis of production data: Practical approaches for hydraulically fractured wells in unconventional reservoirs. *Journal of Petroleum Science and Engineering*, *119*, 54–68.

Fuentes-Cruz, G., Gildin, E., Valkó, P. P., et al. (2014). Analyzing production data from hydraulically fractured wells: the concept of induced permeability field. *SPE Reservoir Evaluation & Engineering*, *17*(02), 220–232.

Furman, A., & Neuman, S. P. (2003). Laplace-transform analytic element solution of transient flow in porous media. *Advances in Water Resources*, *26*(12), 1229–1237.

Gaver Jr, D. P. (1966). Observing stochastic processes, and approximate transform inversion. *Operations Research*, *14*(3), 444–459.

Ge, J., Ghassemi, A., et al. (2011). Permeability enhancement in shale gas reservoirs after stimulation by hydraulic fracturing. In *45th us rock mechanics/geomechanics symposium.*

Gray, J. (1977). Future gas reserve potential western canadian sedimentary basin. In *Canadian gas association's 3rd national technical conference, calgary, canada.*

Holy, R. W. (2016). *Numerical investigation of 1d anomalous diffusion in fractured nanoporous reservoirs* (Unpublished doctoral dissertation). Colorado School of Mines. Arthur Lakes Library.

Javadpour, F., Fisher, D., Unsworth, M., et al. (2007). Nanoscale gas flow in shale gas sediments. *Journal of Canadian Petroleum Technology*, *46*(10).

Kazemi, H., Merrill Jr, L., Porterfield, K., Zeman, P., et al. (1976). Numerical simulation of water-oil flow in naturally fractured reservoirs. *Society of Petroleum Engineers Journal*, *16*(06), 317–326.

La, N.-N. (2015). *Production analysis of oil production from unconventional reservoirs using bottom hole pressures entirely in the laplace space* (Unpublished doctoral dissertation).

Mayerhofer, M. J., Lolon, E. P., Youngblood, J. E., & Heinze, J. R. (2006). Integration of microseismic-fracture-mapping results with numerical fracture network production modeling in the barnett shale. In *Spe annual technical conference and exhibition.*

Metzler, R., Glöckle, W. G., & Nonnenmacher, T. F. (1994). Fractional model equation for anomalous diffusion. *Physica A: Statistical Mechanics and its Applications*, *211*(1), 13–24.

Odeh, A. (1965, Jan). Unsteady-state behavior of naturally fractured reservoirs.

Society of Petroleum Engineers Journal, *5*(01), 60-66. doi: 10.2118/966-pa

Ozcan, O. (2014a). *Fractional diffusion in naturally fractured unconventional reservoirs*. Colorado School of Mines.

Ozcan, O. (2014b). *Fractional Diffusion in Naturally Fractured Unconventional Reservoirs* (Unpublished doctoral dissertation). Colorado School of Mines.

Ozkan, E., Brown, M., Raghavan, R., & Kazemi, H. (2009). SPE 121290 Comparison of Fractured Horizontal-Well Performance in Conventional and Unconventional Reservoirs. *Society*, 1–16. Retrieved from `http://www.onepetro.org/mslib/app/Preview.do?paperNumber=SPE-121290-MS{\&}societyCode=SPE` doi: 10.2118/121290-MS

Palmer, I. D., Moschovidis, Z. A., Cameron, J. R., et al. (2007). Modeling shear failure and stimulation of the barnett shale after hydraulic fracturing. In *Spe hydraulic fracturing technology conference.*

Park, H., Choe, J., & Kang, J. (2000). Pressure behavior of transport in fractal porous media using a fractional calculus approach. *Energy Sources*, *22*(10), 881–890.

Raghavan, R. (2011). Fractional derivatives: application to transient flow. *Journal of Petroleum Science and Engineering*, *80*(1), 7–13.

Salzer, H. E. (1954). A simple method for summing certain slowly convergent series. *Studies in Applied Mathematics*, *33*(1-4), 356–359.

Sonnenberg, S. A. (2011). The niobrara petroleum system: a new resource play in the rocky mountain region.

Stalgorova, E., & Mattar, L. (2013). Analytical Model for Unconventional Multifractured Composite Systems. *SPE Reservoir Evaluation & Engineering*, *16*(03), 246–256.

Stehfest, H. (1970). Algorithm 368: Numerical inversion of laplace transforms [d5]. *Communications of the ACM*, *13*(1), 47–49.

Talbot, A. (1979). The accurate numerical inversion of laplace transforms. *IMA Journal of Applied Mathematics*, *23*(1), 97–120.

Taleghani, A. D., et al. (2011). Modeling simultaneous growth of multi-branch hydraulic fractures. In *45th us rock mechanics/geomechanics symposium.*

Uchaikin, V. V. (2013). *Fractional derivatives for physicists and engineers* (Vol. 2). Springer.

Van Everdingen, A., Hurst, W., et al. (1949). The application of the laplace transformation to flow problems in reservoirs. *Journal of Petroleum Technology*, *1*(12), 305–324.

Wang, W., Shahvali, M., & Su, Y. (2015). A semi-analytical fractal model for production from tight oil reservoirs with hydraulically fractured horizontal wells. *Fuel*, *158*, 612–618.

Wang, W., Su, Y., Sheng, G., Cossio, M., & Shang, Y. (2015). A mathematical model considering complex fractures and fractal flow for pressure transient analysis of fractured horizontal wells in unconventional reservoirs. *Journal of Natural Gas Science and Engineering*, *23*, 139 - 147. Retrieved from `http://www.sciencedirect.com/science/article/pii/S1875510014003898` doi: https://doi.org/10.1016/j.jngse.2014.12.011

Warren, J., & Root, P. J. (1963). The behavior of naturally fractured reservoirs.

Wimp, J. (1981). *Sequence transformations and their applications.* Elsevier.

Wu, Y.-S. (2016). Chapter 2 - multiphase fluids in porous media. In Y.-S. Wu (Ed.), *Multiphase fluid flow in porous and fractured reservoirs* (p. 15 - 27). Boston: Gulf Professional Publishing. Retrieved from `https://www.sciencedirect.com/science/article/pii/B9780128038482000027` doi: https://doi.org/10.1016/B978-0-12-803848-2.00002-7

Xu, W., Li, J., Du, M., et al. (2011). Quick estimate of initial production from stimulated reservoirs with complex hydraulic fracture network. In *Spe annual technical conference and exhibition.*

Yuan, B., Su, Y., Moghanloo, R. G., Rui, Z., Wang, W., & Shang, Y. (2015). A new analytical multi-linear solution for gas flow toward fractured horizontal wells with different fracture intensity. *Journal of Natural Gas Science and Engineer-*

ing, *23*, 227–238.

Zhou, W., Banerjee, R., Poe, B. D., Spath, J., & Thambynayagam, M. (2013). Semianalytical production simulation of complex hydraulic-fracture networks. *SPE Journal*, *19*(01), 6–18.

Zimmerman, R. W., Chen, G., Hadgu, T., & Bodvarsson, G. S. (1993). A numerical dual-porosity model with semianalytical treatment of fracture/matrix flow. *Water resources research*, *29*(7), 2127–2137.

Appendix A

Derivation of Induced Branch-fracture Subdiffusive Flow Model

A.1 Derivation of Pressure Solution for Region 4

Governing diffusivity equation to be applied in the region 4 of the figure 4.1 can be derived from Equation (4.1) and (4.6),

$$\frac{\partial}{\partial x}\left(\frac{k_\beta}{\mu}\frac{\partial^{1-\beta}}{\partial t^{1-\beta}}\frac{\partial \Delta p_4}{\partial x}\right) = (\phi c_t)\frac{\partial \Delta p_4}{\partial t} \tag{A.1}$$

Taking $\frac{\partial^{\beta-1}}{\partial t^{\beta-1}}$ of the both sides of Equation (A.1) yields,

$$\frac{\partial}{\partial x}\left(\frac{\partial \Delta p_4}{\partial x}\right) = \left(\frac{\phi\mu c_t}{k_\beta}\right)_4 \frac{\partial^\beta \Delta p_4}{\partial t^\beta} \tag{A.2}$$

Transformation into dimensionless variables facilitate an analytical solution for fluid flow with easier boundary condition setting and compatibility with different unit systems. Table 4.2 lists the different scaled and dimensionless variables used in this derivation. This transformation reduces Equation (A.2) to,

$$\frac{1}{x_F^2}\frac{\partial^2 p_{4D}}{\partial x_D^2} = \frac{1}{\eta_\beta}\left(\frac{\eta_i}{x_F^2}\right)^\beta \frac{\partial^\beta p_{4D}}{\partial t_D^\beta} \tag{A.3}$$

where, η_β is equivalent to the diffusivity of the region 4. Some rearrangements leads

to,

$$\frac{\partial^2 p_{4D}}{\partial x_D^2} - \left(\frac{x_F^2}{\eta_\beta}\right)\left(\frac{\eta_i}{x_F^2}\right)^\beta \frac{\partial^\beta p_{4D}}{\partial t_D^\beta} = 0 \tag{A.4}$$

Equation (A.4) is the governing diffusivity equation for the region 4 of the outer reservoir. Taking Laplce transform of Equation (A.4) results in,

$$\frac{\partial^2 \overline{p}_{4D}}{\partial x_D^2} - \left(\frac{x_F^2}{\eta_\beta}\right)\left(\frac{\eta_i}{x_F^2}\right)^\beta s^\beta \overline{p}_{4D} = 0 \tag{A.5}$$

The initial reservoir pressure is assumed constant for each flow region of the proposed model. Therefore, $P_D\left(x_D, 0\right) = 0$. Now, identifying the terms that are independent of x_D and lumping them into as a function of s variable yields:

$$\frac{\partial^2 \overline{p}_{4D}}{\partial x_D^2} - \epsilon_4 \overline{p}_{4D} = 0 \tag{A.6}$$

In Equation (A.6), ϵ_4 carries all the necessary subdiffusion information to the neighbouring reservoir segment while coupling is performed.

$$\epsilon_4 = \left(\frac{x_F^2}{\eta_\beta}\right)\left(\frac{\eta_i}{x_F^2}\right)^\beta s^\beta \tag{A.7}$$

By superposition principle, Equation (A.6) has a general solution:

$$\overline{p}_{4D} = A\,\exp\left(-\sqrt{\epsilon_4}\;x_D\right) + B\,\exp\left(\sqrt{\epsilon_4}\;x_D\right) \tag{A.8}$$

Equation (A.8) is subjected to the following initial and boundary conditions which facilitate with the determination of the integration constants.

□ Initial condition (Pressure difference Δp at $t = 0$):

$$\Delta p|_{t=0} = 0 \tag{A.9}$$

□ Boundary condition 1 (No flow boundary at $x = x_2$):

$$\left.\frac{\partial \Delta p_4}{\partial x}\right|_{x=x_2} = 0 \tag{A.10}$$

Assuming a no-flow boundary at $x = x_2$ is realistic when there exists two more horizontal well on the both sides of the interested well. This is an industry practice to drill parallel well in an unconventional reservoir. Now, transforming Equation (A.10) into dimensionless form and taking Laplace transform of both sides leads to,

$$\left.\frac{\partial \overline{p}_{4D}}{\partial x_D}\right|_{x_D=x_{2D}} = 0 \tag{A.11}$$

Taking the derivative of Equation (A.8) and applying the boundary condition 1.

$$\frac{\partial \overline{p}_{4D}}{\partial x_D} = -\sqrt{\epsilon_4}\ A\exp\left(-\sqrt{\epsilon_4}x_D\right) + \sqrt{\epsilon_4}\ B\exp\left(\sqrt{\epsilon_4}x_D\right) \tag{A.12}$$

Substituting (A.11) into Equation (A.12) results in,

$$A = B\exp(2\sqrt{\epsilon_4}\ x_{2D}) \tag{A.13}$$

Equation (A.8) reduces to,

$$\overline{p}_{4D} = B\exp(2\sqrt{\epsilon_4}\ x_{2D})\exp\left(-\sqrt{\epsilon_4}\ x_D\right)\ + B\exp\left(\sqrt{\epsilon_4}\ x_D\right) \tag{A.14}$$

Some rearrangements to Equation (A.14) results in,

$$\overline{p}_{4D} = B\exp\left(\sqrt{\epsilon_4}\ x_{2D}\right)\ \left\{\exp\left[\sqrt{\epsilon_4}\left(\ x_{2D} - \ x_D\right)\right]\ + \exp\left[-\sqrt{\epsilon_4}\left(\ x_{2D} - \ x_D\right)\right]\ \right\} \tag{A.15}$$

The second boundary condition will ultimately solve the pressure solution for region 4. Transforming Equation (4.11) into dimensionless form and taking Laplace transform of both sides leads to,

$$\left(\overline{p}_{4D}\right)\big|_{x_D=x_{1D}} = \left(\overline{p}_{2D}\right)\big|_{x_D=x_{1D}} \tag{A.16}$$

Applying the second boundary condition into Equation (A.15) reduces to,

$$\overline{p}_{2D} = B\exp\left(\sqrt{\epsilon_4}\ x_{2D}\right)\ \left\{\exp\left[\sqrt{\epsilon_4}\left(\ x_{2D} - \ x_{1D}\right)\right]\ + \exp\left[-\sqrt{\epsilon_4}\left(\ x_{2D} - \ x_{1D}\right)\right]\ \right\} \tag{A.17}$$

Solving for B results in,

$$B = \frac{\overline{p}_{2D}}{\exp\left(\sqrt{\epsilon_4}\ x_{2D}\right)\ \left\{\exp\left[\sqrt{\epsilon_4}\,(\ x_{2D} -\ x_D)\right]\ + \exp\left[-\sqrt{\epsilon_4}\,(\ x_{2D} -\ x_D)\right]\ \right\}} \tag{A.18}$$

Therefore, the pressure solution in region 4 is,

$$\overline{p}_{4D} = (\overline{p}_{2D})\,\frac{\cosh\left[\sqrt{\epsilon_4}\,(\ x_{2D} -\ x_D)\right]}{\cosh\left[\sqrt{\epsilon_4}\,(\ x_{2D} -\ x_{1D})\right]} \tag{A.19}$$

Also, derivative at $x_D = x_{1D}$ is calculated for flux from the region 4 to the region 2:

$$\left.\frac{\partial \overline{p}_{4D}}{\partial x_D}\right|_{x_D = x_{1D}} = -\left(\overline{p}_{2D}\right)|_{x_D = x_{1D}}\sqrt{\epsilon_4}\tanh\left[\sqrt{\epsilon_4}\,(x_{2D} - x_{1D})\right] \tag{A.20}$$

A.2 Derivation of Pressure Solution for Region 3

The governing diffusivity equation of region 3 can be written as,

$$\frac{\partial}{\partial x}\left(\frac{k_\beta}{\mu}\frac{\partial^{1-\beta}}{\partial t^{1-\beta}}\frac{\partial \Delta p_3}{\partial x}\right) = (\phi c_t)_3\frac{\partial \Delta p_3}{\partial t} \tag{A.21}$$

According to the rules of fractional calculus (Uchaikin, 2013), we take $\frac{\partial^{\beta-1}}{\partial t^{\beta-1}}$ of the both sides of Equation (A.2) yields,

$$\frac{\partial}{\partial x}\left(\frac{\partial \Delta p_3}{\partial x}\right) = \left(\frac{\phi\mu c_t}{k_\beta}\right)_3\frac{\partial^\beta \Delta p_3}{\partial t^\beta} \tag{A.22}$$

Transforming into dimensionless introducing the variables listed in Table 4.2, Equation reduces to,

$$\frac{1}{x_F^2}\frac{\partial^2 p_{3D}}{\partial x_D^2} = \frac{1}{\eta_\beta}\left(\frac{\eta_i}{x_F^2}\right)^\beta\frac{\partial^\beta p_{3D}}{\partial t_D^\beta} \tag{A.23}$$

where, η_β is equivalent to the diffusivity of the region 3. This parameter is similar as it is in region 4 due to the assumption that the unconventional matrix of the whole reservoir possess same level of sub-diffusive characteristics. Some rearrangements leads to,

$$\frac{\partial^2 p_{3D}}{\partial x_D^2} - \left(\frac{x_F^2}{\eta_\beta}\right)\left(\frac{\eta_i}{x_F^2}\right)^\beta \frac{\partial^\beta p_{3D}}{\partial t_D^\beta} = 0 \tag{A.24}$$

Equation (A.24) is the governing diffusivity equation in terms of scaled and dimensionless variable for the region 3. Taking Laplace transform of Equation (A.24) results in,

$$\frac{\partial^2 \overline{p}_{3D}}{\partial x_D^2} - \left(\frac{x_F^2}{\eta_\beta}\right)\left(\frac{\eta_i}{x_F^2}\right)^\beta s^\beta \overline{p}_{3D} = 0 \tag{A.25}$$

Now, identifying the terms that are independent of x_D and lumping them into as a function of s variable yields:

$$\frac{\partial^2 \overline{p}_{3D}}{\partial x_D^2} - \epsilon_3 \overline{p}_{3D} = 0 \tag{A.26}$$

Like ϵ_3 of the region 3, ϵ_4 carries all the necessary subdiffusive information to the neighbouring SRV segment while coupling is performed by transfer functions.

$$\epsilon_3 = \left(\frac{x_F^2}{\eta_\beta}\right)\left(\frac{\eta_i}{x_F^2}\right)^\beta s^\beta \tag{A.27}$$

By superposition principle, Equation (A.26) has a general solution,

$$\overline{p}_{3D} = A\exp\left(-\sqrt{\epsilon_3}\; x_D\right) \; + B\exp\left(\sqrt{\epsilon_3}\; x_D\right) \tag{A.28}$$

Equation (A.28) is subjected to the following initial and boundary conditions which facilitate with the determination of the integration constants.

- ☐ Boundary Condition 1 (No flow boundary at $x = x_2$) in dimensionless form:

$$\left.\frac{\partial \overline{p}_{3D}}{\partial x_D}\right|_{x_D = x_{2D}} = 0 \tag{A.29}$$

- ☐ Boundary condition 2 (Pressure continuity at the interface of region 3 and SRV) in dimensionless form:

$$(\overline{p}_{3D})|_{x_D = x_{1D}} = (\overline{p}_{1D})|_{x_D = x_{1D}} \tag{A.30}$$

In a similar fashion, applying Equation (A.29) and (A.30) into Equation (A.28) yields,

$$\overline{p}_{3D} = (\overline{p}_{iD})|_{x_D=x_{1D}} \frac{\cosh\left[\sqrt{\epsilon_3}\,(x_{2D}-x_D)\right]}{\cosh\left[\sqrt{\epsilon_3}\,(x_{2D}-x_{1D})\right]} \tag{A.31}$$

Equation (A.31) is the pressure solution for region 3. The derivative at $x_D = x_{1D}$ is calculated for the flux from the region 3 to the region 2,

$$\left.\frac{\partial \overline{p}_{3D}}{\partial x_D}\right|_{x_D=x_{1D}} = -(\overline{p}_{iD})|_{x_D=x_{1D}} \sqrt{\epsilon_3}\tanh\left[\sqrt{\epsilon_3}\,(x_{2D}-x_{1D})\right] \tag{A.32}$$

A.3 Derivation of Pressure Solution for Region 2

The diffusion equation in region 2 involves x and y component of the fluid flux due to the need for coupling of region 4 influx. The governing diffusivity equation can be written as,

$$\frac{\partial}{\partial x}\left(\frac{k_\beta}{\mu}\frac{\partial^{1-\beta}}{\partial t^{1-\beta}}\frac{\partial \Delta p_2}{\partial x}\right) + \frac{\partial}{\partial y}\left(\frac{k_\beta}{\mu}\frac{\partial^{1-\beta}}{\partial t^{1-\beta}}\frac{\partial \Delta p_2}{\partial y}\right) = (\phi c_t)_2 \frac{\partial \Delta p_2}{\partial t} \tag{A.33}$$

Taking $\frac{\partial^{\beta-1}}{\partial t^{\beta-1}}$ of the both sides of Equation (A.33) yields,

$$\frac{\partial}{\partial x}\left(\frac{\partial \Delta p_2}{\partial x}\right) + \frac{\partial}{\partial y}\left(\frac{\partial \Delta p_2}{\partial y}\right) = \left(\frac{\phi\mu c_t}{k_\beta}\right)_\beta \frac{\partial^\beta \Delta p_2}{\partial t^\beta} \tag{A.34}$$

We assumed that the fluid flow in every region is unidirectional. Now, integrating Equation (A.34) with respect to x in $[0, x_F]$ results in,

$$\int_0^{x_F} \frac{\partial^2 \Delta p_2}{\partial x^2} dx + \int_0^{x_F} \frac{\partial^2 \Delta p_2}{\partial y^2} dx = \left(\frac{\phi\mu c_t}{k_\beta}\right)_\beta \int_0^{x_F} \frac{\partial^\beta \Delta p_2}{\partial t^\beta}\, dx \tag{A.35}$$

Since, there is no flow in the x-direction, a pseudo-function assumption is made. According to the derivation procedure of Trilinear (Ozkan et al., 2009) , Five Region (Stalgorova & Mattar, 2013), and FTSGF (Fan & Ettehadtavakkol, 2017b) model, the first derivatives of Δp with respect to y and t are not function of x. This pseudo-function assumption is made to search for an analytical solution.

$$\frac{\partial \Delta p_2}{\partial y}\ , \frac{\partial \Delta p_2}{\partial t} \neq f(x) \tag{A.36}$$

The integration in Equation (A.35) results in,

$$x_F \left(\frac{\partial^2 \Delta p_2}{\partial y^2}\right) + \left(\frac{\partial \Delta p_2}{\partial x}\right)\bigg|_{x_F} = \frac{x_F}{\eta_\beta}\ \frac{\partial^\beta \Delta p_2}{\partial t^\beta} \tag{A.37}$$

Transforming into dimensionless variables reduces Equation (A.37) to,

$$\left(\frac{\partial p_{2D}}{\partial x_D}\right)\bigg|_{x_D=x_{1D}} + \frac{\partial^2 p_{2D}}{\partial y_D^2} = \frac{x_F^2}{\eta_\beta}\left(\frac{\eta_i}{x_F^2}\right)^\beta \frac{\partial^\beta p_{2D}}{\partial t_D^\beta} \tag{A.38}$$

Taking Laplace Transform of both sides,

$$\left(\frac{\partial \overline{p}_{2D}}{\partial x_D}\right)\bigg|_{x_D=x_{1D}} + \frac{\partial^2 \overline{p}_{2D}}{\partial y_D^2} = \frac{x_F^2}{\eta_\beta}\left(\frac{\eta_i}{x_F^2}\right)^\beta s^\beta\left(\overline{p}_{2D}\right) \tag{A.39}$$

- ☐ Boundary condition 1 (Flux continuity at the interface of region 3 and region 2)

$$(q_4)|_{x=x_1} = (q_2)|_{x=x_1} \tag{A.40}$$

- ☐ Boundary condition 2 (No flow boundary at $y = y_2$)

$$\frac{\partial \overline{p}_{2D}}{\partial y_D}\bigg|_{y_D=y_{2D}} = 0 \tag{A.41}$$

- ☐ Boundary condition 3 (Pressure continuity at the interface of SRV branch-fracture and region 3)

$$(\overline{p}_{3D})|_{y_D=y_{1D}} = (\overline{p}_{iD})|_{y_D=y_{1D}} \tag{A.42}$$

Matrix-matrix fluid transfer happens at the interface at $x = x_1$. Therefore, expanding Equation (A.40),

$$\frac{k_\beta}{\mu}\frac{\partial^{1-\beta}}{\partial t^{1-\beta}}\left(\frac{\partial \Delta p_4}{\partial x}\right)\bigg|_{x=x_1} = \frac{k_\beta}{\mu}\frac{\partial^{1-\beta}}{\partial t^{1-\beta}}\left(\frac{\partial \Delta p_2}{\partial x}\right)\bigg|_{x=x_1} \tag{A.43}$$

Transforming into dimensionless variables and taking Laplace transform of both sides,

$$\left(\frac{\partial \overline{p}_{4D}}{\partial x_D}\right)\Big|_{x_D=x_{1D}} = \left(\frac{\partial \overline{p}_{2D}}{\partial x_D}\right)\Big|_{x_D=x_{1D}} \tag{A.44}$$

Substituting Equation (A.44) into Equation (A.39) results in,

$$\left(\frac{\partial \overline{p}_{4D}}{\partial x_D}\right)\Big|_{x_D=x_{1D}} + \frac{\partial^2 \Delta \overline{p}_{2D}}{\partial y_D^2} = \frac{x_F^2}{\eta_\beta}\left(\frac{\eta_i}{x_F^2}\right)^\beta s^\beta\left(\overline{p}_{2D}\right) \tag{A.45}$$

From Equation (A.32) and Equation (A.45), we derive,

$$\frac{\partial^2 \Delta \overline{p}_{2D}}{\partial y_D^2} - \sqrt{\epsilon_4}\tanh\left[\sqrt{\epsilon_4}\left(x_{2D}-x_{1D}\right)\right]\ \left(\overline{p}_{2D}\right)\big|_{x_D=x_{1D}} = \frac{x_F^2}{\eta_\beta}\left(\frac{\eta_i}{x_F^2}\right)^\beta s^\beta\left(\overline{p}_{2D}\right) \tag{A.46}$$

Recalling the pseudo-function assumption and assuming $\left(\overline{p}_{2D}\right)\big|_{x_D=x_{1D}} = \overline{p}_{2D}$. Therefore, identifying the terms that are independent of y_D and lumping them into as a function of s variable yields,

$$\frac{\partial^2 \Delta \overline{p}_{2D}}{\partial y_D^2} - \epsilon_2\left(\overline{p}_{2D}\right) = 0 \tag{A.47}$$

In Equation (A.47), ϵ_2 carries all the important information about region 2 to the region 1.

$$\epsilon_2 = \left[\sqrt{\epsilon_4}\tanh\left[\sqrt{\epsilon_4}\left(x_{2D}-x_{1D}\right)\right] + \frac{x_F^2}{\eta_\beta}\left(\frac{\eta_i}{x_F^2}\right)^\beta s^\beta\right] \tag{A.48}$$

By superposition principle, we write from Equation (A.47),

$$\overline{p}_{2D} = A\exp\left(-\sqrt{\epsilon_2}\ y_D\right)\ + B\exp\left(\sqrt{\epsilon_2}\ y_D\right) \tag{A.49}$$

Applying the boundary conditions from Equation (A.41) and (A.42) into Equation (A.49) leads to,

$$\overline{p}_{2D} = \left(\overline{p}_{iD}\right)\big|_{y=y_{1D}} \frac{\cosh\left[\sqrt{\epsilon_2}\left(y_{2D}-y_D\right)\right]}{\cosh\left[\sqrt{\epsilon_2}\left(y_{2D}-y_{1D}\right)\right]} \tag{A.50}$$

The resulted solution in Equation (A.50) presents the pressure solution for region 2. Also, derivative of (A.50) is calculated at $y_D = y_{1D}$ for flux from region 2 to the

SRV.

$$\left.\frac{\partial \overline{p}_{2D}}{\partial y_D}\right|_{y_D=y_{1D}} = -\left(\overline{p}_{iD}\right)\big|_{y_D=y_{1D}}\sqrt{\epsilon_2}\tanh\left[\sqrt{\epsilon_2}\left(y_{2D}-y_{1D}\right)\right] \tag{A.51}$$

A.4 Derivation of Pressure Solution for Spherical Matrix

The governing diffusivity equation in spherical matrix:

$$\frac{1}{r^2}\frac{\partial}{\partial r}\left(r^2\frac{k_\beta}{\mu}\frac{\partial^{1-\beta}}{\partial t^{1-\beta}}\frac{\partial \Delta p_m}{\partial r}\right) = \left(\phi c_t\right)_\beta \frac{\partial \Delta p_m}{\partial t} \tag{A.52}$$

Taking $\frac{\partial^{\beta-1}}{\partial t^{\beta-1}}$ of the both sides of Equation (A.52) yields,

$$\frac{1}{r^2}\frac{\partial}{\partial r}\left(r^2\frac{\partial \Delta p_m}{\partial r}\right) = \left(\frac{\phi\mu c_t}{k}\right)_\beta \frac{\partial^\beta \Delta p_m}{\partial t^\beta} \tag{A.53}$$

Introducing dimensionless variables in (A.53)

$$\frac{1}{r_D^2}\frac{\partial}{\partial r_D}\left(r_D^2\frac{\partial p_{mD}}{\partial r_D}\right) = \frac{x_F^2}{\eta_\beta}\left(\frac{\eta_i}{x_F^2}\right)^\beta \frac{\partial^\beta p_{mD}}{\partial t_D^\beta} \tag{A.54}$$

Let,

$$M_D = p_{mD} r_D \tag{A.55}$$

From Equation (A.55) and (A.54), we can derive,

$$\frac{\partial^2 M_D}{\partial r_D^2} = \frac{x_F^2}{\eta_\beta}\left(\frac{\eta_i}{x_F^2}\right)^\beta \frac{\partial^\beta M_D}{\partial t_D^\beta} \tag{A.56}$$

Taking Laplace transform of both sides of Equation (A.56).

$$\frac{\partial^2 \overline{M_D}}{\partial r_D^2} - \left(\frac{x_F^2}{\eta_\beta}\right)\left(\frac{\eta_i}{x_F^2}\right)^\beta s^\beta \overline{M_D} = 0 \tag{A.57}$$

Identifying the parameters that remain constant at a fixed time in Laplace domain and lumping them together in ϵ_m:

$$\frac{\partial^2 \overline{M_D}}{\partial r_D^2} - \epsilon_m \overline{M_D} = 0 \tag{A.58}$$

Where,

$$\epsilon_m = \left(\frac{x_F^2}{\eta_\beta}\right)\left(\frac{\eta_i}{x_F^2}\right)^{\beta} s^{\beta} \tag{A.59}$$

Therefore, the general solution of Equation (A.58) in Laplace domain is,

$$\overline{M_D} = A\exp\left(-\sqrt{\epsilon_m}\ r_D\right)\ + B\exp\left(\sqrt{\epsilon_m}\ r_D\right) \tag{A.60}$$

where, A and B are constants that needs to be evaluated by applying necessary boundary conditions. The boundary conditions are,

- Boundary condition 1

$$\begin{aligned} \Delta p_m\left(r=0,t\right) &= 0 \\ \overline{M_D}\left(r_D=0,\ s\right) &= 0 \end{aligned} \tag{A.61}$$

- Boundary condition 2 (Pressure continuity at the interface of spherical matrix and branch-fracture medium)

$$\overline{p_{mD}}\big|_{r_D=r_{mD}} = \overline{(p_{iD})}\Big|_{r_D=r_{mD}} \tag{A.62}$$

Applying the boundary condition 1 from Equation (A.61) into Equation (A.60) yields the following,

$$\overline{M_D} = 2B\{\sinh\left(\sqrt{\epsilon_m}\ r_D\right)\} \tag{A.63}$$

Plugging the relation of $\overline{M_D}$ from Equation (A.55),

$$\overline{p}_{mD} = \frac{2}{r_D}\ B\sinh\left(\sqrt{\epsilon_m} r_D\right) \tag{A.64}$$

Now, applying boundary condition 2 from Equation (A.62) results in,

$$\overline{p}_{iD}\big|_{r_D=r_{mD}} = \frac{2}{r_{mD}} B\ \sinh\left(\sqrt{\epsilon_m} r_{mD}\right) \tag{A.65}$$

Evaluating for B,

$$B = \frac{r_{mD}}{2\sinh\left(\sqrt{\epsilon_m}\ r_{mD}\right)}\{\left(\overline{p}_{iD}\right)|\}_{r_D=r_{mD}} \tag{A.66}$$

Therefore, we obtain the pressure solution in Laplace domain for the spherical matrix.

$$\overline{p}_{mD} = \frac{r_{mD}}{r_D} \frac{\sinh\left(\sqrt{\epsilon_m}\ r_D\right)}{\sinh\left(\sqrt{\epsilon_m}\ r_{mD}\right)}\ \left(\overline{p}_{iD}\right)|_{r_D = r_{mD}} \tag{A.67}$$

A.5 Derivation of Pressure Solution for Branch-fracture

The governing equation for the branch-fracture domain can be written as,

$$\frac{\partial}{\partial x}\left(\frac{\overline{k_x}}{\mu}\frac{\partial \Delta p_i}{\partial x}\right) + \frac{\partial}{\partial y}\left(\frac{k\,(y)}{\mu}\frac{\partial \Delta p_i}{\partial y}\right) + \dot{Q} = (\phi c_t)_i \frac{\partial \Delta p_i}{\partial t} \tag{A.68}$$

where, $\dot{Q}$ denotes the transient fluid transfer from the SRV matrix spheres into the branch-fracture. According to de Swaan O et al. (1976), the matrix source term should be the ratio of the total flux across the surface of a spherical matrix to the half of the fracture volume envelope around each sphere.

$$\dot{Q} = -\frac{k_\beta\,(4\pi r_m^2)}{\mu}\frac{\partial^{1-\beta}}{\partial t^{1-\beta}}\left(\frac{\partial \Delta p_m}{\partial r}\right)_{r=r_m} \frac{1}{4\pi r_m^2 (h_f/2\ )} \tag{A.69}$$

After some rearrangements, Equation A.69 reduces to,

$$\dot{Q} = -\frac{2k_\beta}{\mu h_f}\frac{\partial^{1-\beta}}{\partial t^{1-\beta}}\left(\frac{\partial \Delta p_m}{\partial r}\right)_{r=r_m} \tag{A.70}$$

Plugging equation A.70 into equation A.68 yields,

$$\frac{\partial}{\partial x}\left(\frac{\overline{k_x}}{\mu}\frac{\partial \Delta p_i}{\partial x}\right) + \frac{\partial}{\partial y}\left(\frac{k\,(y)}{\mu}\frac{\partial \Delta p_i}{\partial y}\right) - \frac{2k_\beta}{\mu h_f}\frac{\partial^{1-\beta}}{\partial t^{1-\beta}}\left(\frac{\partial \Delta p_m}{\partial r}\right)_{r=r_m} = (\phi c_t)_i \frac{\partial \Delta p_i}{\partial t} \tag{A.71}$$

Now, integrating Equation A.71 over $[0, x_F]$,

$$\int_0^{x_F} \frac{\partial}{\partial x}\left(\frac{\overline{k_x}}{\mu}\frac{\partial \Delta p_i}{\partial x}\right)dx + \int_0^{x_F} \frac{\partial}{\partial y}\left(\frac{k\,(y)}{\mu}\frac{\partial \Delta p_i}{\partial y}\right)dx$$

$$- \int_0^{x_F} \frac{2k_\beta}{\mu h_f}\frac{\partial^{1-\beta}}{\partial t^{1-\beta}}\left(\frac{\partial \Delta p_m}{\partial r}\right)_{r=r_m} dx = (\phi c_t)_i \int_0^{x_F} \frac{\partial \Delta p_i}{\partial t}\, dx \tag{A.72}$$

The fluid flow is unidirectional and pressure gradient only varies in the y-direction. Applying the pseudo-function assumption which states that the first derivatives of Δp with respect to y and t are not function of x.(Ozkan et al., 2009). The fluid flow is unidirectional and pressure gradient only varies in the y-direction. Hence, we write,

$$\frac{\partial \Delta p_i}{\partial y} \neq f(x) \tag{A.73}$$

$$\frac{\partial \Delta p_i}{\partial t} \neq f(x) \tag{A.74}$$

$$k\,(y) \neq f(x) \tag{A.75}$$

From Equation (A.73), (A.74), (A.75) and (A.72), we obtain,

$$\frac{\overline{k_x}}{\mu}\left(\frac{\partial \Delta p_i}{\partial x}\right)\Big|_{x=x_F} + x_F \frac{\partial}{\partial y}\left(\frac{k\,(y)}{\mu}\frac{\partial \Delta p_i}{\partial y}\right) - \frac{2x_F k_\beta}{\mu h_f}\frac{\partial^{1-\beta}}{\partial t^{1-\beta}}\left(\frac{\partial \Delta p_m}{\partial r}\right)_{r=r_m} = x_F(\phi c_t)_i \frac{\partial \Delta p_i}{\partial t} \tag{A.76}$$

Introducing dimensionless variables and transforming the variables into dimensionless form,

$$\frac{\overline{k_x}}{\mu}\left(\frac{\partial p_{iD}}{\partial x_D}\right)\Big|_{x_D=x_{1D}} + \frac{\partial}{\partial y_D}\left(\frac{k\,(y)}{\mu}\frac{\partial p_{iD}}{\partial y_D}\right) - \frac{2x_F k_\beta}{\mu h_f}\left(\frac{\eta_i}{x_F^2}\right)^{1-\beta}\frac{\partial^{1-\beta}}{\partial t^{1-\beta}}\left(\frac{\partial p_{mD}}{\partial r_D}\right)_{r_D=r_{mD}} = (\phi c_t)_i\,(\eta_i)\,\frac{\partial p_{iD}}{\partial t_D} \tag{A.77}$$

Multiplying both sides of (A.77) by $\frac{\mu}{k_i}$ yields,

$$\frac{\overline{k_x}}{k_i}\left(\frac{\partial p_{iD}}{\partial x_D}\right)\Big|_{x_D=x_{1D}} + \frac{\partial}{\partial y_D}\left(\frac{k\left(y\right)}{k_i}\frac{\partial p_{iD}}{\partial y_D}\right) - \frac{2k_\beta x_F}{k_i h_f}\left(\frac{\eta_i}{x_F^2}\right)^{1-\beta}\frac{\partial^{1-\beta}}{\partial t^{1-\beta}}\left(\frac{\partial p_{mD}}{\partial r_D}\right)_{r_D=r_{mD}} = \frac{\partial p_{iD}}{\partial t_D} \tag{A.78}$$

Introducing the dimensionless permeability $k_D\left(y_D\right)$ and dimensionless fracture slab thickness h_{fD} to Equation (A.78) results in,

$$k_{xD}\left(\frac{\partial p_{iD}}{\partial x_D}\right)\Big|_{x_D=x_{1D}} + \frac{\partial}{\partial y_D}\left(k_D\left(y_D\right)\frac{\partial p_{iD}}{\partial y_D}\right) - \frac{2k_\beta}{k_i h_{fD}}\left(\frac{\eta_i}{x_F^2}\right)^{1-\beta}\frac{\partial^{1-\beta}}{\partial t^{1-\beta}}\left(\frac{\partial p_{mD}}{\partial r_D}\right)_{r_D=r_{mD}} = \frac{\partial p_{iD}}{\partial t_D} \tag{A.79}$$

Here, $k_{xD} = \frac{\overline{k_x}}{k_i}$. Now, taking Laplace transform of Equation (A.79) and applying the initial condition, $p_D\left(y_D, 0\right) = 0$:

$$k_{xD}\left(\frac{\partial \overline{p}_{iD}}{\partial x_D}\right)\Big|_{x_D=x_{1D}} + \frac{\partial}{\partial y_D}\left(k_D\left(y_D\right)\frac{\partial \overline{p}_{iD}}{\partial y_D}\right) - \frac{2k_\beta}{k_i h_{fD}}\left(\frac{\eta_i}{x_F^2}\right)^{1-\beta} s^{1-\beta}\left(\frac{\partial \overline{p}_{mD}}{\partial r_D}\right)_{r_D=r_{mD}} = s\left(\overline{p}_{iD}\right) \tag{A.80}$$

Recalling the pressure solution for spherical matrix stated in Equation (A.67) and taking derivative,

$$\frac{\partial p_{mD}}{\partial r_D} = \frac{r_{mD}\left(p_{iD}\right)|_{r_D=r_{mD}}}{\sinh\left(\sqrt{\epsilon_m}\, r_{mD}\right)}\left[\frac{-\sinh\left(\sqrt{\epsilon_m}\, r_D\right)}{r_D^2} + \frac{\sqrt{\epsilon_{\mathrm{m}}}\cosh\left(\sqrt{\epsilon_m}\, r_D\right)}{r_D}\right] \tag{A.81}$$

Now, evaluating Equation (A.81) at $r_D = r_{mD}$, we obtain,

$$\left(\frac{\partial p_{mD}}{\partial r_D}\right)\Big|_{r_D=r_{mD}} = r_{mD}\,(p_{iD})|_{r_D=r_{mD}}\left[\frac{-1}{r_{mD}^2} + \frac{\sqrt{\epsilon_{\rm m}}\,\cosh\left(\sqrt{\epsilon_m}\;r_{mD}\right)}{r_{mD}\sinh\left(\sqrt{\epsilon_m}\;r_{mD}\right)}\right] \tag{A.82}$$

After some rearrangements, the derivative take the form,

$$\left(\frac{\partial p_{mD}}{\partial r_D}\right)\Big|_{r_D=r_{mD}} = \frac{(p_{iD})|_{r_D=r_{mD}}}{r_{mD}}\;\left[r_{mD}\sqrt{\epsilon_{\rm m}}\coth\left(\sqrt{\epsilon_m}\;r_{mD}\right)\;-1\right] \tag{A.83}$$

Substituting Equation (A.83) in Equation (A.80), we obtain the following:

$$\begin{aligned} &k_{xD}\left(\frac{\partial \overline{p}_{iD}}{\partial x_D}\right)\Big|_{x_D=x_{1D}} + \frac{\partial}{\partial y_D}\left(k_D\,(y_D)\,\frac{\partial \overline{p}_{iD}}{\partial y_D}\;\right) \\ &-\frac{2k_\beta}{k_i h_{fD}}\left(\frac{\eta_i}{x_F^2}s\right)^{1-\beta}\frac{(p_{iD})|_{r_D=r_{mD}}}{r_{mD}}\;\left[r_{mD}\sqrt{\epsilon_{\rm m}}\coth\left(\sqrt{\epsilon_m}\;r_{mD}\right)\;-1\right] = s\;\;(\overline{p}_{iD}) \end{aligned} \tag{A.84}$$

The branch-fracture diffusivity equation is subjected to the following boundary conditions,

☐ Boundary condition 1 (Flux continuity at the interface of SRV and region 3)

$$(q_1)|_{x=x_1} = (q_3)|_{x=x_1} \tag{A.85}$$

☐ Boundary condition 2 (Flux continuity at the interface of SRV and region 2)

$$(q_1)|_{y=y_1} = (q_2)|_{y=y_1} \tag{A.86}$$

☐ Boundary condition 3 (Pressure continuity at $y = w_F/2$)

$$(p_i)|_{y=w_F/2} = (p_F)|_{y=w_F/2} \tag{A.87}$$

☐ Boundary condition 4 (Pressure continuity at $y = y_1$)

$$(p_i)|_{y=y_1} = (p_2)|_{y=y_1} \tag{A.88}$$

Expanding the boundary condition 1, we obtain,

$$\frac{\overline{k_x}A_i}{\mu}\left(\frac{\partial \Delta p_i}{\partial x}\right)\bigg|_{x=x_1} = \frac{k_\beta A_h}{\mu}\frac{\partial^{1-\beta}}{\partial t^{1-\beta}}\left(\frac{\partial \Delta p_3}{\partial x}\right)\bigg|_{x=x_1} \tag{A.89}$$

Where A_i represents the area of the induced fractures intersecting at the interface of the region 1 and region 3. This area of the fracture continuum plays as the sole medium of fluid transport. On the other hand, the matrix continuum only acts as a storage of fluid and does not produce to the well bore. The term A_h on the right side represents the area of the region 3 that produce fluid and transport to the region 1. If the fracture height is h_f and there exists n_f number of fractures in induced region, Equation (A.89) can be written as:

$$\overline{k_x}\left(n_f h_f y_1\right)\left(\frac{\partial \Delta p_i}{\partial x}\right)\bigg|_{x=x_1} = k_\beta\left(n_f h_f + n_f h_m\right) y_1 \frac{\partial^{1-\beta}}{\partial t^{1-\beta}}\left(\frac{\partial \Delta p_3}{\partial x}\right)\bigg|_{x=x_1} \tag{A.90}$$

In Equation (A.91), the total fracture height, h_{ft} equals $n_f h_f$.

$$\left(\overline{k_x}h_{ft}\right)\left(\frac{\partial \Delta p_i}{\partial x}\right)\bigg|_{x=x_1} = \left(k_\beta h\right)\frac{\partial^{1-\beta}}{\partial t^{1-\beta}}\left(\frac{\partial \Delta p_3}{\partial x}\right)\bigg|_{x=x_1} \tag{A.91}$$

Introducing the bulk permeability $\left(\widetilde{k_x} = \frac{\overline{k_x}h_{ft}}{h}\right)$ in Equation (A.91) gives us,

$$\widetilde{k_x}\left(\frac{\partial \Delta p_i}{\partial x}\right)\bigg|_{x=x_1} = k_\beta\frac{\partial^{1-\beta}}{\partial t^{1-\beta}}\left(\frac{\partial \Delta p_3}{\partial x}\right)\bigg|_{x=x_1} \tag{A.92}$$

where, $\widetilde{k_x}$ represents the bulk permeability at the interface of the induced region and region 3. Now transforming Equation(A.92) into dimensionless and then taking Laplace transform of both sides:

$$\left(\frac{\partial \overline{p}_{iD}}{\partial x_D}\right)\bigg|_{x_D=x_{1D}} = \frac{k_\beta}{\widetilde{k_x}}\left(\frac{\eta_i}{x_F^2}s\right)^{1-\beta}\left(\frac{\partial \overline{p}_{3D}}{\partial x_D}\right)\bigg|_{x_D=x_{1D}} \tag{A.93}$$

Recalling Equation(A.32) and substituting in Equation (A.93), we obtain the follow-

ing,

$$\left(\frac{\partial \overline{p}_{iD}}{\partial x_D}\right)\Big|_{x_D=x_{1D}} = -\frac{k_\beta}{\widetilde{k_x}} \left(\frac{\eta_i}{x_F^2}s\right)^{1-\beta} \sqrt{\epsilon_3}\tanh\left[\sqrt{\epsilon_3}\left(x_{2D}-x_{1D}\right)\right] \left(\overline{p}_{1D}\right)|_{x_D=x_{1D}} \quad \text{(A.94)}$$

Plugging Equation (A.93) in Equation (A.84) results in,

$$-\frac{k_{xD}k_\beta}{\widetilde{k_x}} \left(\frac{\eta_i}{x_F^2}s\right)^{1-\beta} \sqrt{\epsilon_3}\tanh\left[\sqrt{\epsilon_3}\left(x_{2D}-x_{1D}\right)\right] \left(\overline{p}_{iD}\right)|_{x_D=x_{1D}} + \frac{\partial}{\partial y_D}\left(k_D\left(y_D\right)\frac{\partial \overline{p}_{iD}}{\partial y_D}\right)$$

$$-\frac{2k_\beta}{k_i h_{fD}}\left(\frac{\eta_i}{x_F^2}s\right)^{1-\beta} \frac{\left(p_{iD}\right)|_{r_D=r_{mD}}}{r_{mD}} \left[r_{mD}\sqrt{\epsilon_{\mathrm{m}}}\coth\left(\sqrt{\epsilon_m}\ r_{mD}\right) - 1\right] = s\ \left(\overline{p}_{iD}\right) \quad \text{(A.95)}$$

Now, identifying the constant terms at a fixed time and lumping them together into single parameter simplify Equation (A.95) to,

$$-\epsilon_a\left(\overline{p}_{iD}\right)|_{x_D=x_{1D}} + \frac{\partial}{\partial y_D}\left(k_D\left(y_D\right)\frac{\partial \overline{p}_{iD}}{\partial y_D}\right) - \epsilon_b\left(p_{iD}\right)|_{r_D=r_{mD}} - s\ \left(\overline{p}_{iD}\right) = 0 \quad \text{(A.96)}$$

where, the lumped parameters ϵ_a and ϵ_b are defined as:

$$\begin{aligned} \epsilon_a &= \frac{k_{xD}k_\beta}{\widetilde{k_x}} \left(\frac{\eta_i}{x_F^2}s\right)^{1-\beta} \sqrt{\epsilon_3}\tanh\left[\sqrt{\epsilon_3}\left(x_{2D}-x_{1D}\right)\right] \\ \epsilon_b &= \frac{2k_{\beta D}}{h_{fD}r_{mD}}\left(\frac{\eta_i}{x_F^2}s\right)^{1-\beta} \left[r_{mD}\sqrt{\epsilon_{\mathrm{m}}}\coth\left(\sqrt{\epsilon_m}\ r_{mD}\right) - 1\right] \end{aligned} \quad \text{(A.97)}$$

The fluid flow in SRV branch-fractures is necessarily unidirectional. Hence, $\overline{p}_{iD}$ only depends on y direction. Again, recalling the pseudo-function assumption and assuming $\left(\overline{p}_{iD}\right)|_{x_D=x_{1D}} = \overline{p}_{iD}$ and $\left(\overline{p}_{iD}\right)|_{r_D=r_{mD}} = \overline{p}_{iD}$ lets us write,

$$\frac{\partial}{\partial y_D}\left(k_D\left(y_D\right)\frac{\partial \overline{p}_{iD}}{\partial y_D}\right) - \epsilon_i\ \left(\overline{p}_{iD}\right) = 0 \quad \text{(A.98)}$$

where,

$$\epsilon_i = \epsilon_a + \epsilon_b + s \quad \text{(A.99)}$$

Next, we incorporate the exponential branch-fracture permeability field to the diffusivity equation of fracture medium. Recalling the branch-fracture permeability field in dimensionless form,

$$k_D(y_D) = (k_{\beta D})^{\left(\frac{y_D - w_D/2}{y_{1D} - w_D/2}\right)} \tag{A.100}$$

Transforming it into an exponential form gives us flexibility to deal with the complexity it introduces to the diffusivity equation,

$$k_D\left(y_D\right) = e^{(\ln k_{\beta D})\ \left(\frac{y_D - w_D/2}{y_{1D} - w_D/2}\right)} \tag{A.101}$$

From Equation (A.98) and (A.101), we find,

$$\frac{\partial}{\partial y_D}\left(e^{(\ln k_{\beta D})\ \left(\frac{y_D - w_D/2}{y_{1D} - w_D/2}\right)}\ \frac{\partial \overline{p}_{iD}}{\partial y_D}\ \right) - \epsilon_i\ \ (\overline{p}_{iD}) = 0 \tag{A.102}$$

Now, expanding Equation (A.102):

$$e^{(\ln k_{\beta D})\ \left(\frac{y_D - w_D/2}{y_{1D} - w_D/2}\right)}\ \frac{\partial^2 \overline{p}_{iD}}{\partial y_D^2} + \frac{\partial \overline{p}_{iD}}{\partial y_D}\left(\frac{\ln k_{\beta D}}{y_{1D} - w_D}\right) e^{(\ln k_{\beta D})\ \left(\frac{y_D - w_D/2}{y_{1D} - w_D/2}\right)}\ - \epsilon_i\ \ (\overline{p}_{iD}) = 0 \tag{A.103}$$

To simplify the diffusivity equation, we let the following:

$$M = \left(\frac{\ln k_{\beta D}}{y_{1D} - w_D/2}\right), \quad z_D\ = e^{M(y_D - w_D/2)} \tag{A.104}$$

Now the diffusivity equation becomes,

$$z_D \frac{\partial^2 \overline{p}_{iD}}{\partial y_D^2} + \frac{\partial \overline{p}_{iD}}{\partial y_D} M z_D - \epsilon_i\ \ (\overline{p}_{iD}) = 0 \tag{A.105}$$

Recalling Chain Rule of differentiation and finding the derivative terms of Equation (A.105) in terms of z_D.

$$\frac{\partial \overline{p}_{iD}}{\partial y_D} = \frac{\partial \overline{p}_{iD}}{\partial z_D}\ \frac{\partial z_D}{\partial y_D}$$
$$\frac{\partial \overline{p}_{iD}}{\partial y_D} = \frac{\partial \overline{p}_{iD}}{\partial z_D}\ Me^{M(y_D - w_D/2)} \tag{A.106}$$

In a similar fashion, we obtain:

$$\frac{\partial^2 \overline{p}_{iD}}{\partial y_D^2} = M^2 z_D^2 \frac{\partial^2 \overline{p}_{iD}}{\partial z_D^2} + M^2 z_D \frac{\partial \overline{p}_{iD}}{\partial z_D} \tag{A.107}$$

Substituting Equation (A.106) and (A.107) into Equation (A.105) yields:

$$z_D^2 \frac{\partial^2 \overline{p}_{iD}}{\partial z_D} + 2 z_D \frac{\partial \overline{p}_{iD}}{\partial z_D} - \left(\frac{\epsilon_i}{M^2}\right)\left(\frac{1}{z_D}\right)\overline{p}_{iD} = 0 \tag{A.108}$$

Equation (A.108) resembles to the modified Bessel differential equation. In order to find the solution to this equation, we complement the techniques of determining solutions from a standard Bessel differential equation. Therefore, according to Bowman (2012), the general solution to the modified Bessel differential equation can be written as below:

$$\overline{p}_{iD} = z_D^{-1/2}\ \left[AI_1\left(\frac{2\sqrt{\epsilon_i}}{M}\ z_D^{-\frac{1}{2}}\right) + BK_1\left(\frac{2\sqrt{\epsilon_i}}{M}\ z_D^{-\frac{1}{2}}\right)\right] \tag{A.109}$$

Here, I_1 and K_1 are the modified Bessel function of first and second kind. A and B are two constants which needs to be evaluated with the available boundary conditions. For the ease of algebraic manipulation, we let the argument of Bessel functions as:

$$X = \frac{2\sqrt{\epsilon_i}}{M}\ z_D^{-\frac{1}{2}} \tag{A.110}$$

This simplifies to,

$$\overline{p}_{iD} = z_D^{-1/2}\ \left[AI_1(X) + BK_1(X)\right] \tag{A.111}$$

The differentiation rules for I_ν and K_ν are given by:

$$\begin{aligned} I_\nu^{'}(x) &= I_{\nu-1}(x) - \frac{\nu}{x}\, I_\nu(x) \\ K_\nu^{'}(x) &= -K_{\nu-1}(x) - \frac{\nu}{x}\, K_\nu(x) \end{aligned} \tag{A.112}$$

Utilizing the differential rules given in Equation (A.112), the derivative of Equation (A.109) is evaluated. We write:

$$\begin{aligned} \frac{\partial \overline{p}_{iD}}{\partial y_D} = \frac{1}{\sqrt{z_D}} \Bigg[-A\frac{\sqrt{\epsilon_i}}{\sqrt{z_D}}\, I_0(X) + \frac{AM}{2}\, I_1(X) + B\frac{\sqrt{\epsilon_i}}{\sqrt{z_D}}\, K_0(X) + \frac{BM}{2}\, K_1(X) \Bigg] \\ - \frac{M}{2\sqrt{z_D}} \left[AI_1(X) + BK_1(X) \right] \end{aligned} \tag{A.113}$$

Which simplifies to,

$$\frac{\partial \overline{p}_{iD}}{\partial y_D} = \frac{\sqrt{\epsilon_i}}{z_D} \left[BK_0(X) - AI_0(X) \right] \tag{A.114}$$

When Equation is evaluated at $y_D = y_{1D}$, Equation (A.114) takes the form:

$$\left(\frac{\partial \overline{p}_{iD}}{\partial y_D} \right)\Bigg|_{y_D = y_{1D}} = \frac{\sqrt{\epsilon_i}}{k_{\beta D}} \left[BK_0(X_1) - AI_0(X_1) \right] \tag{A.115}$$

In Equation (A.115), we define X_1 as X evaluated at $y_D = y_{1D}$. We did this to keep our equations and terms tidy and distinguishable. Hence, we write,

$$X_1 = (X)|_{y_D = y_{1D}} = \frac{2\sqrt{\epsilon_i}}{M} \frac{1}{\sqrt{k_{\beta D}}} \tag{A.116}$$

Recalling the boundary condition 2 in Equation (A.86) and expanding it yields:

$$\frac{k_{\beta i} A_i}{\mu} \left(\frac{\partial \Delta p_i}{\partial y} \right)\Bigg|_{y=y_1} = \frac{k_\beta A_h}{\mu} \frac{\partial^{1-\beta}}{\partial t^{1-\beta}} \left(\frac{\partial \Delta p_2}{\partial y} \right)\Bigg|_{y=y_1} \tag{A.117}$$

Where A_i represents the area of the induced fractures intersecting at the interface of the SRV and region 2. This area of the fracture continuum plays the as the sole medium of fluid transport. On the other hand, the matrix continuum only acts as a storage of fluid and does not produce to the well bore. The term A_h on the right side represents the area of the region 2 that produce fluid and transport to the SRV.

If the fracture height is h_f and there exists n_f number of fractures in induced region, Equation (A.117) can be written as:

$$k_{\beta i}\left(n_f h_f x_F\right)\left(\frac{\partial \Delta p_i}{\partial x}\right)\Big|_{y=y_1} = k_\beta\left(n_f h_f + n_f h_m\right) x_F \frac{\partial^{1-\beta}}{\partial t^{1-\beta}}\left(\frac{\partial \Delta p_2}{\partial x}\right)\Big|_{y=y_1} \tag{A.118}$$

Total branch-fracture height, $h_{ft} = n_f h_f$,

$$\left(k_{\beta i} h_{ft}\right)\left(\frac{\partial \Delta p_i}{\partial y}\right)\Big|_{y=y_1} = \left(k_\beta h\right)\frac{\partial^{1-\beta}}{\partial t^{1-\beta}}\left(\frac{\partial \Delta p_2}{\partial y}\right)\Big|_{y=y_1} \tag{A.119}$$

Introducing bulk permeability to Equation (A.119) results in,

$$\widetilde{k_y}\left(\frac{\partial \Delta p_i}{\partial y}\right)\Big|_{y=y_1} = k_\beta \frac{\partial^{1-\beta}}{\partial t^{1-\beta}}\left(\frac{\partial \Delta p_2}{\partial y}\right)\Big|_{y=y_1} \tag{A.120}$$

Here,$\widetilde{k_y}$ represents the bulk permeability at the interface of the induced region and region 2. Now transforming Equation (A.120) into dimensionless and then taking Laplace transform of both sides:

$$\left(\frac{\partial \overline{p}_{iD}}{\partial y_D}\right)\Big|_{y_D=y_{1D}} = \frac{k_\beta}{\widetilde{k_y}}\ \left(\frac{\eta_i}{x_F^2}s\right)^{1-\beta}\ \left(\frac{\partial \overline{p}_{2D}}{\partial x_D}\right)\Big|_{y_D=y_{1D}} \tag{A.121}$$

Recalling Equation (A.51) which is the derivative of the pressure solution from region 2 and applying in Equation (A.121).

$$\left(\frac{\partial \overline{p}_{iD}}{\partial y_D}\right)\Big|_{y_D=y_{1D}} = -\frac{k_\beta}{\widetilde{k_y}}\ \left(\frac{\eta_i}{x_F^2}s\right)^{1-\beta}\sqrt{\epsilon_2}\tanh\left[\sqrt{\epsilon_2}\left(y_{2D}-y_{1D}\right)\right]\ \left(\overline{p}_{iD}\right)\big|_{y_D=y_{1D}} \tag{A.122}$$

Plugging Equation (A.122) in (A.115), we obtain the following:

$$\begin{aligned} -\left(\frac{\sqrt{\epsilon_2}}{\sqrt{\epsilon_i}}\right)\ \left(\frac{k_\beta k_{\beta D}}{\widetilde{k_y}}\right)\ \left(\frac{\eta_i}{x_F^2}s\right)^{1-\beta}&\tanh\left[\sqrt{\epsilon_2}\left(y_{2D}-y_{1D}\right)\right]\ \left(\overline{p}_{iD}\right)\big|_{y_D=y_{1D}} \\ &= \left[BK_0\left(X_1\right) - AI_0\left(X_1\right)\right] \end{aligned} \tag{A.123}$$

Now, lumping the important parameters that remain constant at a fixed time. We define it as ϵ_α which equals to:

$$\epsilon_\alpha = \left(\frac{\sqrt{\epsilon_2}}{\sqrt{\epsilon_i}}\right)\left(\frac{k_\beta k_{\beta D}}{\widetilde{k_y}}\right)\ \left(\frac{\eta_i}{x_F^2}s\right)^{1-\beta}\tanh\left[\sqrt{\epsilon_2}\left(y_{2D}-y_{1D}\right)\right] \tag{A.124}$$

Then, Equation (A.123) reduces to:

$$\epsilon_\alpha\left(\overline{p}_{iD}\right)\big|_{y_D=y_{1D}} = AI_0\left(X_1\right) - BK_0\left(X_1\right) \tag{A.125}$$

Recalling Equation (A.109) and evaluating at $y_D = y_{1D}$ reduces Equation (A.109) in terms of $\left(\overline{p_{iD}}\right)\big|_{y_D=y_{1D}}$ which is desirable to compute the coefficients of integration.

$$\left(\overline{p}_{iD}\right)\big|_{y_D=y_{1D}} = \frac{1}{\sqrt{k_{\beta D}}}\ \left[AI_1\left(X_1\right) + BK_1\left(X_1\right)\right] \tag{A.126}$$

Evaluating for A:

$$A = \frac{\sqrt{k_{\beta D}}\left(\overline{p}_{iD}\right)\Big|_{y_D=y_{1D}}}{I_1\left(X_1\right)} - \left(\frac{K_1\left(X_1\right)}{I_1\left(X_1\right)}\right)B \tag{A.127}$$

From Equation (A.127) and (A.125), we derive:

$$\epsilon_\alpha\left(\overline{p}_{iD}\right)\big|_{y_D=y_{1D}} = \left[\frac{\sqrt{k_{\beta D}}\left(\overline{p}_{iD}\right)\Big|_{y_D=y_{1D}}}{I_1\left(X_1\right)} - \left(\frac{K_1\left(X_1\right)}{I_1\left(X_1\right)}\right)B\right]I_0\left(X_1\right) - BK_0\left(X_1\right) \tag{A.128}$$

Evaluating for B:

$$B = \left[\frac{\sqrt{k_{\beta D}}I_0\left(X_1\right) - \epsilon_\alpha I_1\left(X_1\right)}{K_1\left(X_1\right)I_0\left(X_1\right) + K_0\left(X_1\right)I_1\left(X_1\right)}\right]\left(\overline{p}_{iD}\right)\big|_{y_D=y_{1D}} \tag{A.129}$$

We identify the constants and let:

$$B = C\ \left(\overline{p}_{iD}\right)\big|_{y_D=y_{1D}} \tag{A.130}$$

Here,

$$C = \left[\frac{\sqrt{k_{\beta D}}I_0\left(X_1\right) - \epsilon_\alpha I_1\left(X_1\right)}{K_1\left(X_1\right)I_0\left(X_1\right) + K_0\left(X_1\right)I_1\left(X_1\right)}\right] \tag{A.131}$$

Equation (A.127) reduces to the following after putting Equation for B:

$$A = \left[\frac{\sqrt{k_{\beta D}}}{I_1(X_1)} - \left(\frac{K_1(X_1)}{I_1(X_1)}\right)C\right] \ (\overline{p}_{iD})|_{y_D=y_{1D}} \tag{A.132}$$

Again, we let:

$$D = \left[\frac{\sqrt{k_{\beta D}}}{I_1(X_1)} - \left(\frac{K_1(X_1)}{I_1(X_1)}\right)C\right] \tag{A.133}$$

This simplifies Equation (A.132) to:

$$A = D\,(\overline{p}_{iD})|_{y_D=y_{1D}} \tag{A.134}$$

Here, the two coefficients A and B have been expressed in $(\overline{p_{iD}})|_{y_D=y_{1D}}$ and C and D are constant at a fixed value of time. Then, applying the boundary condition 3 from Equation (A.87), the value of $(\overline{p_{iD}})|_{y_D=y_{1D}}$ can be obtained. Now, the general solution (eq. (A.111)) takes the form as:

$$(\overline{p}_{iD})| = z_D^{-1/2}[DI_1(X) + CK_1(X)\ ]\ (\overline{p}_{iD})|_{y_D=y_{1D}} \tag{A.135}$$

Transforming the boundary condition 3 into dimensionless form:

$$(\overline{p}_{iD})|_{y_D=w_D/2} = (\overline{p}_{FD})|_{y_D=w_D/2} \tag{A.136}$$

Now, in order to evaluate the term $(\overline{p_{iD}})|_{y_D=y_{1D}}$, we apply the boundary condition 3. First, if we set $y_D = w_D/2$ in Equation (A.111), Equation (A.111) reduces to:

$$(\overline{p}_{iD})|_{y_D=w_D/2} = [DI_1(X_0) + CK_1(X_0)\ ]\ (\overline{p}_{iD})|_{y_D=y_{1D}} \tag{A.137}$$

Where,

$$X_0 = (X)|_{y_D=w_D/2} = \frac{2\sqrt{\epsilon_i}}{M} \tag{A.138}$$

From Equation (A.136) and (A.137), we obtain,

$$(\overline{p}_{iD})|_{y_D=y_{1D}} = \frac{(\overline{p}_{FD})|_{y_D=\frac{w_D}{2}}}{[DI_1(X_0) + CK_1(X_0)]} \tag{A.139}$$

Therefore, the general solution (stated in Eq.(A.111)) can be written in terms of hydraulic fracture pressure term as following:

$$\overline{p}_{iD} = z_D^{-\frac{1}{2}} \left[\frac{DI_1(X) + CK_1(X)}{DI_1(X_0) + CK_1(X_0)} \right] (\overline{p}_{FD})|_{y_D = \frac{w_D}{2}} \tag{A.140}$$

Recalling the differentiation rules for I_ν and K_ν and differentiating Equation (A.141) yields,

$$\left(\frac{\partial \overline{p}_{iD}}{\partial y_D} \right) = \left(\frac{(\overline{p}_{FD})|_{y_D = \frac{w_D}{2}}}{DI_1(X_0) + CK_1(X_0)} \right) \frac{\partial}{\partial y_D} \left[z_D^{-\frac{1}{2}} \{ DI_1(X) + CK_1(X) \} \right] \tag{A.141}$$

Expanding the differentiation and rearranging Equation (A.142),

$$\left(\frac{\partial \overline{p}_{iD}}{\partial y_D} \right) = \left(\frac{(\overline{p}_{FD})|_{y_D = \frac{w_D}{2}}}{DI_1(X_0) + CK_1(X_0)} \right) \left[\frac{1}{\sqrt{z_D}} \left(-D \frac{\sqrt{\epsilon_i}}{\sqrt{z_D}} \; I_0(X) + \frac{DM}{2} \; I_1(X) \right. \right.$$
$$\left. \left. + C \frac{\sqrt{\epsilon_i}}{\sqrt{z_D}} \; K_0(X) + \frac{CM}{2} \; K_1(X) \right) \; - \frac{M}{2\sqrt{z_D}} \left[DI_1(X) + CK_1(X) \right] \right] \tag{A.142}$$

Equation (A.142) simplifies to,

$$\left(\frac{\partial \overline{p}_{iD}}{\partial y_D} \right) = \left(\frac{(\overline{p}_{FD})|_{y_D = \frac{w_D}{2}}}{DI_1(X_0) + CK_1(X_0)} \right) \frac{\sqrt{\epsilon_i}}{z_D} \left[C \; K_0(X) - D \; I_0(X) \right] \tag{A.143}$$

Evaluating Equation (A.143) at $y_d = w_D/2$ results in,

$$\left(\frac{\partial \overline{p}_{iD}}{\partial y_D} \right) \Bigg|_{y_D = w_D/2} = \sqrt{\epsilon_i} \left[\frac{C \; K_0(X_0) - D \; I_0(X_0)}{DI_1(X_0) + CK_1(X_0)} \right] (\overline{p}_{FD})|_{y_D = \frac{w_D}{2}} \tag{A.144}$$

Identifying the constant term for a fixed value of time and letting:

$$\epsilon_\gamma = \sqrt{\epsilon_i} \left[\frac{C \; K_0(X_0) - D \; I_0(X_0)}{DI_1(X_0) + CK_1(X_0)} \right] \tag{A.145}$$

Where the argument X_0 represents the X evaluated at $y_D = w_D/2$. Since, for negative argument X, I_ν and K_ν produce complex values, we can avoid that by placing positive argument while keeping the expression coherent by factoring a term δ. Hence,

$$\epsilon_\gamma = \delta\sqrt{\epsilon_i}\left[\frac{C\ K_0\left(X_0\right) - D\ I_0\left(X_0\right)}{DI_1\left(X_0\right) + CK_1\left(X_0\right)}\right] \tag{A.146}$$

In the above equation, when $k_{\beta D} = \frac{k_\beta}{k_i} < 1, \delta = -1$ and the arguments and become:

$$\begin{aligned} X &= \frac{2\sqrt{\epsilon_i}\ln\left(\frac{1}{k_{\beta D}}\right)}{y_{1D} - w_D}\ e^{(\ln k_{\beta D})\ \left(\frac{y_D - w_D/2}{y_{1D} - w_D/2}\right)} \\ X_1 &= \frac{2\sqrt{\epsilon_i}\ln\left(\frac{1}{k_{\beta D}}\right)}{y_{1D} - w_D/2}\ \frac{1}{\sqrt{k_{\beta D}}} \\ X_0 &= \frac{2\sqrt{\epsilon_i}\ln\left(\frac{1}{k_{\beta D}}\right)}{y_{1D} - w_D/2} \end{aligned} \tag{A.147}$$

Finally, Equation (A.144) takes the following form:

$$\left(\frac{\partial\overline{p}_{iD}}{\partial y_D}\right)\Bigg|_{y_D = w_D/2} = \epsilon_\gamma\ \left(\overline{p}_{FD}\right)|_{y_D = \frac{w_D}{2}} \tag{A.148}$$

Here, Equation (A.148) is now ready to be coupled with the hydraulic fracture region to incorporate the effect of all the four regions. The term ϵ_γ accounts for the effect of outer regions, inner unfractured region, the branch-fracture permeability distribution in the SRV and the effect of fractional diffusion in spherical matrix.

A.6 Derivation of Pressure Solution for Primary Fracture Plane

The diffusivity equation for the primary fracture plane is,

$$\frac{\partial}{\partial x}\left(\frac{k_F}{\mu}\frac{\partial\Delta p_F}{\partial x}\right) + \frac{\partial}{\partial y}\left(\frac{k_F}{\mu}\frac{\partial\Delta p_F}{\partial y}\right) = \left(\phi c_t\right)_F\frac{\partial\Delta p_F}{\partial t} \tag{A.149}$$

In order to incorporate the influx from the SRV into the fracture continuum, we should integrate the above equation along the width of the fracture. Also, Equation (A.149) becomes $1D$ after integration,

$$\int_0^{w_F/2} \frac{\partial^2 \Delta p_F}{\partial x^2} dy + \int_0^{w_F/2} \frac{\partial^2 \Delta p_F}{\partial y^2} dy = \left(\frac{\phi \mu c_t}{k_\beta}\right)_F \int_0^{w_F/2} \frac{\partial \Delta p_F}{\partial t}\, dy \tag{A.150}$$

The flow inside the primary hydraulic fracture is necessarily unidirectional. Therefore, according to pseudo-function assumption (Ozkan et al., 2009), the first derivatives of Δp with respect to x and t are not function of y.

$$\frac{\partial \Delta p_F}{\partial x}\ , \frac{\partial \Delta p_F}{\partial t} \neq f(y) \tag{A.151}$$

The integration in Equation (A.150) simplifies to,

$$\left(\frac{\partial^2 \Delta p_F}{\partial x^2}\right) \frac{w_F}{2} + \left(\frac{\partial p_F}{\partial y}\right)\Big|_0^{w_F/2} = \frac{1}{\eta_F} \frac{w_F}{2} \frac{\partial \Delta p_F}{\partial t} \tag{A.152}$$

Transforming Equation (A.152) into dimensionless form yields,

$$\frac{\partial^2 p_{FD}}{\partial x_{FD}^2} + \frac{2}{w_D} \left.\frac{\partial p_{FD}}{\partial y_D}\right|_{y_D = w_D/2} = \frac{\eta_i}{\eta_F} \frac{\partial p_{FD}}{\partial t_D} \tag{A.153}$$

Now, we take the Laplace transform of both sides of Equation (A.153)

$$\frac{\partial^2 \overline{p}_{FD}}{\partial x_D^2} + \frac{2}{w_D} \left.\frac{\partial \overline{p}_{FD}}{\partial y_D}\right|_{y_D = w_D/2} = \frac{s}{\eta_{FD}} \overline{p}_{FD} \tag{A.154}$$

Equation (A.154) is the diffusivity equation in Laplace domain for the hydraulic fracture region. Equation (A.154) is subjected to the following boundary conditions,

- Boundary condition 1 (Flux continuity at the interface of SRV and primary fracture region)

$$(q_F)|_{y=w_F/2} = (q_i)|_{y=w_F/2} \tag{A.155}$$

- Boundary condition 2 (Flux continuity at the interface of primary fracture plane and the wellbore)

$$\left(\frac{Bq_f}{4}\right)\Big|_{x=0} = (q_F)|_{x=0} \tag{A.156}$$

□ Boundary condition 3 (No flow boundary at $x = x_1$) in dimensionless form

$$\left(\frac{\partial p_{FD}}{\partial x_D}\right)\Big|_{x_D=x_{1D}} = 0 \tag{A.157}$$

Expanding the boundary condition from Equation (A.155) using Darcy's law results in,

$$\frac{A_h k_F}{\mu}\left(\frac{\partial \Delta p_F}{\partial y}\right)\Big|_{y=w_F/2} = \frac{A_i k_i}{\mu}\left(\frac{\partial \Delta p_i}{\partial y}\right)\Big|_{y=w_F/2} \tag{A.158}$$

The effective area through which the primary fracture plane connects with the branch-fracture volume can be found from the individual fracture height.

$$A_i = n_f h_{ft} x_F \tag{A.159}$$

Equation (A.160) simplifies to,

$$k_F\left(\frac{\partial \Delta p_F}{\partial y}\right)\Big|_{y=w_F/2} = \frac{k_i h_{ft}}{h}\left(\frac{\partial \Delta p_i}{\partial y}\right)\Big|_{y=w_F/2} \tag{A.160}$$

The bulk branch-fracture permeability at the interface of SRV and primary fracture region can be written as:

$$\widetilde{k_i} = \left(\frac{h_{ft}}{h}\right) k_i \tag{A.161}$$

Therefore, Equation (A.160) becomes,

$$\left(\frac{\partial \Delta p_F}{\partial y}\right)\Big|_{y=w_F/2} = \frac{\widetilde{k_i}}{k_F}\left(\frac{\partial \Delta p_i}{\partial y}\right)\Big|_{y=w_F/2} \tag{A.162}$$

Transforming into dimensionless form and taking laplace transform of both sides of Equation (A.162),

$$\left(\frac{\partial \overline{p}_{FD}}{\partial y_D}\right)\Big|_{y_D=w_D/2} = \left(\frac{\widetilde{k_i}}{k_F}\right)\left(\frac{\partial \overline{p}_{iD}}{\partial y_D}\right)\Big|_{y_D=w_D/2} \tag{A.163}$$

From Equation (A.154) and Equation (A.163) , the fracture diffusivity equation can be rearranged as:

$$\frac{\partial^2 \overline{p}_{FD}}{\partial x_D^2} + \frac{2}{w_D} \left(\frac{\widetilde{k}_i}{k_F}\right) \left(\frac{\partial \overline{p}_{iD}}{\partial y_D}\right)\Bigg|_{y_D = w_D/2} = \frac{s}{\eta_{FD}} \overline{p}_{FD} \tag{A.164}$$

Defining the dimensionless fracture conductivity,

$$C_{FD} = \frac{k_F w_D}{\widetilde{k}_i} = \frac{k_F w_F h}{k_i x_F h_{ft}} \tag{A.165}$$

Introducing C_{FD} into Equation (A.164),

$$\frac{\partial^2 \overline{p}_{FD}}{\partial x_D^2} + \frac{2}{C_{FD}} \left(\frac{\partial \overline{p}_{iD}}{\partial y_D}\right)\Bigg|_{y_D = w_D/2} = \frac{s}{\eta_{FD}} \overline{p}_{FD} \tag{A.166}$$

Substituting Equation (A.148) into Equation (A.166), we obtain:

$$\frac{\partial^2 \overline{p}_{FD}}{\partial x_D^2} + \frac{2}{C_{FD}} \left.\epsilon_\gamma \left(\overline{p}_{FD}\right)\right|_{y_D = \frac{w_D}{2}} = \frac{s}{\eta_{FD}} \overline{p}_{FD} \tag{A.167}$$

Recalling the pseudo-function assumption, we set $\left.\left(\overline{p}_{FD}\right)\right|_{y_D = \frac{w_D}{2}} = \overline{p}_{FD}$. Now, identifying the terms that are independent of x_D of primary fracture domain and lumping them into as a function of s variable,

$$\epsilon_F = \frac{s}{\eta_{FD}} - \frac{2}{C_{FD}} \epsilon_\gamma \tag{A.168}$$

Then, Equation (A.167) reduces to,

$$\frac{\partial^2 \overline{p}_{FD}}{\partial x_D^2} - \epsilon_F \overline{p}_{FD} = 0 \tag{A.169}$$

Applying superposition principle, we obtain a general solution to Equation (A.169),

$$\overline{p}_{FD} = A \exp\left(-\sqrt{\epsilon_F}\ x_D\right) + B \exp\left(\sqrt{\epsilon_F}\ x_D\right) \tag{A.170}$$

As the boundary condition 2 defines that one-fourth of the individual fracture flowrate (Bq_f) is producing through each symmetry element. The total well flowrate $q_t = n_F q_f$ where n_F is the number of primary hydraulic fractures intercepting the horizontal well. Therefore, expanding the boundary condition 2 from equation A.156 using Darcy's law results in,

$$\int_0^{w_F/2}\int_0^{h}(v_x)|_{x=0}\ \partial z\partial y = -\frac{k_F}{\mu}\int_0^{w_F/2}\int_0^{h}\left(\frac{\partial \Delta p_F}{\partial x}\right)\Big|_{x=0}\partial z\partial y \tag{A.171}$$

Evaluating the integration yields,

$$\left(\frac{Bq_f}{4}\right) = -\frac{k_F}{\mu}\frac{w_F}{2}\ h\ \left(\frac{\partial \Delta p_F}{\partial x}\right)\Big|_{x=0} \tag{A.172}$$

Introducing dimensionless fracture variables and dimensionless flow conductivity C_{FD} into Equation (A.172),

$$\begin{aligned} 1 &= -\frac{k_F w_F h}{k_i x_F h_{ft}}\frac{1}{\pi}\left(\frac{\partial p_{FD}}{\partial x_D}\right)\Big|_{x_D=0} \\ \left(\frac{\partial p_{FD}}{\partial x_D}\right)\Big|_{x_D=0} &= -\frac{\pi}{C_{FD}} \end{aligned} \tag{A.173}$$

Now, taking Laplace transform of Equation (A.173),

$$\left(\frac{\partial \overline{p}_{FD}}{\partial x_D}\right)\Big|_{x_D=0} = -\frac{\pi}{sC_{FD}} \tag{A.174}$$

Recalling the boundary condition 3 from Equation (A.157) and taking Laplace transform of both sides yields,

$$\left(\frac{\partial \overline{p}_{FD}}{\partial x_D}\right)\Big|_{x_D=x_{1D}} = 0 \tag{A.175}$$

The boundary condition 3 defines that there exists a no flow boundary at the tip of the primary fracture plane. Applying Equation (A.175) and (A.174) into the general solution (eq. (A.170)) yields the particular pressure solution in Laplace domain for the SIBFF model,

$$\overline{p}_{FD} = \frac{\pi}{sC_{FD}\sqrt{\epsilon_F}}\frac{\cosh\left[\sqrt{\epsilon_F}\ (1-x_D)\right]}{\sinh\left[\sqrt{\epsilon_F}\ \right]} \tag{A.176}$$

Setting $x_D = 0$ in (A.176), we obtain the wellbore pressure solution,

$$\overline{p}_{FD}|_{x_D=0} = \overline{p}_{WD} = \frac{\pi}{s\ C_{FD}\ \sqrt{\epsilon_F}\tanh\left[\sqrt{\epsilon_F}\ \right]} \tag{A.177}$$

Equation (A.177) presents the constant rate solution for the buttomhole pressure of the proposed SIBFF model in Laplace domain.